AFML-TR-76-122

GRADED PYROLYTIC GRAPHITE/SILICON CARBIDE COATING DEPOSITION STUDIES

ATLANTIC RESEARCH CORPORATION
5390 CHEROKEE AVENUE
ALEXANDRIA, VIRGINIA 22314

APRIL 1977

TECHNICAL REPORT AFML-TR-76-122
Final Report for Period July 1974 – October 1975

Approved for public release; distribution unlimited.

AIR FORCE MATERIALS LABORATORY
AIR FORCE SYSTEMS COMMAND
WRIGHT-PATTERSON AIR FORCE BASE, OHIO 45433

NOTICE

When government drawings, specifications, or other data are used for any purpose other than in connection with a definitely related Government procurement operation, the United States Government thereby incurs no responsibility nor any obligation whatsoever; and the fact that the Government may have formulated, furnished, or in any way supplied the said drawings, specifications, or other data, is not to be regarded by implication or otherwise as in any manner licensing the holder or any other person or corporation, or conveying any rights or permission to manufacture, use, or sell any patented invention that may in any way be related thereto.

This final report was submitted by Atlantic Research Corporation, 5390 Cherokee Avenue, Alexandria, Virginia under Contract F33615-74-C-5103, Project 7340, Task 734001 with the Air Force Materials Laboratory, Wright Patterson Air Force Base, Ohio. Mr. John D. Latva, AFML/MXS was the laboratory project monitor.

This report has been reviewed and cleared for open publication and/or public release by the appropriate Office of Information (OI) in accordance with AFR 190-17 and DODD 5230.9. There is no objection to unlimited distribution of this report to the public at large, or by DDC to the National Technical Information Service (NTIS).

This technical report has been reviewed and is approved for publication.

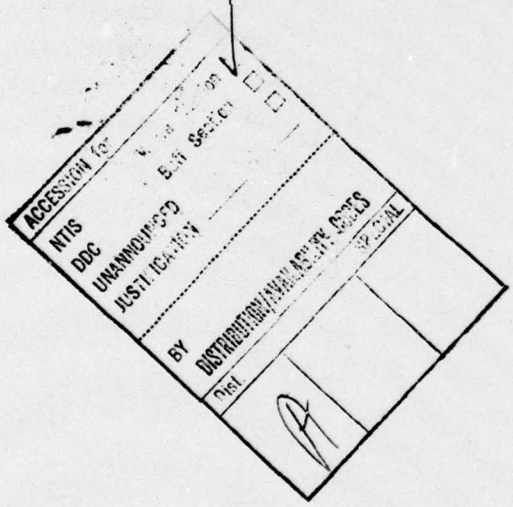

John D. Latva

JOHN D. LATVA
Project Monitor

FOR THE DIRECTOR

Albert Olevitch

A. OLEVITCH
Chief, Non-Metals Engineering Branch
Systems Support Division

Copies of this report should not be returned unless return is required by security considerations, contractual obligations, or notice on a specific document.

AIR FORCE/56780/28 September 1977 — 100

UNCLASSIFIED

SECURITY CLASSIFICATION OF THIS PAGE (When Data Entered)

REPORT DOCUMENTATION PAGE

READ INSTRUCTIONS BEFORE COMPLETING FORM

1. REPORT NUMBER: AFML-TR-76-122	2. GOVT ACCESSION NO.
3. RECIPIENT'S CATALOG NUMBER	
4. TITLE (and Subtitle): Graded Pyrolytic Graphite/Silicon Carbide Coating Deposition Studies	5. TYPE OF REPORT & PERIOD COVERED: Final Report, July 1974 - October 1975
	6. PERFORMING ORG. REPORT NUMBER
7. AUTHOR(s): Joseph P. Copeland; Kenneth E. Undercoffer	8. CONTRACT OR GRANT NUMBER(s): F33615-74-C-5103
9. PERFORMING ORGANIZATION NAME AND ADDRESS: Atlantic Research Corporation, 5390 Cherokee Avenue, Alexandria, Virginia 22314	10. PROGRAM ELEMENT, PROJECT, TASK AREA & WORK UNIT NUMBERS: 7340, 734001, 73400157
11. CONTROLLING OFFICE NAME AND ADDRESS: Air Force Materials Laboratory, Wright-Patterson AFB, Dayton, Ohio 45433	12. REPORT DATE: April 1977
	13. NUMBER OF PAGES: 143
14. MONITORING AGENCY NAME & ADDRESS (if different from Controlling Office)	15. SECURITY CLASS. (of this report): Unclassified
	15a. DECLASSIFICATION DOWNGRADING SCHEDULE

16. DISTRIBUTION STATEMENT (of this Report)

Approved for public release; distribution unlimited.

17. DISTRIBUTION STATEMENT (of the abstract entered in Block 20, if different from Report)

18. SUPPLEMENTARY NOTES

19. KEY WORDS (Continue on reverse side if necessary and identify by block number)

Coatings
Pyrolytic Graphite
Silicon Carbide
Chemical Vapor Deposition
Composites

20. ABSTRACT (Continue on reverse side if necessary and identify by block number)

Codeposited coatings of pyrolytic graphite/silicon carbide were fabricated by chemical vapor deposition at temperatures ranging from 3000°F to 3800°F using methane and methyltrichlorosilane as precursors and nitrogen as a diluent and carrier. The effect of temperature and methyltrichlorosilane concentration on coating composition (SiC content) and morphology were determined. Specimens of codeposited coatings were fabricated to determine the physical properties, thermal stress state and erosion characteristics of various PG/SiC compositions. Coating samples were examined and characterized microscopically, by X-ray diffraction and by electron microprobe.

DD FORM 1 JAN 73 1473 EDITION OF 1 NOV 65 IS OBSOLETE

UNCLASSIFIED

SECURITY CLASSIFICATION OF THIS PAGE (When Data Entered)

045550

4B

PREFACE

This technical report was prepared in partial fulfillment of the requirements of Contract F33615-74-C-5103, AFML Project No. 7340, Task No. 734001 with the Space and Missiles Systems Branch, Systems Support Division, Air Force Materials Laboratory. Mr. John D. Latva, AFML/MXS, provided technical direction for the Air Force Materials Laboratory.

This report covers work conducted during the period July 1974 through October 1975 and constitutes the final report under this contract.

This study was conducted within the Materials Technology Department, Research and Technology Division, Atlantic Research Corporation, 5390 Cherokee Avenue, Alexandria, Virginia 22314. The Principal Investigator was Dr. Joseph Copeland. Mr. Kenneth Undercoffer supervised the deposition and characterization effort.

TABLE OF CONTENTS

Section			Page
I	INTRODUCTION		1
II	SUMMARY		2
III	DEPOSITION EXPERIMENTS		3
	1.	Objective and Approach	3
	2.	Apparatus	3
	3.	Experimental Runs	6
	4.	Analysis of Results	60
	5.	Application of Correlations	63
IV	FABRICATION OF TEST SPECIMENS		66
	1.	Physical Properties Specimens	66
	2.	Thermal Stress Specimens	78
	3.	Erosion Test Specimens	85
V	MATERIALS CHARACTERIZATION PROCEDURES		111
	1.	Physical Properties	111
	2.	Thermal/Mechanical Properties	120
VI	CONCLUSIONS AND RECOMMENDATIONS		122
APPENDIX – General Atomic Report			125

LIST OF ILLUSTRATIONS

Figure		Page
1	Water-Cooled Injector (0.310 inch bore)	4
2	CH_3SiCl_3 Delivery System	5
3	3.5-inch Tubular Deposition Assembly	8
4	2.0-inch Tubular Deposition Assembly	9
5	Run 002-85 Coating Microstructure 13 Inches from Injector	11
6	Coating Thickness and Density Profiles of Pin Located 15 Inches from Injector. Run No. 002-85	14
7	Electron Microprobe Scan of Coating Deposited at 3000°F	21
8	Electron Microprobe Scan of Coating Deposited at 3200°F	22
9	Electron Microprobe Scan of Coating Deposited at 3400°F	23
10	Electron Microprobe Scan of Coating Deposited at 3600°F	24
11	Electron Microprobe Scan of Coating Deposited at 3800°F	25
12	Run 006-3, 3000°F, Coating Microstructure 13 Inches from Injector	27
13	Run 006-3, 3200°F, Coating Microstructure 13 Inches from Injector	28
14	Run 006-3, 3400°F, Coating Microstructure 13 Inches from Injector	29
15	Run 006-3, 3600°F, Coating Microstructure 13 Inches from Injector	30
16	Run 006-3, 3800°F, Coating Microstructure 13 Inches from Injector	31
17	Electron Microprobe Scan of Coating from Run 006-18, Layer 1, Deposited at 3000°F	34
18	Electron Microprobe Scan of Run 006-10, Layer 2, Deposited at 3200°F	35
19	Electron Microprobe Scan of Run 006-10, Layer 3, Deposited at 3400°F	36
20	Electron Microprobe Scan of Run 006-10, Layer 4, Deposited at 3600°F	37

LIST OF ILLUSTRATIONS (Continued)

Figure		Page
21	Run 006-10, 3000°F, Coating Microstructure	39
22	Run 006-10, 3200°F, Coating Microstructure	40
23	Run 006-10, 3400°F, Coating Microstructure	41
24	Run 006-10, 3600°F, Coating Microstructure	42
25	Electron Microprobe Scan of Coating from Run 002-81, Layer 1	48
26	Electron Microprobe Scan of Coating from Run 002-81, Layer 2	49
27	Electron Microprobe Scan of Coating from Run 002-81, Layer 3	50
28	Electron Microprobe Scan of Coating from 006-8, Layer 1	51
29	Electron Microprobe Scan of Coating from 006-8, Layer 2	52
30	Electron Microprobe Scan of Coating from Run 006-18, Layer 1	53
31	Electron Microprobe Scan of Coating from Run 006-18, Layer 2	54
32	Electron Microprobe Scan of Coating from Run 006-18, Layer 3	55
33	Run 002-81, Layer 1 (0.080% CH_3SiCl_3), Coating Microstructure 13 Inches from Injector	56
34	Run 002-81, Layer 2 (0.040% CH_3SiCl_3), Coating Microstructure 13 Inches from Injector	56
35	Run 002-81, Layer 3 (0.021% CH_3SiCl_3), Coating Microstructure 13 Inches from Injector	57
36	Run 006-8, Layer 1 (0.094% CH_3SiCl_3), Coating Microstructure 12 Inches from Injector	57
37	Run 006-8, Layer 2 (0.048% CH_3SiCl_3), Coating Microstructure 12 Inches from Injector	58
38	Run 006-18, Layer 1 (0.022% CH_3SiCl_3), Coating Microstructure 12 Inches from Injector	58

LIST OF ILLUSTRATIONS (Continued)

Figure		Page
39	Run 006-18, Layer 2 (0.070% CH_3SiCl_3), Coating Microstructure 12 Inches from Injector	59
40	Run 006-18, Layer 3 (0.120% CH_3SiCl_3), Coating Microstructure 12 Inches from Injector	59
41	Effect of Temperature	62
42	Effect of CH_3SiCl_3 Flowrate	64
	Run 006-22 Coating Microstructure 6 Inches from Injector	70
44	Run 006-22 Coating Microstructure 9 Inches from Injector	70
45	Run 006-22 Coating Microstructure 12 Inches from Injector	71
46	Electron Microprobe Scan of Coating from Run 006-22, 10 Inches from Injector	72
47	Electron Microprobe Scan of Coating from Run 006-22, 12 Inches from Injector	73
48	Electron Microprobe Scan of Coating from Run 006-22, 14 Inches from Injector	74
49	Run 006-23 Coating Microstructure 12 Inches from Injector	76
50	Run 006-23 Coating Microstructure 14 Inches from Injector	76
51	Electron Microprobe Scan of Coating from Run 006-23, 12 Inches from Injector	77
52	Run 006-24 Coating Microstructure 12 Inches from Injector	79
53	Run 006-24 Coating Microstructure 14 Inches from Injector	79
54	Electron Microprobe Scan of Coating from Run 006-24, 12 Inches from Injector	80
55	Nominal CH_3SiCl_3 Rate vs. Time for Run No. 008-11	81

LIST OF ILLUSTRATIONS (Continued)

Figure		Page
56	Nominal CH_3SiCl_3 Rate vs. Time for Run No. 008-23	82
57	Run 008-11, Entrance End, Coating Microstructure (Full Thickness)	86
58	Run 008-11, Entrance End, Coating Microstructure Near Coating Surface	87
59	Run 008-11, Entrance End, Coating Microstructure at Coating Mid-Thickness	87
60	Run 008-11, Entrance End, Coating Microstructure Near Substrate	88
61	Run 008-11, Exit End, Coating Microstructure (Full Thickness)	89
62	Run 008-11, Exit End, Coating Microstructure Near Coating Surface	90
63	Run 008-11, Exit End, Coating Microstructure at Coating Mid-Thickness	90
64	Run 008-11, Exit End, Coating Microstructure Near Substrate	91
65	Run 008-23, Entrance End, Coating Microstructure (Full Thickness)	92
66	Run 008-23, Entrance End, Coating Microstructure Near Coating Surface	93
67	Run 008-23, Entrance End, Coating Microstructure at Coating Mid-Thickness	93
68	Run 008-23, Entrance End, Coating Microstructure Near Substrate	94
69	Run 008-23, Exit End, Coating Microstructure (Full Thickness)	95
70	Run 008-23, Exit End, Coating Microstructure Near Coating Surface	96
71	Run 008-23, Exit End, Coating Microstructure at Coating Mid-Thickness	96
72	Run 008-23, Exit End, Coating Microstructure Near Substrate	97
73	Coated Erosion Test Specimen Configuration	98
74	Run 008-9 Coating Microstructure at Entrance End	102
75	Run 008-9 Coating Microstructure at Throat	102
76	Run 008-9 Coating Microstructure at Exit End	103

LIST OF ILLUSTRATIONS (Continued)

Figure		Page
77	Run 008-12 Coating Microstructure at Entrance End	104
78	Run 008-12 Coating Microstructure at Throat	104
79	Run 008-12 Coating Microstructure at Exit End	105
80	Run 008-20 Coating Microstructure at Entrance End	107
81	Run 008-20 Coating Microstructure at Throat	107
82	Run 008-20 Coating Microstructure at Exit End	108
83	Run 008-21 Coating Microstructure at Entrance End	109
84	Run 008-21 Coating Microstructure at Exit End	109
85	Run 008-22 Coating Microstructure at Entrance End	110
86	Run 008-22 Coating Microstructure at Exit End	110
87	Typical Group 5 PG/SiC Microstructure	114
88	Typical Group 6 PG/SiC Microstructure	114
89	Typical Group 10 PG/SiC Microstructure	115
90	Typical Group 11 PG/SiC Microstructure	115
91	Typical Group 20 PG/SiC Microstructure	116
92	Typical Group 21 PG/SiC Microstructure	116
93	Typical Group 30 PG/SiC Microstructure	117
94	Typical Group 40 PG/SiC Microstructure	117
95	Typical Group 70 PG/SiC Microstructure	118
96	Relationship Between Coating Density, SiC Concentration and Pyrolytic Graphite Matrix Density	119

LIST OF ILLUSTRATIONS (Continued)

Table		Page
1	Deposition Conditions for Run 002-85	10
2	Coating Characterization Data for Run 002-85	13
3	Circumferential Coating Thickness Variation of Tube Wall Coating of Run 002-85	15
4	Deposition Conditions for Run 006-1	17
5	Deposition Conditions for Run 006-3	18
6	Coating Characterization Data for Run 006-1	19
7	Coating Characterization Data for Run 006-3	20
8	Deposition Conditions for Run 006-10	32
9	Coating Data for Run 006-10	33
10	Deposition Conditions for Runs 002-81, 006-8 and 006-18	44
11	Coating Characterization Data for Run 002-81	45
12	Coating Characterization Data for Run 006-8	46
13	Coating Characterization Data for Run 006-18	47
14	Interlayer Spacing of PG Phase in Coating Layers Deposited During Run 006-18	61
15	Deposition Conditions for Runs 002-86, 002-87, 006-22, 006-23 and 006-24	67
16	Coating Characterization Data for Runs 002-86, 002-87, 006-22, 006-23 and 006-24	68
17	"C" Direction Density and SiC Concentration Profile of Coating from Run 006-22 at 13 Inches from Injector	75
18	Deposition Conditions for Thermal Stress Specimen Coating Runs	83
19	Coating Characterization Data for Thermal Stress Specimens	84

LIST OF ILLUSTRATIONS (Continued)

Table		Page
20	Coating Deposition Conditions for Erosion Test Specimen Deposition Runs	100
21	Coating Characterization Data for Erosion Test Specimens	101
22	Description of Various PG/SiC Coating Microstructural Groups	112
23	Summary of General Atomic Results	121

SECTION I

INTRODUCTION

When silicon carbide (SiC) is codeposited with pyrolytic graphite (PG) under appropriate conditions, the carbide appears as a discrete separate phase in the form of well defined aciculae which are more or less evenly dispersed through the PG phase. The aciculae or needles tend to orient in the growth direction, and in so doing, they reinforce the PG primarily in its weaker C-direction. Compared to PG, the codeposit possesses higher strength and lower anisotropy.

The mechanical properties of PG/SiC codeposits can be adjusted by varying the structure and amount of the carbide. Hence, the material can be tailored to achieve structural compatibility with various substrate materials.

Homogeneous coatings which contained from ~10 to ~20 weight percent (w/o) SiC deposited on fine grained bulk graphites (primarily ATJ) have exhibited acceptable structural performance in several rocket firings. The erosion rate of the material is higher than that of pure PG, however, when exposed to modern high temperature rocket environments.

The program described herein addresses the matter of improving the erosion resistance of PG/SiC codeposits. The approach involves deposition of a coating with a SiC concentration gradient through its thickness, i.e., a graded coating. This concept involves initially depositing a codeposit which contains sufficient SiC to be structurally compatible with the substrate and then decreasing the SiC content as the coating thickens until the last material deposited is pure PG. While several process schemes can be envisioned for depositing graded coatings, two were selected for emphasis during this program, i.e., variation of temperature and variation of methyltrichlorosilane (CH_3SiCl_3 the SiC precursor) flow rate. The first stems from previous observations of the inverse relationship between deposition temperature and SiC content. The second recognizes the direct relationship between CH_3SiCl_3 concentration in the inlet gas mixture and the resultant SiC content of the coating.

The overall objectives of this program were to develop a subscale process for depositing graded coatings, to evaluate methods for characterizing the coatings and to fabricate test specimens coated with both graded and homogeneous low SiC content codeposits. This report describes the work done to accomplish these objectives. Deposition experiments, conducted to establish the dependence of coating characteristics on temperature and gas composition are discussed in Section III. Section IV describes the runs conducted to fabricate thermal stress, erosion and physical property test specimens. Procedures and techniques used to characterize the coatings are described in Section V. Conclusions and recommendations are summarized in Section VI.

SECTION II

SUMMARY

This report describes an exploratory program conducted to develop a subscale process for depositing graded PG/SiC coatings. The major elements of the program were: (1) experimental deposition runs to establish the relationships between selected process conditions and coating composition and structure, (2) fabrication deposition runs to produce samples for test purposes, and (3) materials characterization.

The experimental run series was oriented toward establishing the independent effects of deposition temperature and CH_3SiCl_3 flow rate. The experiments involved deposition on the inside surface of cylindrical substrates contained in a resistively heated tubular furnace. Gases were introduced at the centerline of the substrate through a single port injector. Several homogeneous coatings were produced which contained from 0 to ~20 w/o SiC. Correlations of SiC content, rate, and density with temperature and CH_3SiCl_3 flow rate were derived from the results of these runs.

The fabrication runs produced specimens for erosion and thermal stress tests and yielded material for physical property measurements. Conditions for these runs were selected on the basis of the correlations established from the results of the experimental runs.

The coatings were characterized with respect to SiC content and microstructure. Various techniques were considered for determining SiC content and electron microprobe analysis was ultimately selected for routine analyses. Coating microstructures were determined primarily by optical microscopy.

The major conclusions of this program are: (1) PG/SiC graded coatings can be deposited by scheduled variation of deposition temperature or CH_3SiCl_3 flow rate, (2) when deposited by either single-variable method, the coating microstructure changes as the coating thickens, and (3) in a PG/SiC codeposit, the PG matrix density increases with deposition temperature.

SECTION III

DEPOSITION EXPERIMENTS

1. OBJECTIVE AND APPROACH

The objective of the experimental deposition series was to determine the independent effects of temperature and gas composition on silicon carbide concentration and microstructure. A series of runs were conducted in which multiple layers of coating were applied to cylindrical substrates, each layer involving a different deposition temperature or CH_3SiCl_3 concentration in the process gas.

2. APPARATUS

Deposition runs were conducted in a 6-inch tubular resistance furnace manufactured by the Pereny Corporation. The furnace was modified, at ARC, by installing an angular sight port which penetrates the deposition chamber at the aft end and views the coating surface during deposition. This procedure allowed continuous and accurate monitoring of the coating surface temperature throughout the deposition cycle.

The deposition gases were introduced into the deposition chamber through a water-cooled multiple-walled injector as shown in Figure 1.

Most of the carrier nitrogen was introduced through the injector. A small amount of nitrogen was introduced through the annular area between the drive shaft and the injector to keep the process gases from depositing material on the injector centering device which would cause binding and prevent rotation of the canister. (See Figure 3 for example.)

The canister and substrate were rotated continuously during deposition at 4 rpm to eliminate the effects of slight injector misalignments.

The CH_3SiCl_3 was stored in a 5-gallon pressurized stainless steel reservoir and controlled in the liquid phase using a standard Fischer and Porter rotameter. After leaving the rotameter the liquid CH_3SiCl_3 entered a heated (120 to 160°F) stainless steel plenum where it vaporized and mixed with the carrier nitrogen and methane before entry into the deposition furnace. A diagram of the CH_3SiCl_3 delivery system is shown in Figure 2.

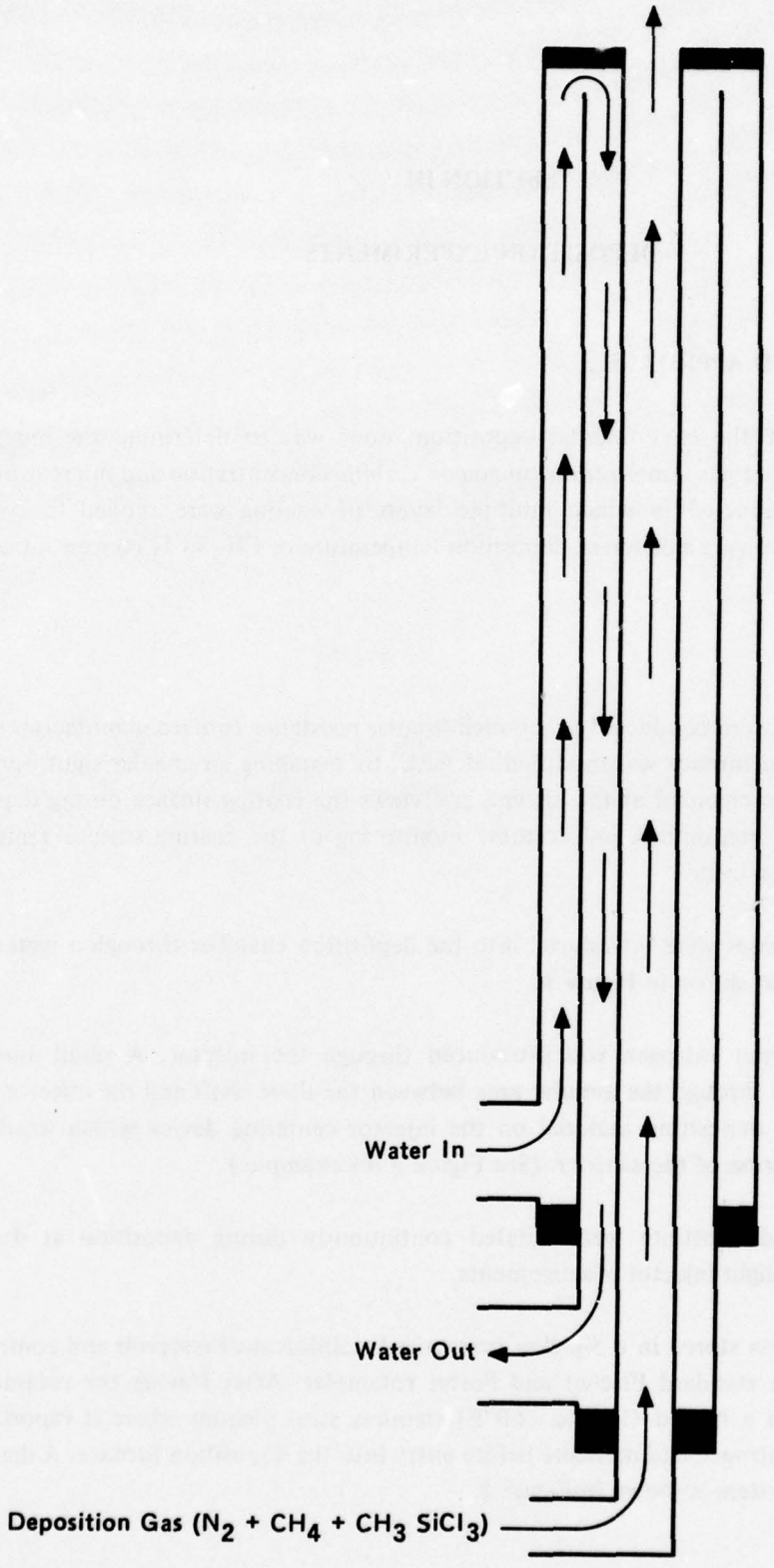

Figure 1. Water-Cooled Injector (0.310 inch bore).

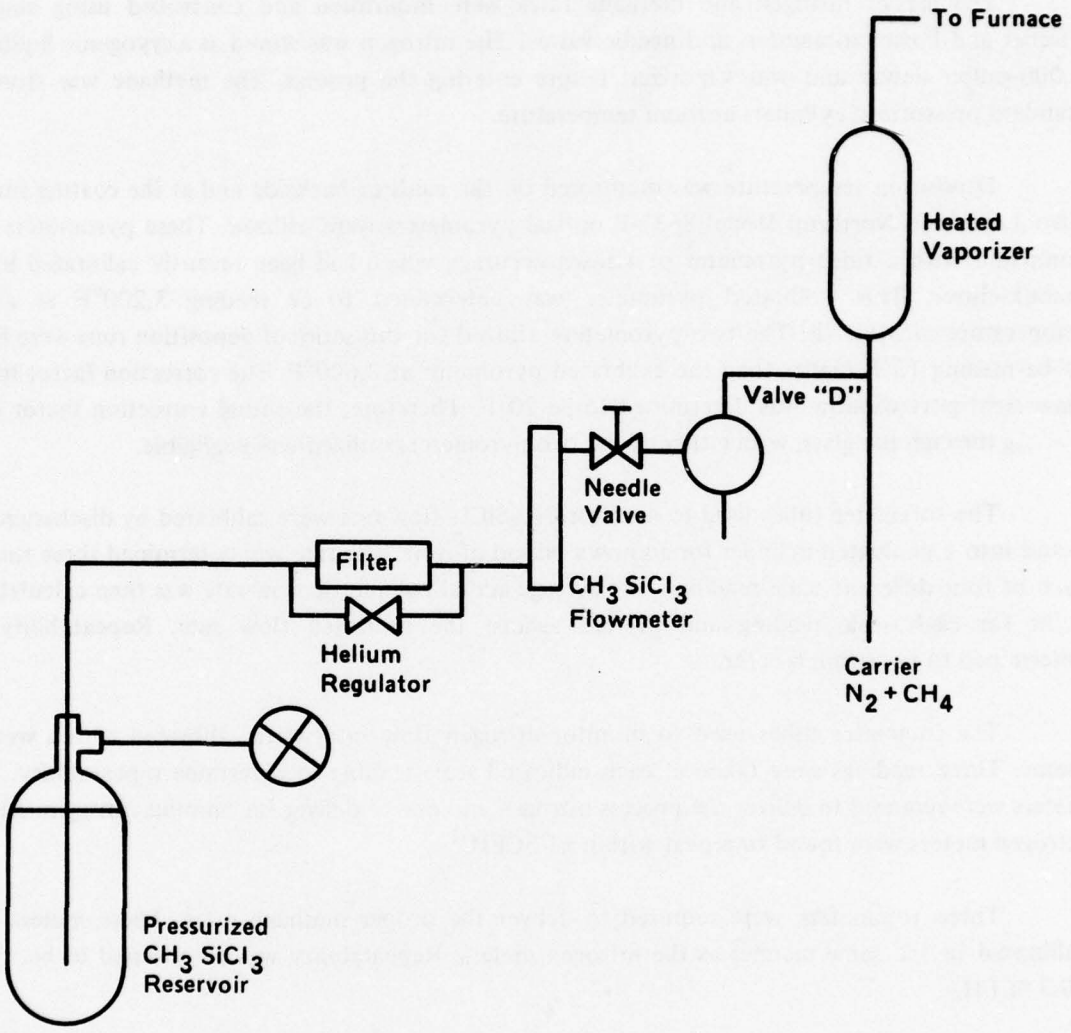

Figure 2. CH_3SiCl_3 Delivery System.

The carrier nitrogen and methane rates were monitored and controlled using standard Fischer and Porter rotameters and needle valves. The nitrogen was stored as a cryogenic liquid in a 2,000-gallon dewar and was vaporized before entering the process. The methane was stored in standard pressurized cylinders at room temperature.

Deposition temperature was monitored on the canister backside and at the coating surface. Two Leeds and Northrup Model 8632-F optical pyrometers were utilized. These pyrometers were compared with a third pyrometer of known accuracy which had been recently calibrated by the manufacturer. This calibrated pyrometer was determined to be reading 3,200°F at a true temperature of 3,[illegible] F. The two pyrometers utilized for this series of deposition runs were found to be reading 15°F higher than the calibrated pyrometer at 3,600°F. The correction factor for the glass sight port window was determined to be 20°F. Therefore, the actual correction factor when [illegible]ng through the glass, with either of the two pyrometers utilized was negligible.

The rotameter tubes used to monitor CH_3SiCl_3 flow rate were calibrated by discharging the liquid into a graduated cylinder for a known period of time. The rate was determined three times at each of four different scale readings. The average actual volumetric flow rate was then calculated in cc/hr for each scale reading and plotted against the indicated flow rate. Repeatability was determined to be within 6 cc/hr.

The rotameter tubes used to monitor nitrogen flow rates were calibrated with a wet test meter. Three readings were taken at each indicated scale reading to determine repeatability. Four meters were required to deliver the process nitrogen and one to deliver the annulus nitrogen. All five nitrogen meters were found to repeat within ±1 SCFH.[1]

Three rotameters were required to deliver the proper methane rates. These meters were calibrated in the same manner as the nitrogen meters. Repeatability was determined to be within ±0.3 SCFH.

The delivery pressure for the nitrogen and methane was 50 psig in all cases. All line pressure gauges were calibrated with a Heise test gauge and found to be accurate within ±1 psig.

3. EXPERIMENTAL RUNS

Seven deposition runs were conducted to investigate the effects of flow, temperature and CH_3SiCl_3 concentration on the coating composition and morphology.

---

[1]SCFH, Standard Cubic Feet per Hour.

Runs 002-81, 002-85, 006-1, 006-3, 006-8 and 006-18 utilized tubular HLM graphite substrates 3.5 inches I.D. by 15.5 inches long. The basic deposition configuration was the same in all six runs and is shown in Figure 3.

Run 006-10 utilized a tubular ATJ graphite substrate 2.16 inches I.D. by 1.0 inch long. The deposition configuration is shown in Figure 4.

Multilayered coatings were deposited in those runs conducted to investigate the effects of temperature and CH_3SiCl_3 concentration. Each layer was of a different composition and was separated by a thin layer of unalloyed pyrolytic graphite so the codeposited layers could be distinguished. This procedure permitted the investigation of several parameters with a minimum of deposition runs.

a. Flow Characterization

One deposition run, 002-85, was conducted to investigate the conditions which exist within the core of the deposition chamber as well as those at the walls. To accomplish this, five 0.25-inch-diameter pins were installed radially in the substrate tube at 3-, 7-, 11-, 13- and 15-inch intervals from the injector. The substrate tube was not rotated so the effect of injector misalignment on coating deposition rate could be determined. Deposition conditions are shown in Table 1.

The target coating was 100/150 mils in thickness with a 15 w/o SiC concentration. At the temperature measuring position, 13 inches from the injector, the average coating thickness was 120 mils and the SiC concentration[1] was estimated to be 11 w/o, after deposition.

The coating microstructure, achieved during this run, is shown in Figure 5. This microstructure is typical of a 10 to 30 w/o SiC containing PG coating deposited at 3,200°F. The SiC can be seen as bright acicular needles growing more-or-less normal to the AB plane of the PG matrix. Notice how the SiC concentration and crystal size increase near the PG cone boundaries. This phenomenon is highly temperature dependent. Above 3,200°F all or nearly all of the SiC phase concentrates in the cone boundaries as large needles and crystalline growths. Below 3,200°F the SiC crystal size decreases markedly and the dispersion appears to become uniform below 3,100°F. Figure 5 was taken at the coating temperature measuring position. In most cases photomicrographs and other coating characterization data were obtained from the temperature measuring position to assure that the data represent coating fabricated at the desired deposition temperature.

---

[1]Estimated SiC concentration derived from Figure 96 and assumes a PG matrix density of 2.14 g/cc.

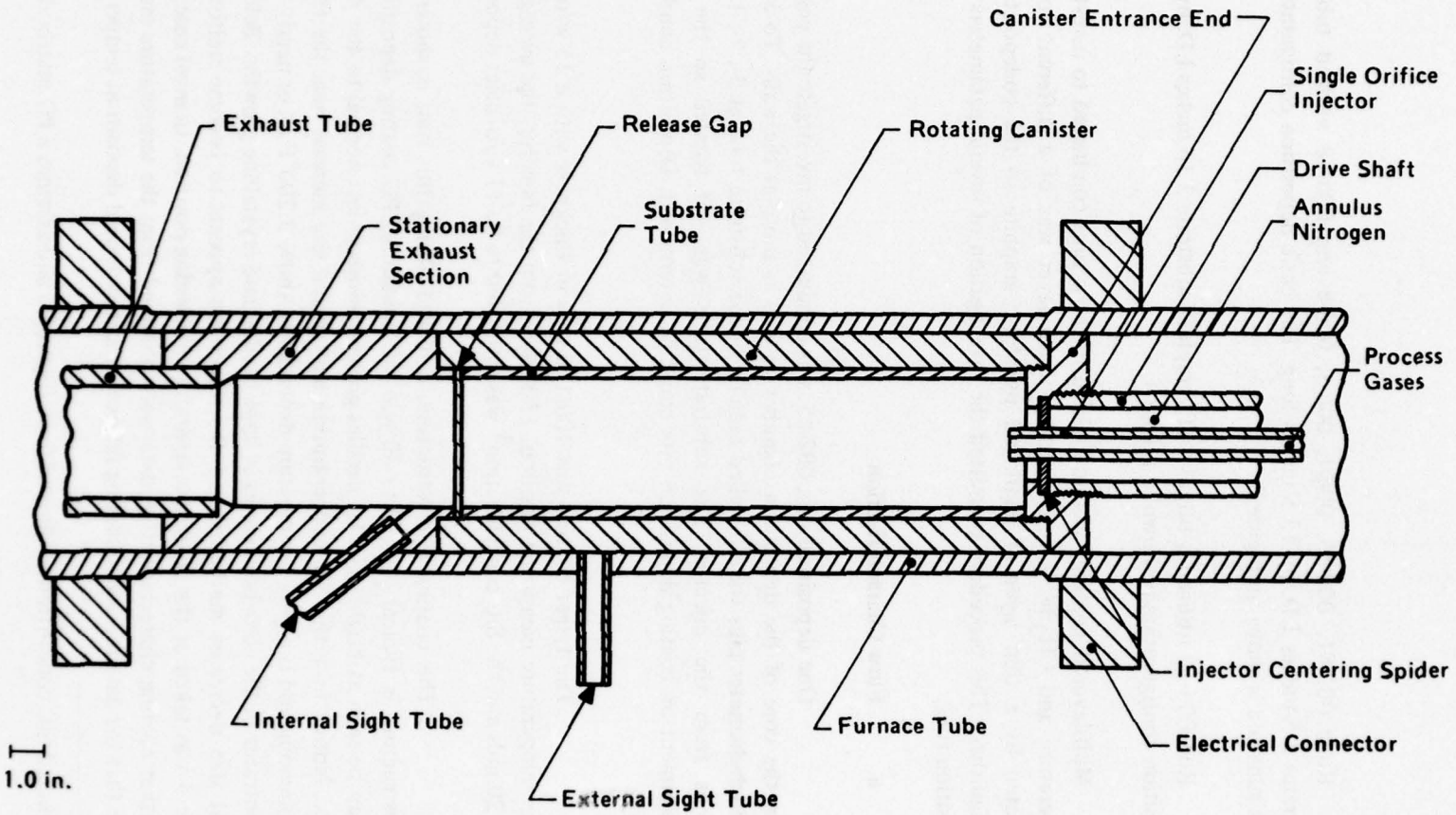

Figure 3. 3.5-inch Tubular Deposition Assembly.

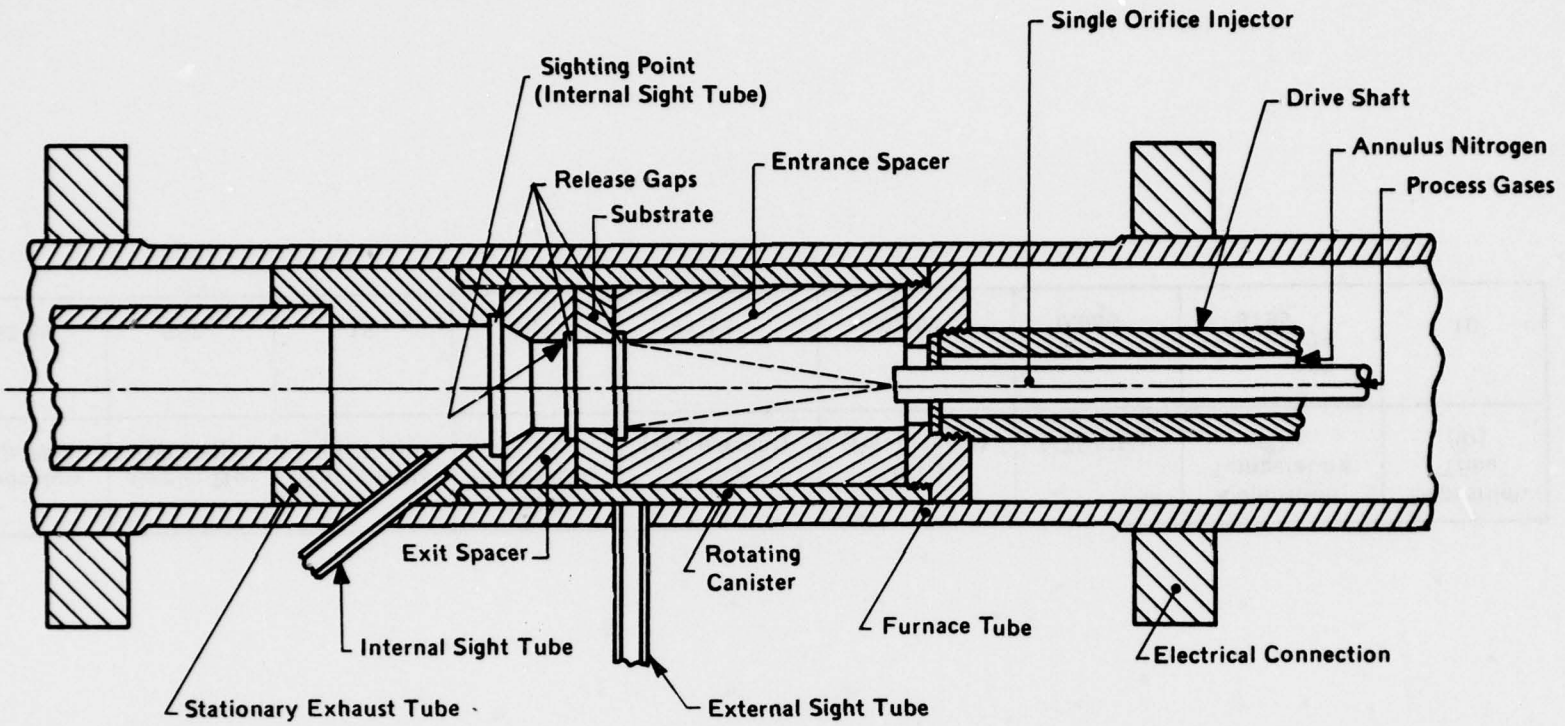

Figure 4. 2.0-inch Tubular Deposition Assembly.

Table 1. Deposition Conditions for Run 002-85.

Deposition Run No.	Carrier N_2 (SCFH)	Annulus N_2 (SCFH)	Total Process Gas (SCFH)	CH_4 (vol. percent)	MTS (vol. percent)	MTS/CH_4	Deposition Temperature ($^{\circ}F$)	Deposition Time (hr)
002-85	953	15	981	1.19	0.102	0.086	3195^{+45}_{-75}	10

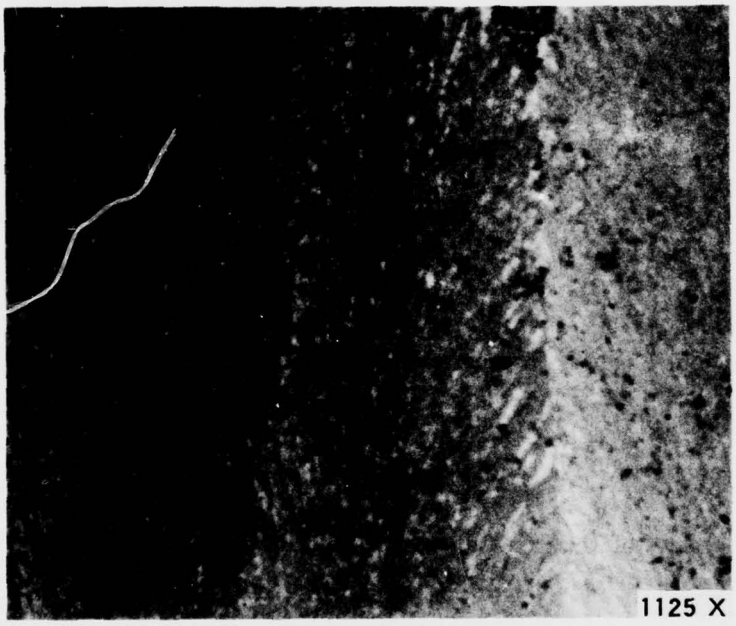

Figure 5. Run 002-85 Coating Microstructure 13 Inches From Injector.

Post-deposition examination was conducted by sectioning the substrate tube radially 3, 7, 10, 13 and 15 inches from the injector. See Table 2. The "15"-inch pin was sectioned radially at six positions to determine its coating thickness and density. These data are shown in Figure 6. The other four pins were examined visually to determine the approximate flow pattern of the deposition gas stream.

The circumferential variation in tube wall coating thickness, caused by injector misalignment, is shown in Table 3. As can be seen, this variation is minimal at the forward and midsections and rather severe at the exhaust end of the coating. Tube wall coating densities were obtained at the zero degree position only so the circumferential variation in tube wall density could not be determined. Some measure of this variation was evident in the data obtained in examining the coating from the "15"-inch pin. (Figure 6) The coating thickness and density were greatest on the upstream side of the "15"-inch pin. The overall density and coating thickness of the pin were both much higher than that of the coating on the tube wall in the same plane. The average coating thickness on the other four pins declined steadily as the distance to the injector declined. The coating thickness of the pins tended to increase at the ends. This effect was especially pronounced on the two pins nearest to the injector. The reduction in average thickness is believed to be the result of reduced gas stream and substrate temperature nearer the injector. The increased coating thickness at the ends of the pins indicate that these areas were being heated by the substrate walls and were, therefore, much higher in temperature than the center portions. The 7-inch pin contained a nodular growth about 1/2-inch long by 3/16-inch wide by 3/16-inch thick at the center, on the upstream side. This growth was hard and of low density. It appears to be analogous to those which often occur on the centerbody in large diameter deposition runs.

The results of this run indicated that some assymmetry existed in the flow field which was probably related to injector/substrate misalignment. Therefore, substrate rotation was utilized in subsequent runs to eliminate circumferential variations in coating thickness and SiC concentration.

b. Effect of Temperature

Two deposition runs, 006-1 and 006-3, were conducted to investigate the effect of deposition temperature on the composition and microstructure of codeposited coatings applied to a nominal 3.5-inch I.D. cylindrical substrate.

Five layers of coating were applied during each run. Nominal deposition temperatures were 3,000, 3,200, 3,400, 3,600 and 3,800°F. Each codeposited layer was separated by a thin layer of unalloyed pyrolytic graphite.

Table 2. Coating Characterization Data for Run 002-85.

Inches from Injector	1	2	3	4	5	6	7	8	9	10	11	12	13	14	15	Comments
002-85 Density (g/cc)	—	—	2.28	—	—	—	2.31	—	—	2.29	—	—	2.22	—	2.18	No rotation. 1/4-in. diameter pins installed in substrate tube, across diameter, at 3, 7, 11, 13, and 15 inch positions.

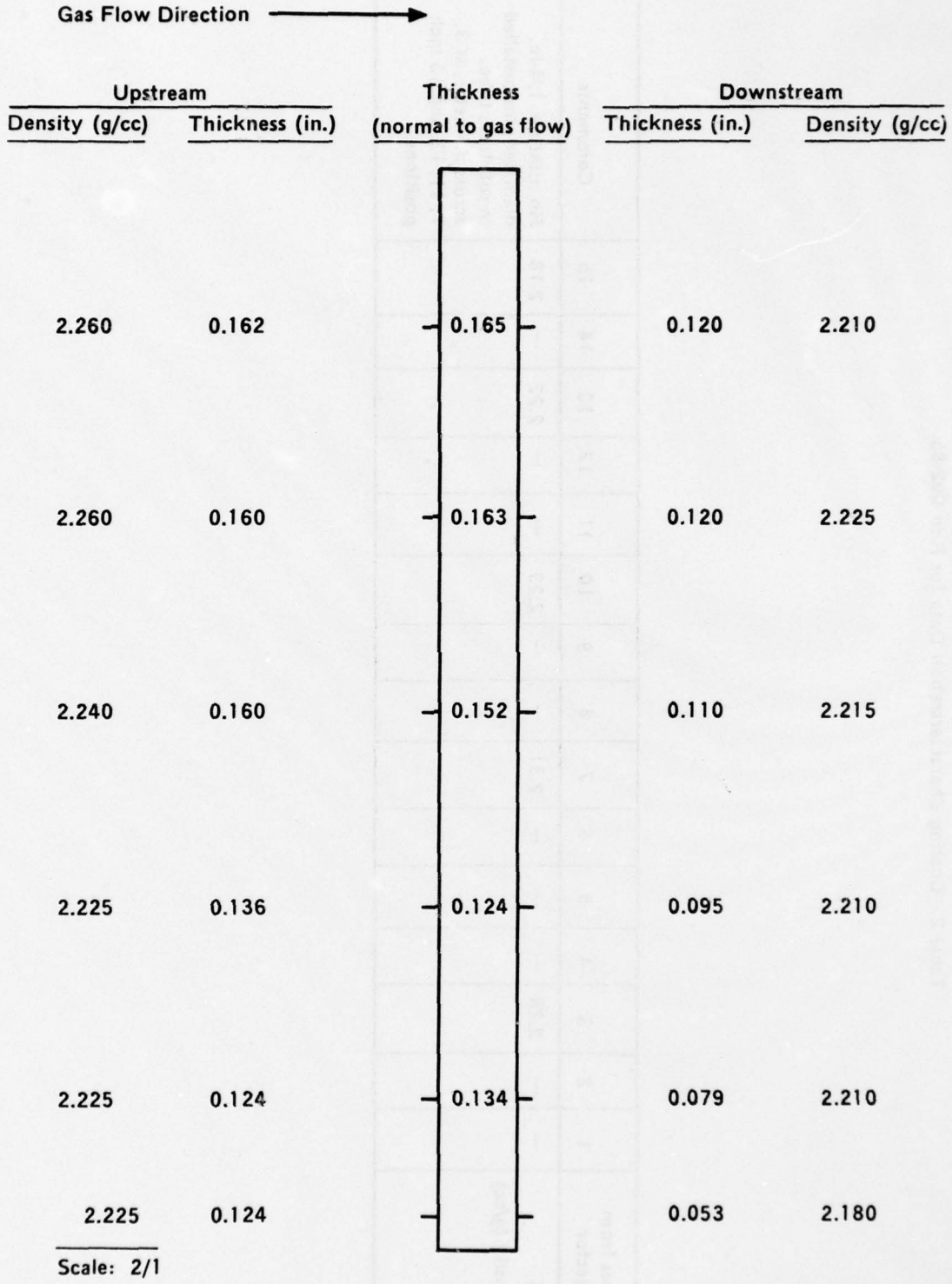

Figure 6. Coating Thickness and Density Profiles of Pin Located 15 Inches From Injector. Run No. 002-85.

Table 3. Circumferential Coating Thickness Variation of Tube Wall Coating of Run 002-85.

Inches from Injector		3	7	10	13	15
Mils of Coating at–	0°	80	98	106	106	70
	90°	73	95	110	120	80
	180°	70	96	110	140	110
	270°	68	93	114	114	94

Deposition conditions for 006-1 and 006-3 are shown in Tables 4 and 5.

Deposition temperature was monitored on the coating surface 13 inches from the injector during both runs. Temperature was controlled automatically on the canister backside at a location approximately 12 inches from the injector. Continuous upward adjustments in the controller set point were necessary to maintain a constant surface temperature as the coating thickness and, therefore, the thermal gradient between the coating surface and the canister backside increased. Deposition was initiated at a temperature somewhat higher than the desired deposition temperature to compensate for the reaction endotherm at the coating surface. The coating surface deposition temperature control was acceptable throughout 006-1. Temperature control was somewhat erratic during the fifth case (3,800°F) of 006-3 when the controller failed and manual control became necessary.

After Run 006-1, the graphite deposition fixturing showed some evidence of oxidation near the injector tip. It was felt that the existence of small amounts of oxygen in the deposition gas would probably alter the deposition rate and the properties of the coating. Prior to 006-3, a repeat of 006-1, the deposition fixturing was thoroughly examined for potential leaks and a new injector air seal was installed. Although no water leaks could be detected in the injector, a new one was fabricated to eliminate this possibility. The fixturing for 006-3 was then assembled and the furnace heated to deposition temperature. Nitrogen was introduced into the assembly at nominal deposition flow rates, and samples were withdrawn from the exhaust pipe using a Drager tube. Carbon monoxide content was measured to indicate the amount of oxygen present as the result of either water or air entering the deposition chamber. At nominal deposition nitrogen flow rates, the CO concentration was less than 7 ppm. The fixturing was disassembled after this test and examined for evidence of oxidation. None was present. The fixturing was then reassembled and run 006-3 conducted.

Post-deposition examination of Runs 006-1 and 006-3 was conducted on specimens fabricated by slicing a 1-inch-wide axial section the length of each tube. The five coating layers were separated and examined at 1-inch increments from the injector tip. Coating density, thickness and, in a few cases, microstructures were determined for each position in each layer. Coating characterization data are shown in Tables 6 and 7. The microstructure groups referred to on these and subsequent tables were derived during past programs and are described in Section V, pages 111 through 118. Electron microprobe traces of all five layers of 006-3 were taken at the 13-inch position, and these are shown in Figures 7 through 11.

Table 4. Deposition Conditions for Run 006-1.

Deposition Run No.	Carrier N_2 (SCFH)	Annulus N_2 (SCFH)	Total Process Gas (SCFH)	CH_4 (vol. percent)	MTS (vol. percent)	MTS/CH_4	Deposition Temperature[a] (°F)	Deposition Time (hr)	Comments
006-1 (3000°F)	953	15	981	1.19	0.085	0.071	3005^{+25}_{-05}	5	
006-1 (3200°F)	953	15	981	1.19	0.085	0.071	3180^{+40}_{-20}	5	Injector centering spider broke loose, passed through deposition chamber and lodged at exit end of subs. tube
006-1 (3400°F)	953	15	981	1.19	0.085	0.071	3365^{+35}_{-35}	5	
006-1 (3600°F)	953	15	981	1.19	0.085	0.071	3590^{+70}_{-20}	5	Deposition started and then stopped after 1/2 hour because of temperature control difficulties. A second PG precoat was applied and deposition started over.
006-1 (3800°F)	953	15	981	1.19	0.085	0.071	3810^{+50}_{-30}	5	

[a]Average coating surface temperature 13 inches from injector. No sight glass correction.

Table 5. Deposition Conditions for Run 006-3.

Deposition Run No.	Carrier N_2 (SCFH)	Annulus N_2 (SCFH)	Total Process Gas (SCFH)	CH_4 (vol. percent)	MTS (vol. percent)	MTS/CH_4	Deposition Temperature[a] (°F)	Deposition Time (hr)	Comments
006-3 (3000°F)	953	15	981	1.19	0.085	0.071	3010^{+45}_{-0}	5	
006-3 (3200°F)	953	15	981	1.19	0.085	0.071	3194^{+55}_{-05}	5	
006-3 (3400°F)	953	15	981	1.19	0.085	0.071	3395^{+55}_{-15}	5	
006-3 (3600°F)	953	15	981	1.19	0.085	0.071	3600^{+60}_{-60}	5	Controller malfunctioned making temperature control difficult. Changed to manual control at 4 1/2 hours when temperature dropped to 3540°F.
006-3 (3800°F)	953	15	981	1.19	0.085	0.071	3815^{+145}_{-125}	5	Temperature control erratic throughout run. First hour deposited near 3700°F. Deposition temperature rose to 3900°F at 3 hours and one hour was required to reduce it to 3800°F.

[a]Average coating surface temperature 13 inches from injector. No sight glass correction.

Table 6. Coating Characterization Data for Run 006-1.

Inches from Injector	1	2	3	4	5	6	7	8	9	10	11	12	13	14	15
006-1 (3000°F)															
Density (g/cc)	—	—	—	—	—	2.28	2.30	2.32	2.34	2.34	—	2.32	2.29	2.27	2.27
Thickness (mils)	<10	<10	<10	<10	18	27	19	26	26	25	—	30	34	57	44
Dep. Rate (mils/hr)	—	—	—	—	3.6	5.4	3.8	5.2	5.2	5.0	—	6.0	6.8	11.4	8.8
Microstructure (Grp.)	—	—	—	20	—	—	—	10	—	—	—	10	—	10	—
006-1 (3200°F)															
Density (g/cc)	—	—	—	—	2.25	2.24	2.24	2.25	2.27	2.26	—	2.25	2.24	2.27	2.25
Thickness (mils)	<10	<10	<10	<10	10	27	27	29	33	34	—	54	53	36	18
Dep Rate (mils/hr)	—	—	—	—	2.0	5.4	5.4	5.8	6.6	6.8	—	10.8	10.6	7.1	3.6
Microstructure (Grp.)	—	—	—	10	—	—	—	10	—	—	—	10	—	10	—
006-1 (3400°F)															
Density (g/cc)	2.22	2.23	2.24	2.23	2.23	2.22	2.24	2.24	2.26	2.25	2.26	2.25	2.24	2.23	2.23
Thickness (mils)	16	24	16	19	23	20	25	26	26	25	—	—	—	35	31
Dep Rate (mils/hr)	3.2	4.8	3.2	3.8	4.6	4.0	5.0	5.2	5.2	5.0	—	—	—	7.0	6.2
Microstructure (Grp.)	—	—	—	10	—	—	—	10	—	—	—	10	—	10	—
006-1 (3600°F)															
Density (g/cc)	2.21	2.22	2.24	2.21	2.23	2.20	2.20	2.21	2.21	2.21	2.21	2.25	2.21	2.20	2.20
Thickness (mils)	10	24	18	18	20	46	54	60	70	80	75	81	73	73	86
Dep. Rate (mils/hr)	2.0	4.8	3.6	3.6	4.0	9.2	10.8	12.0	14.0	16.0	15.0	16.2	14.6	14.6	17.2
Microstructure (Grp.)	—	—	—	11	—	—	—	10	—	—	—	10	—	30	—
006-1 (3800°F)															
Density (g/cc)	2.20	2.18	2.18	2.15	2.16	2.15	2.15	2.15	2.15	2.16	2.17	2.15	2.16	2.15	2.15
Thickness (mils)	39	45	61	80	95	86	95	102	130	139	140	142	156	189	165
Dep. Rate (mils/hr)	7.8	9.0	12.2	16.0	19.0	17.2	19.0	20.4	26.0	27.8	28.0	28.4	31.2	37.8	33.0
Microstructure (Grp.)	—	—	—	—	—	—	—	—	—	—	—	—	—	—	—

Table 7. Coating Characterization Data for Run 006-3.

Inches from Injector	1	2	3	4	5	6	7	8	9	10	11	12	13	14	15
006-3 (3000°F)															
Density (g/cc)	—	—	—	2.24	2.28	2.30	2.28	—	2.29	2.32	2.32	2.29	2.27	2.27	—
SiC Concentration(w/o)[a]	—	—	—	—	—	—	—	—	—	—	—	—	18	—	—
Thickness (mils)	<10	<10	<10	21	23	28	29	31	33	36	40	47	49	50	—
Dep. Rate (mils/hr)	—	—	—	4.2	4.6	5.6	5.8	6.2	6.6	7.2	8.0	9.4	9.8	10.0	—
Microstructure (Grp.)	—	—	—	10	—	—	—	40	—	—	—	—	—	40	—
006-3 (3200°F)															
Density (g/cc)	2.27	2.24	2.24	2.24	2.24	2.25	2.25	2.25	2.25	2.25	2.25	2.23	2.24	2.23	—
SiC Concentration(w/o)[a]	—	—	—	—	—	—	—	—	—	—	—	—	10	—	—
Thickness (mils)	18	18	22	30	36	40	43	50	50	54	57	57	61	59	—
Dep. Rate (mils/hr)	3.6	3.6	4.4	6.0	7.2	8.0	8.6	10.0	10.0	10.8	11.4	11.4	12.2	11.8	—
Microstructure (Grp.)	—	10	—	40	—	—	—	10	—	—	—	40	—	11	—
006-3 (3400°F)															
Density (g/cc)	2.22	2.21	2.21	2.21	2.22	2.21	2.21	2.21	2.21	2.21	2.21	2.21	2.21	2.20	2.21
SiC Concentration(w/o)[a]	—	—	—	—	—	—	—	—	—	—	—	—	~0.6	—	—
Thickness (mils)	25	26	31	35	39	45	52	57	65	66	66	69	66	63	56
Dep. Rate (mils/hr)	5.0	5.2	6.2	7.0	7.8	9.0	10.4	11.4	13.0	13.2	13.2	13.8	13.2	12.6	11.2
Microstructure (Grp.)	—	11	—	11	—	—	—	30	—	—	—	—	—	—	—
006-3 (3600°F)															
Density (g/cc)	2.20	2.18	2.20	2.17	2.17	2.16	2.18	2.19	2.19	2.18	2.19	2.19	2.18	2.15	2.18
SiC Concentration(w/o)[a]	—	—	—	—	—	—	—	—	—	—	—	—	0	—	—
Thickness (mils)	25	26	29	37	40	54	64	67	73	75	76	76	77	30[b]	61[b]
Dep. Rate (mils/hr)	5.0	5.2	5.8	7.4	8.0	10.8	12.8	13.4	14.6	15.0	15.2	15.2	15.4	—	—
Microstructure (Grp.)	—	—	—	—	—	—	—	—	—	—	—	—	—	—	—
006-3 (3800°F)															
Density (g/cc)	2.15	2.15	2.15	2.15	2.15	2.15	2.15	2.15	2.15	2.15	2.15	2.15	2.15	2.15	2.15
SiC Concentration(w/o)[a]	—	—	—	—	—	—	—	—	—	—	—	—	0	—	—
Thickness (mils)	25	25	27	30	35	54	63	63	64	69	65	69	68	100[b]	120[b]
Dep. Rate (mils/hr)	5.0	5.0	5.4	6.0	7.0	10.8	12.6	12.6	12.8	13.8	13.0	13.8	13.6	—	—
Microsturcture (Grp.)	—	—	—	—	—	—	—	—	—	—	—	—	—	—	—

[a]Derived from electron microprobe traces.

[b]Coating layers did not separate properly. 3800°F layer contains material from 3600°F layer.

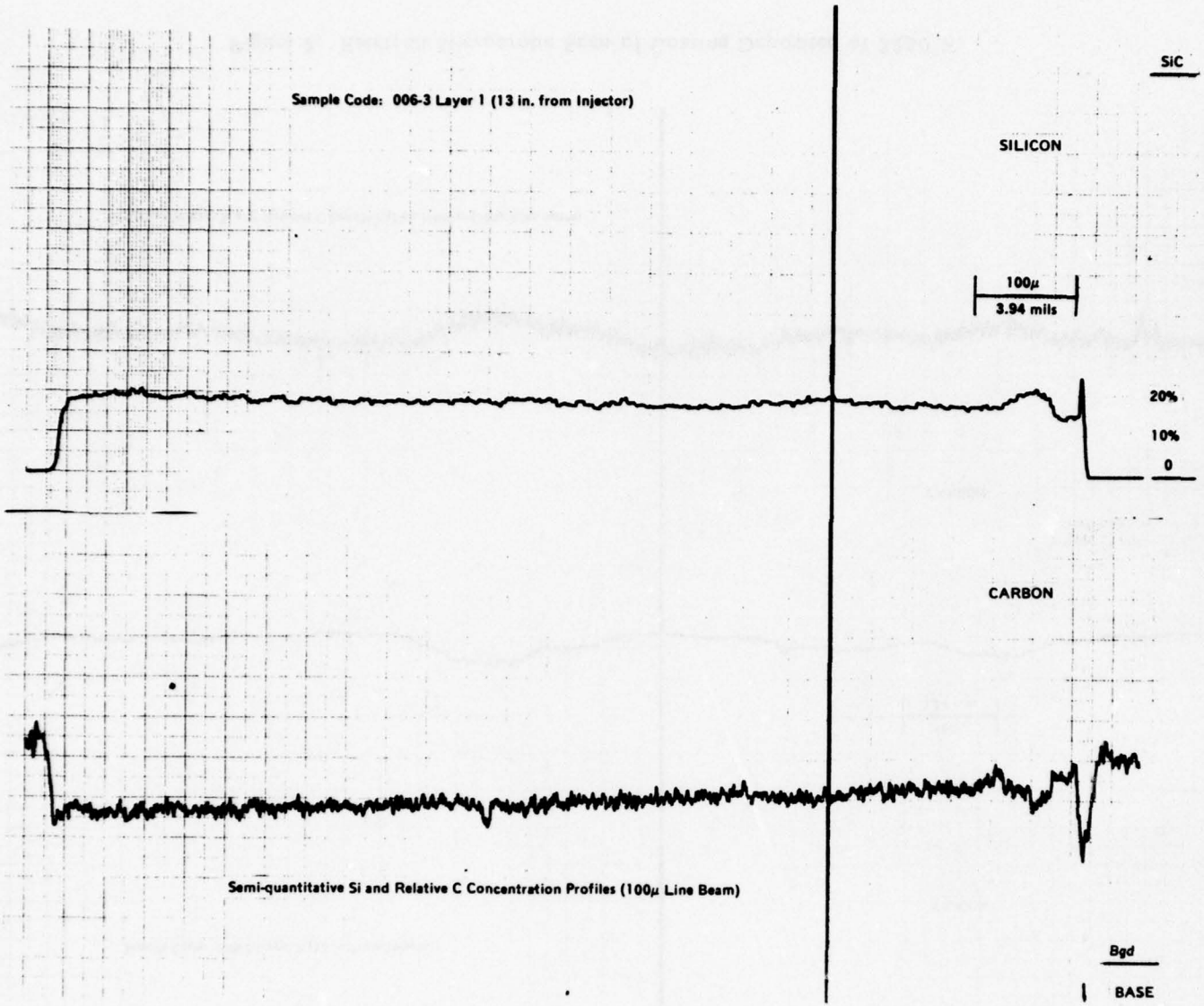

Figure 7. Electron Microprobe Scan of Coating Deposited at 3000°F.

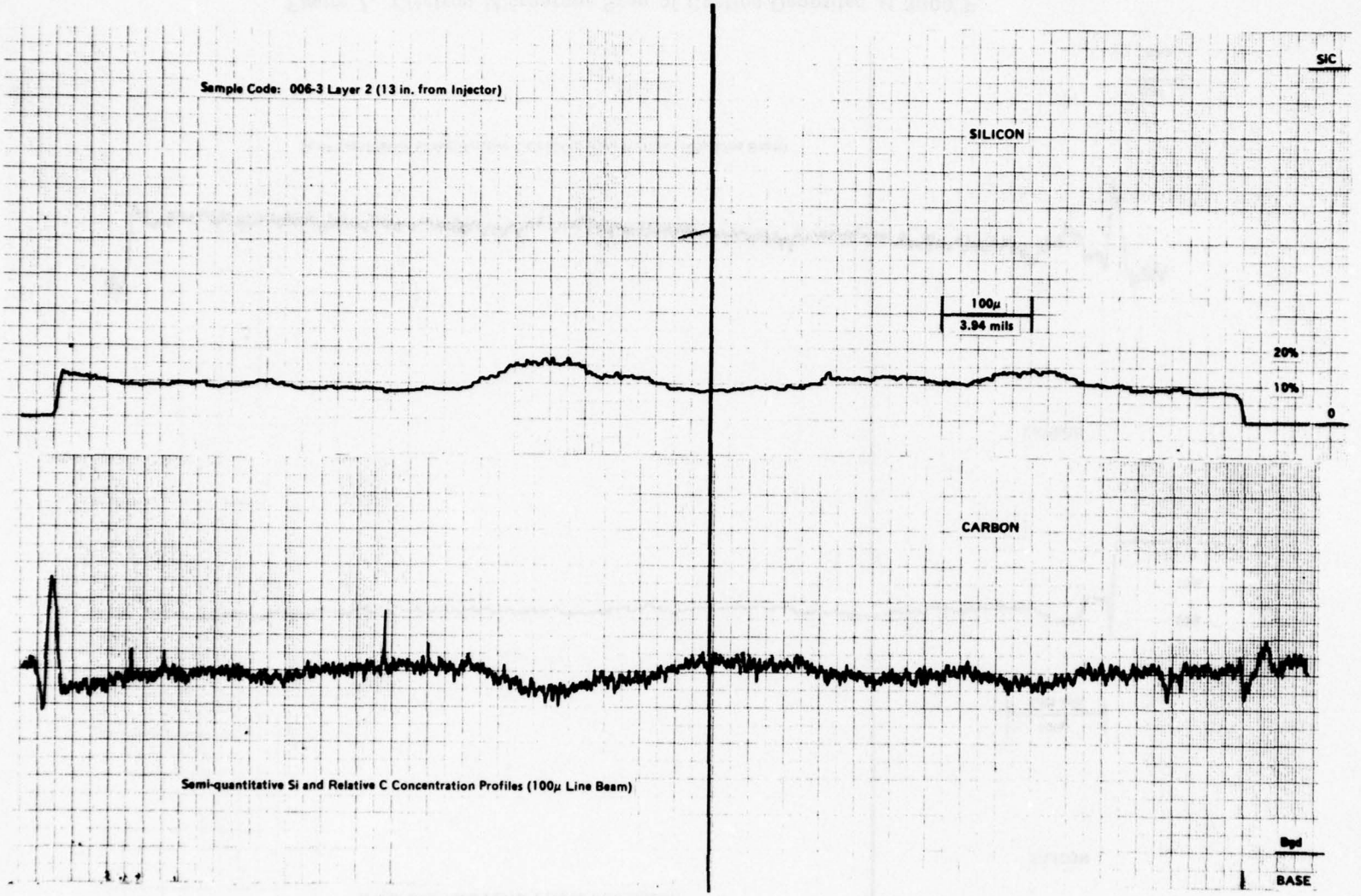

Figure 8. Electron Microprobe Scan of Coating Deposited at 3200°F.

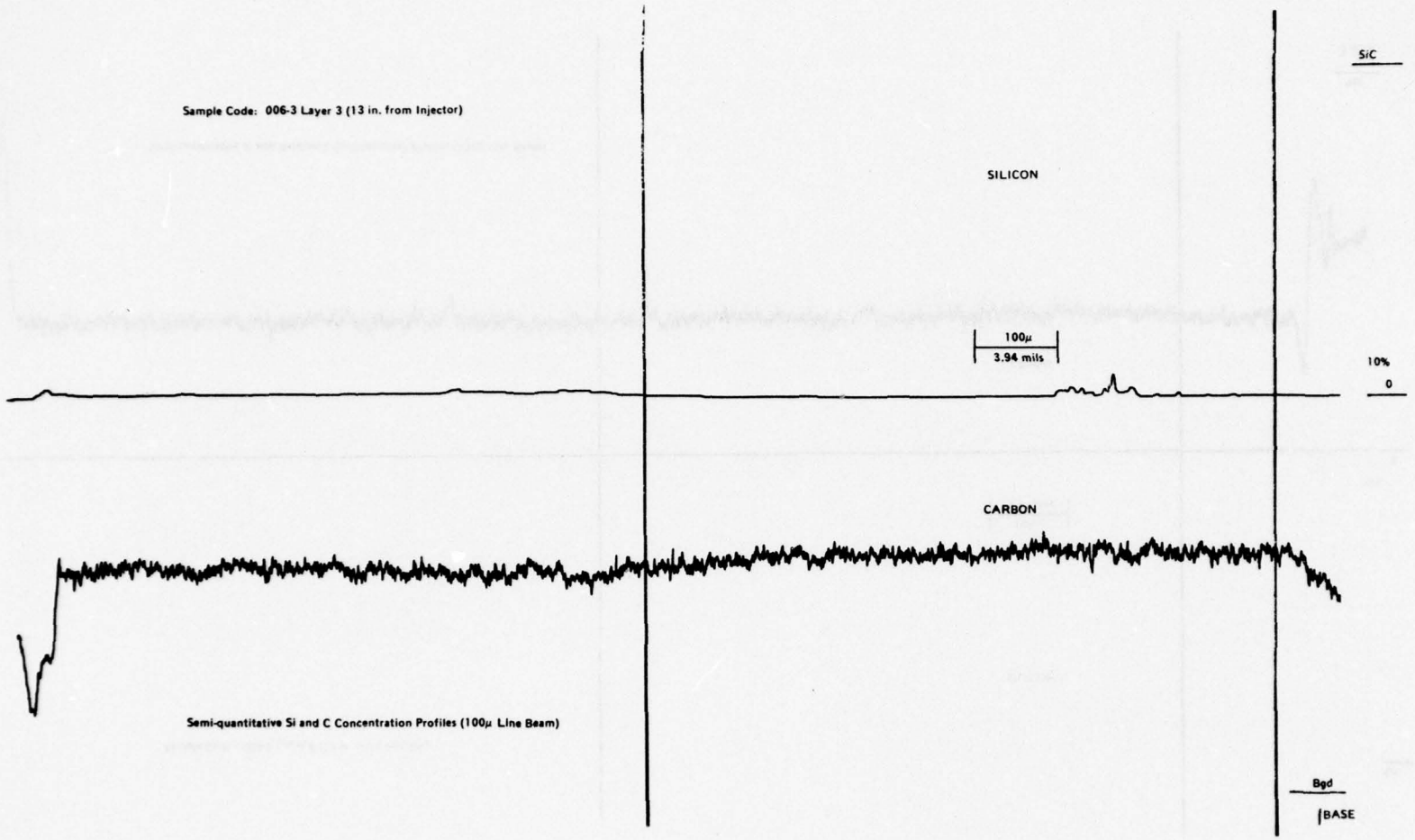

Figure 9. Electron Microprobe Scan of Coating Deposited at 3400°F.

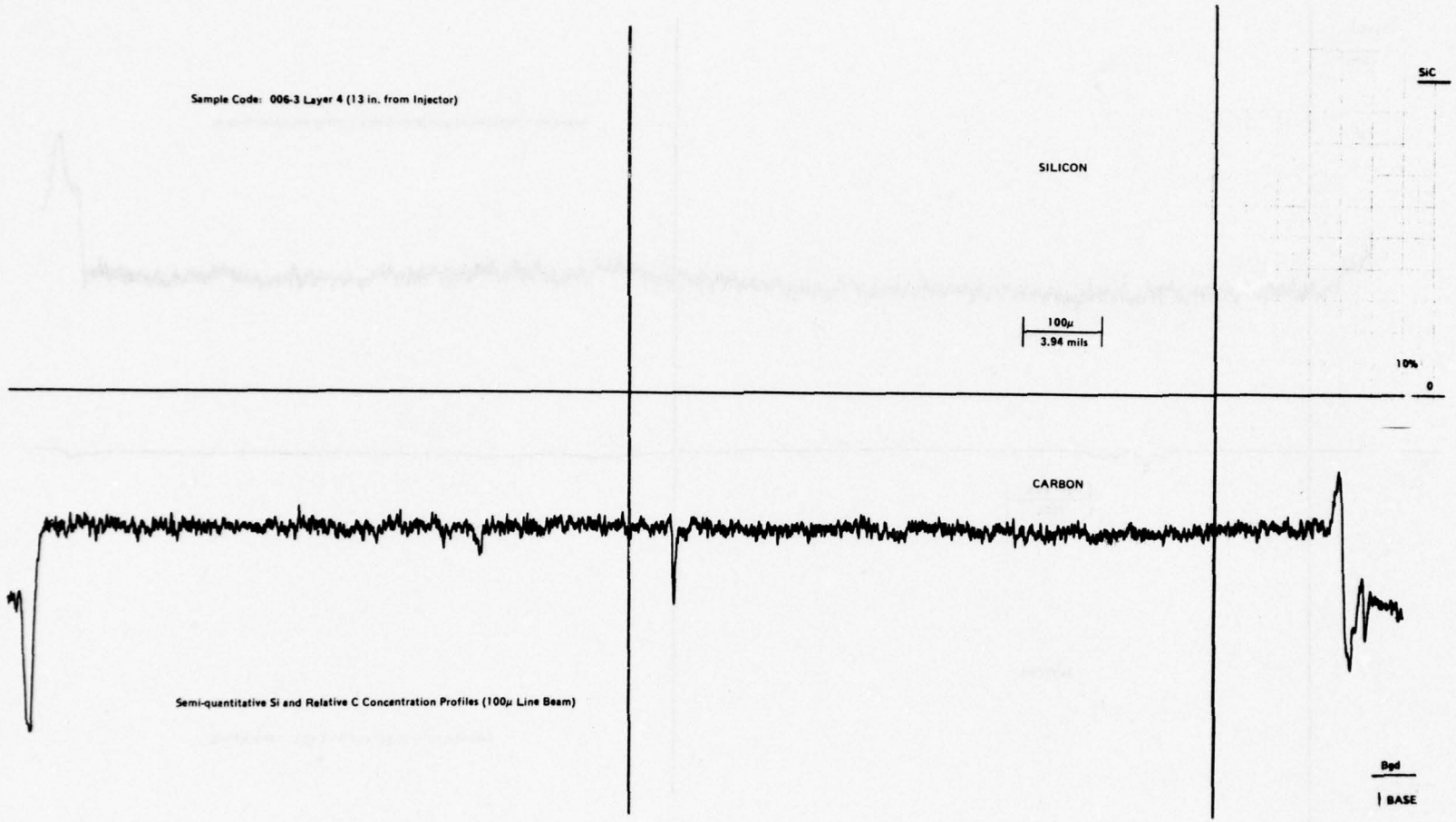

Figure 10. Electron Microprobe Scan of Coating Deposited at 3600°F.

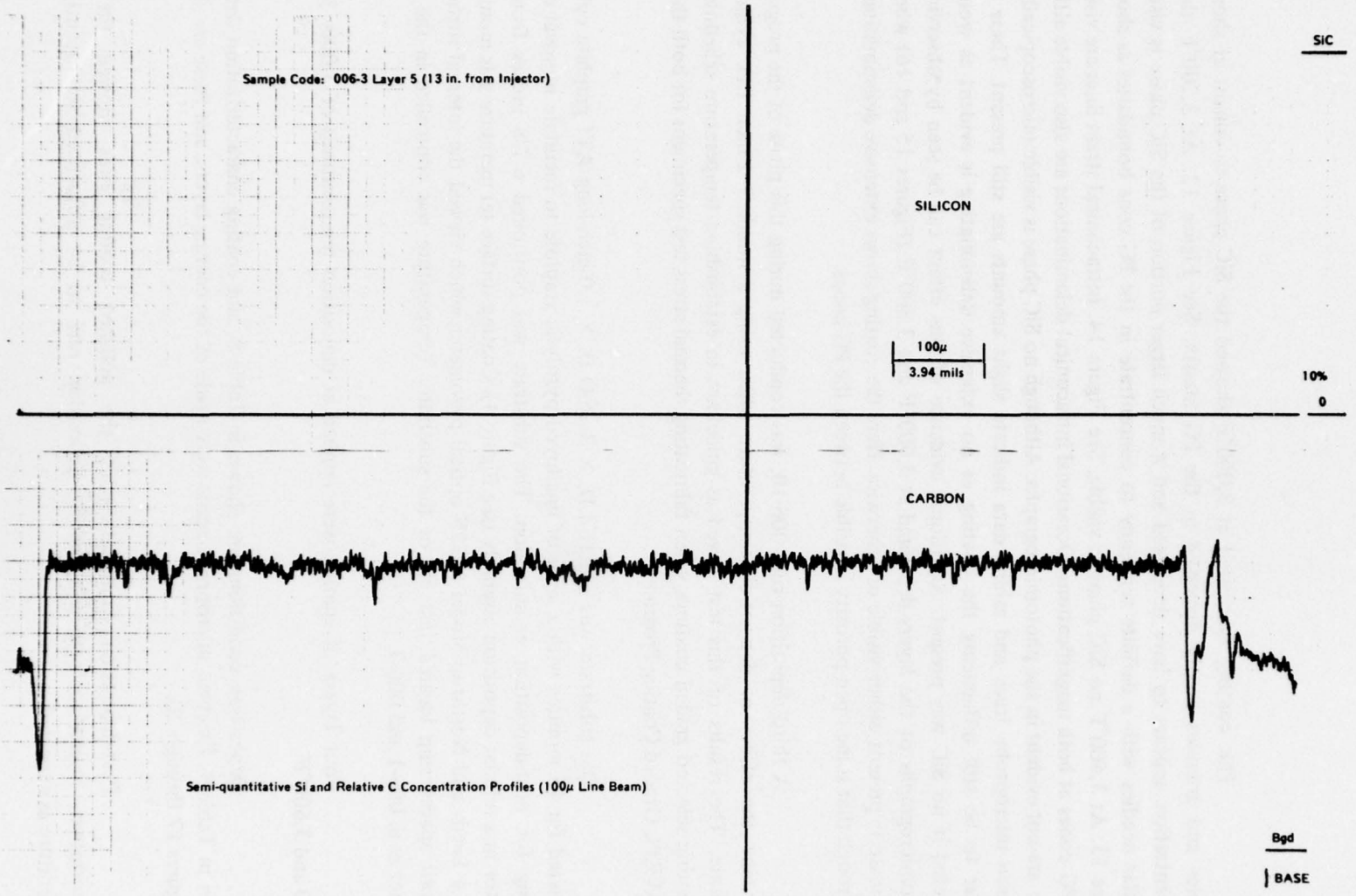

Figure 11. Electron Microprobe Scan of Coating Deposited at 3800°F.

The coating fabricated at 3,000°F showed the SiC phase to consist of short fine needles and granules evenly dispersed in the PG matrix. See Figure 12. At 3,200°F the SiC concentration appears to have decreased and a much larger portion of the SiC phase is visible as acicular needles with a definite tendency to concentrate in the PG cone boundaries as shown in Figure 13. At 3,400°F no SiC phase is visible. See Figure 14. Intraconical strain lines are visible in the PG cones at both magnifications. Occasional intraconical delaminations are also visible although these are not evident in the photomicrographs. Although no SiC phase is visible microscopically, the electron microprobe trace and ashing data indicate slight amounts are still present. These traces appear to be still influencing the coating as no extensive delaminating is evident as would be expected if no SiC was present. Additional evidence of this effect can be seen by observing the photomicrographs of the layers deposited at 3,600°F and 3,800°F (Figures 15 and 16) where no SiC phase is present either visible or otherwise. Here the coating shows extensive delaminations and is so rough that some open porosity is visible between the PG cones.

A third deposition run, 006-10, was conducted during this phase of the program to determine the effect of deposition temperature when using a nominal 2-inch I.D. cylindrical substrate. The results of this test served as guidelines in establishing temperature schedules for depositing selected graded coatings when fabricating thermal stress test specimens for both this and the AFRPL Graded Coating Programs.

The substrate was a 2.16-I.D. X 3.16-O.D. X 1.0-inch-long ATJ graphite cylinder precoated for 15 minutes with a layer of unalloyed pyrolytic graphite to facilitate removal of the coating for post-deposition examination. The substrate was positioned 6 7/8 inches from the injector in a tubular deposition assembly (see Figure 4). Coating surface temperature was monitored with a Leeds and Northrup Model 8632F optical pyrometer which viewed the internal surface of the exit spacer ring located just aft of the substrate. Temperature was controlled in the same manner as in 006-1 and 006-3.

Four layers of coating were applied at deposition temperatures of 3,000, 3,200, 3,400 and 3,600°F.

Deposition conditions are shown in Table 8, and coating characterization data are shown in Table 9. Electron microprobe scans were made of the coating layers, and these are shown in Figures 17 through 20.

Post-deposition examination of the polished coating ends showed the SiC concentration, microstructure, and coating deposition rate to be influenced significantly by temperature as expected.

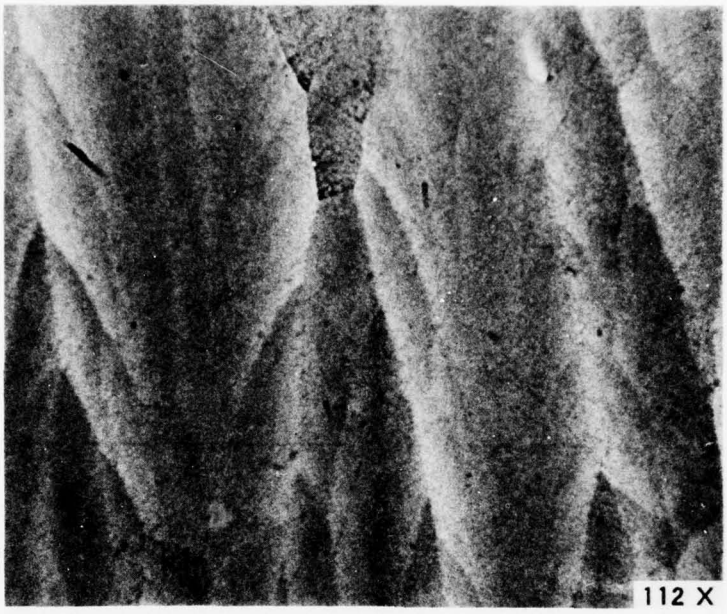

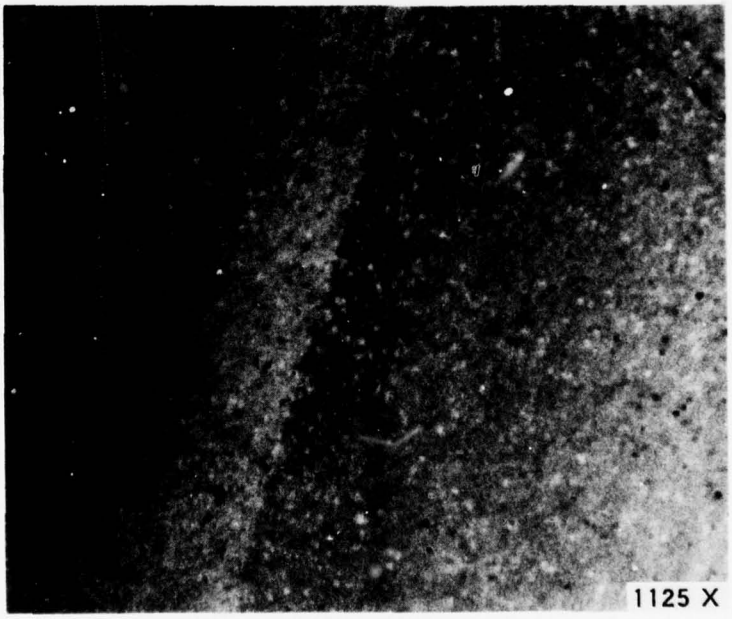

Figure 12. Run 006-3, 3000°F, Coating Microstructure 13 Inches From Injector.

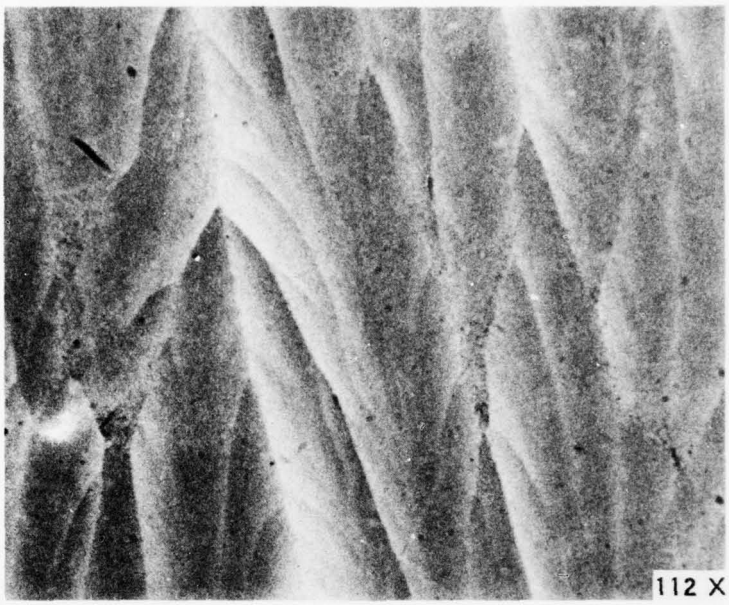

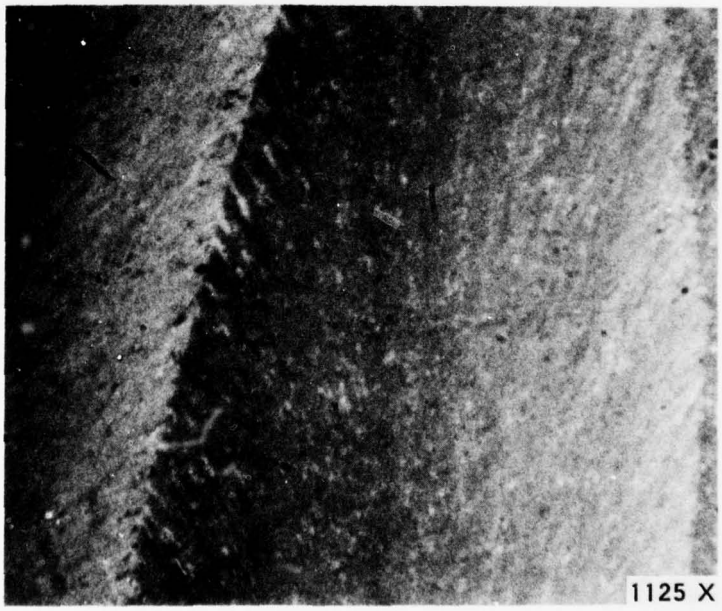

Figure 13. Run 006-3, 3200°F, Coating Microstructure 13 Inches From Injector.

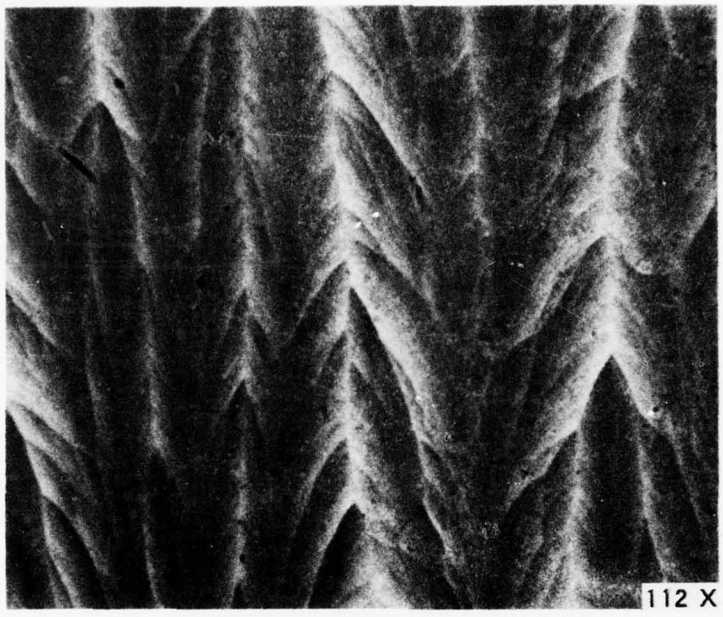

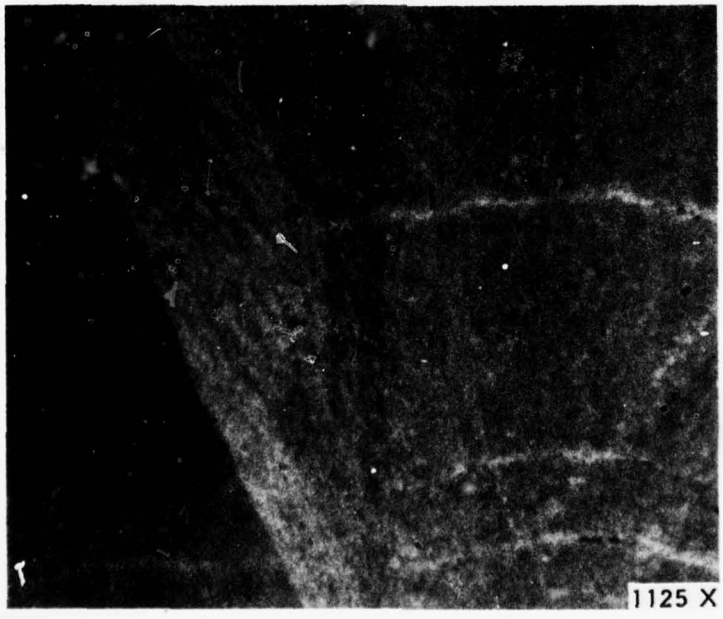

Figure 14. Run 006-3, 3400°F, Coating Microstructure 13 Inches From Injector.

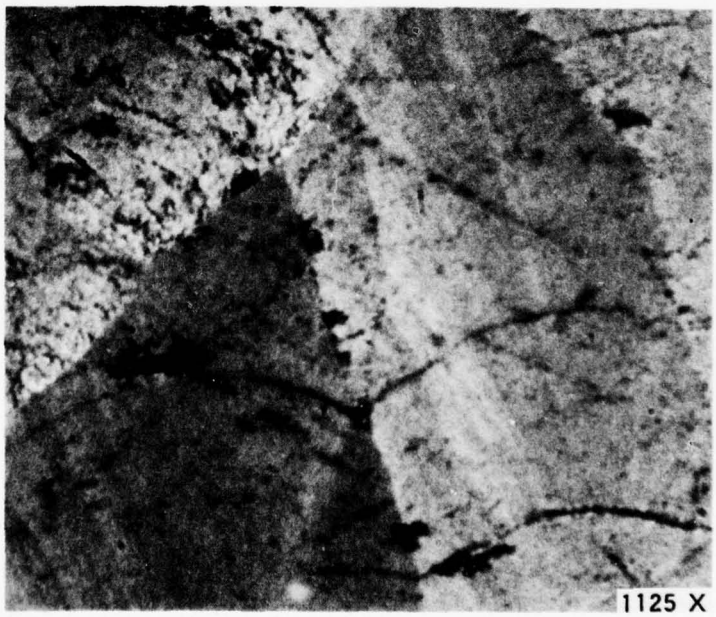

Figure 15. Run 006-3, 3600°F, Coating Microstructure 13 inches From Injector.

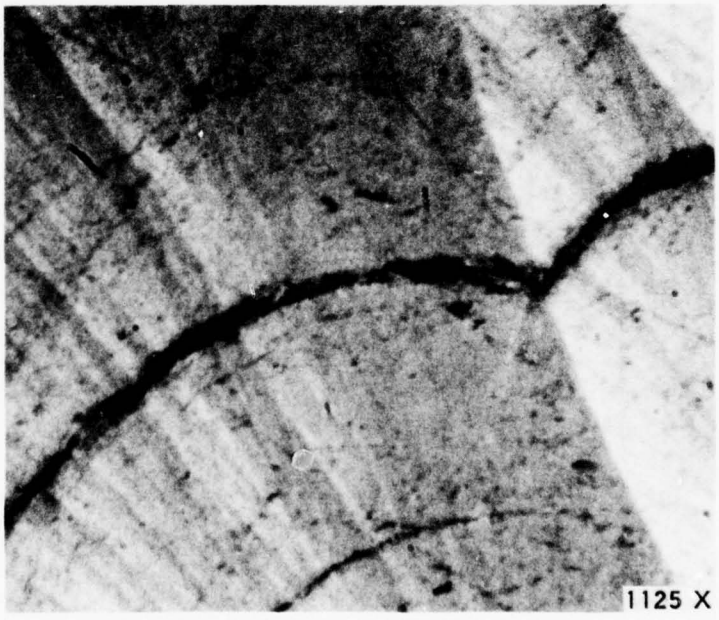

Figure 16. Run 006-3, 3800°F, Coating Microstructure 13 Inches From Injector.

Table 8. Deposition Conditions for Run 006-10.

Layer No.	Carrier N_2 (SCFH)	Annulus N_2 (SCFH)	Process Gas (SCFH)	CH_4 (vol. percent)	MTS (vol. percent)	MTS/CH_4	Deposition Temperature (°F)	Deposition Time (hr)	Comments
1	296	15	315	1.14	0.132	0.116	3005^{+25}_{-15}	3.5	
2	296	15	315	1.14	0.132	0.116	3200^{+20}_{-10}	3.5	
3	296	15	315	1.14	0.132	0.116	3400^{+20}_{-20}	3.5	
4	296[a] 262[b]	15[a] 13[b]	315[a] 279[b]	1.14[a] 1.29[b]	0.132[a] 0.149[b]	0.116[a] 0.116[b]	3610^{+15}_{-25}	3.5	N_2 delivery pressure decreased steadily during last 2 1/4 hours. Final delivery pressure was 36 psig.

[a]Maintained for first 1 1/4 hours of deposition while delivery pressure was 50 psig.

[b]Calculated values at end of cycle when delivery pressure had declined to 36 psig.

Table 9. Coating Data for Run 006-10.

Layer No.	Coating Thickness (mils)		Deposition Rate (mils/hr)		Density (g/cc)	SiC Concentration (w/o)		Microstructure (Group)
	Entr.	Exit	Entr.	Exit		Ashing[a]	Microprobe[b]	
1	28	29	8.0	8.3	2.340	26.7	29.6	10
2	39	38	11.1	10.9	2.240 2.250	13.8	7/21 (13.4 avg.)	11 21
3	45	41	12.9	11.7	2.180 2.190	0.13	0/6.5 (0.8 avg.)	No Visible SiC Phase
4	50	43	14.3	12.3	2.100 2.150	0.21	0	No visible SiC phase

[a]Determined by ashing at 1950°F for 216 hours

[b]Determined by electron microprobe.

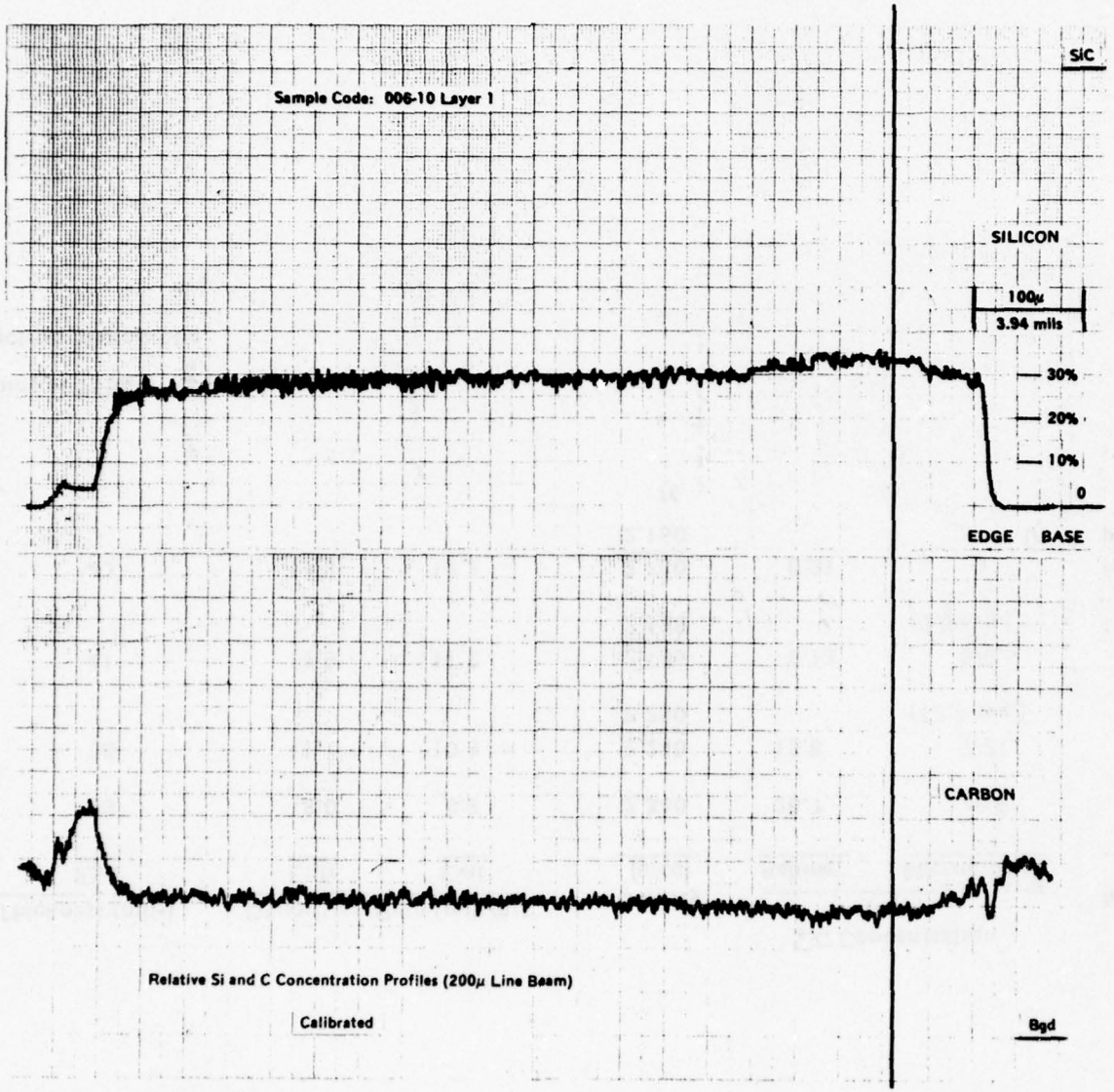

Figure 17. Electron Microprobe Scan of Coating from Run 006-18, Layer 1, Deposited at 3000°F.

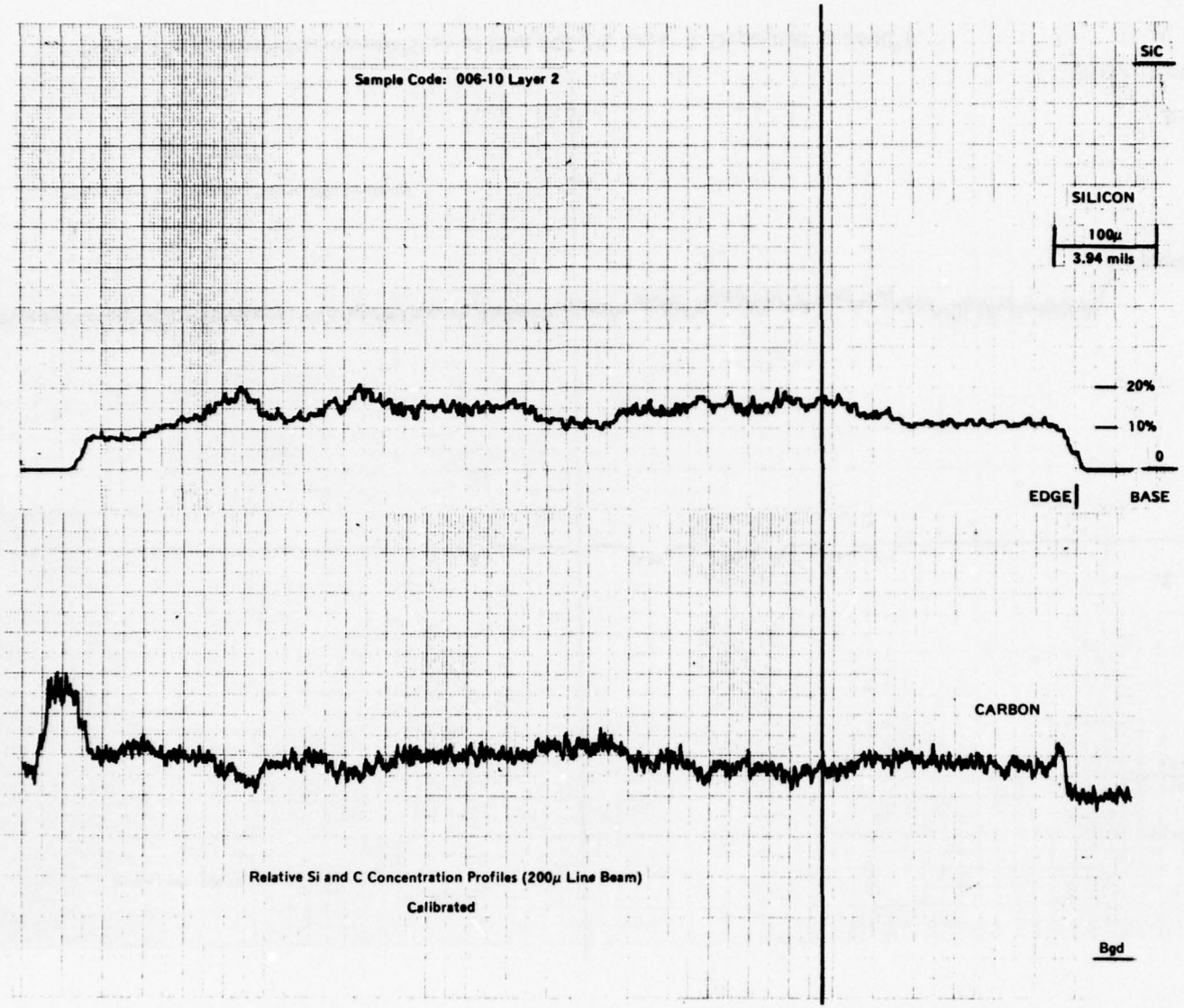

Figure 18. Electron Microprobe Scan of Run 006-10, Layer 2, Deposited at 3200°F.

Figure 19. Electron Microprobe Scan of Run 006-10, Layer 3. Deposited at 3400°F.

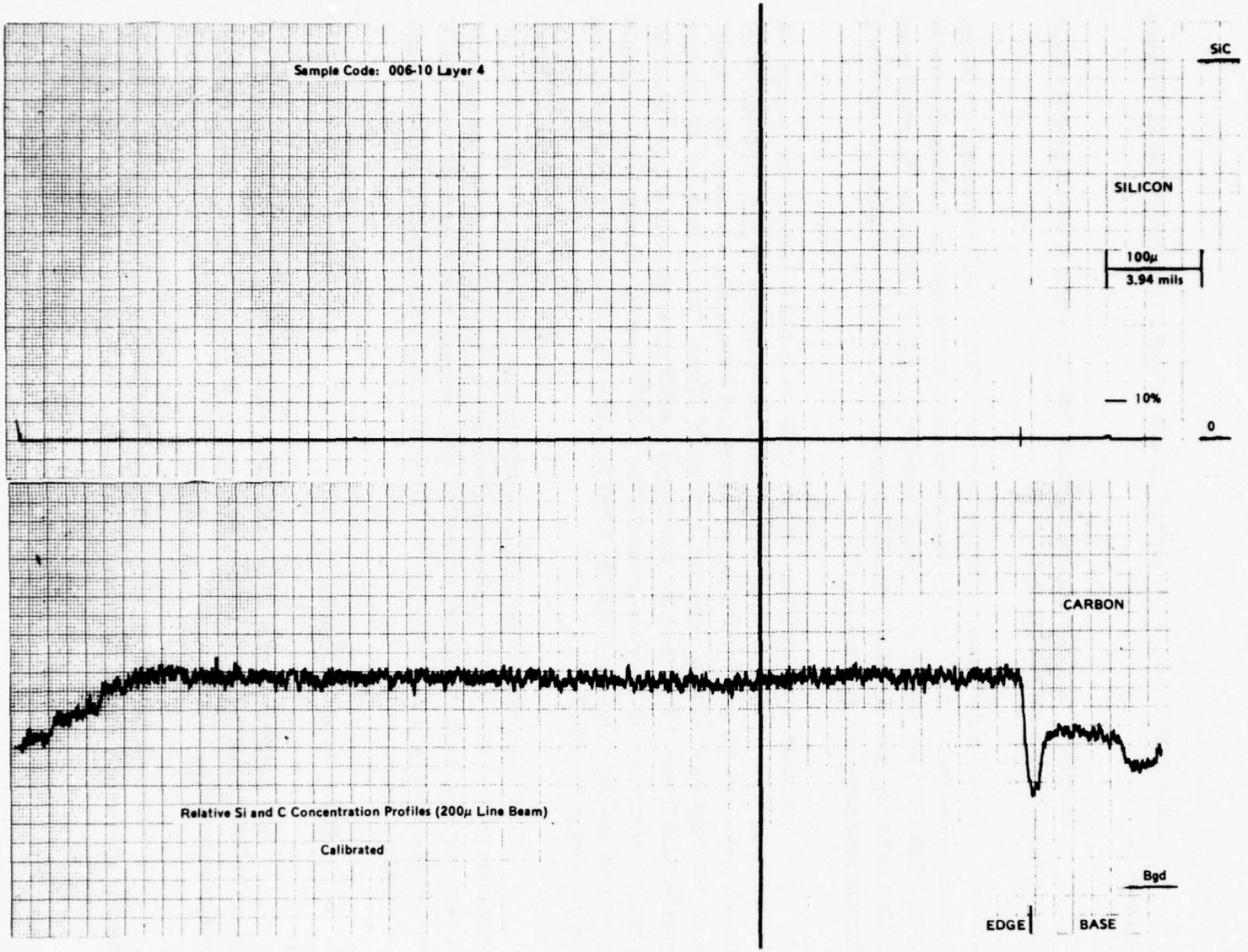

Figure 20. Electron Microprobe Scan of Run 006-10, Layer 4, Deposited at 3600°F.

Four distinct coating microstructures were achieved and these are shown in Figures 21 through 24.

At 3,000°F the SiC phase was visible as very fine, evenly dispersed needles with an average diameter of 0.025 mil. See Figure 21.

Increasing the deposition temperature from 3,000 to 3,200°F decreased the average SiC concentration from 28.2 w/o to 13.6 w/o and increased the average coating deposition rate by 35%. At 3,200°F the SiC phase had an average diameter of 0.025 mil within the PG growth cones and 0.065 mil in the cone boundaries. The SiC phase also began to show a tendency to concentrate in the cone boundaries as shown in Figure 22.

Increasing the temperature from 3,200 to 3,400°F reduced the average SiC concentration to below 1 w/o and increased the coating deposition rate by 12%. Although no SiC phase was visible, see Figure 23, the degree of intraconical delaminating was much less at 3,400° than in the subsequent coating deposited at 3,600°F (Figure 24). A study of the electron microprobe scan (Figure 19) of the layer deposited at 3,400°F shows identifiable quantities of SiC still present. Apparently the SiC phase present in the 3,400°F coating, although much reduced in concentration and dispersion over that in the 3,200°F coating, was still enough to affect the coating as was indicated in Run 006-3.

The final increase in deposition temperature from 3,400 to 3,600°F reduced the SiC concentration to near zero. The ashing determinations gave a slight indication; but the margin of error, when using this method, probably exceeds the values obtained in both the 3,400 and 3,600°F determinations. Again, as in Run 006-3, the 3,600°F coating contained extensive delaminations and was of a coarse microstructure.

c. Effect of Gas Composition

Three deposition runs, 002-81, 006-8 and 006-18, were conducted to investigate the effect of CH_3SiCl_3 concentration in the deposition gas on the SiC concentration and morphology of codeposited coatings.

Multiple-layer coatings were utilized to minimize the number of deposition runs required. In all cases only the CH_3SiCl_3 rate was varied. All other parameters were unchanged.

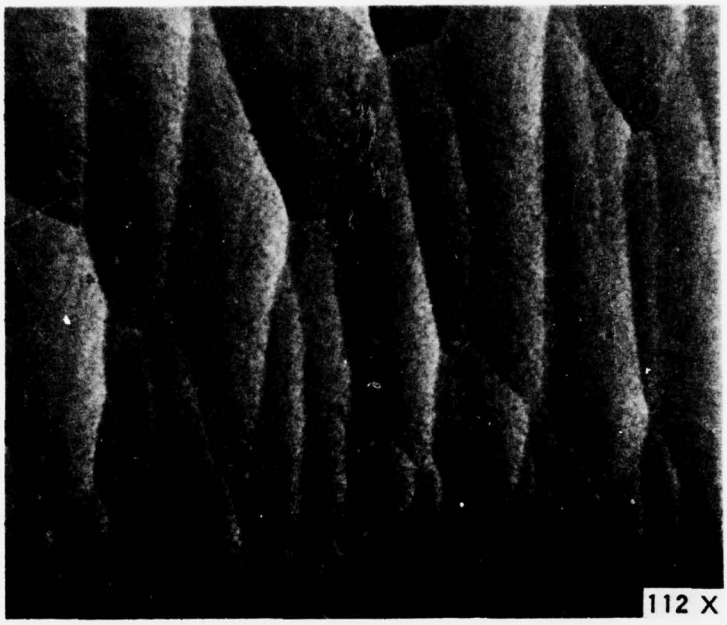

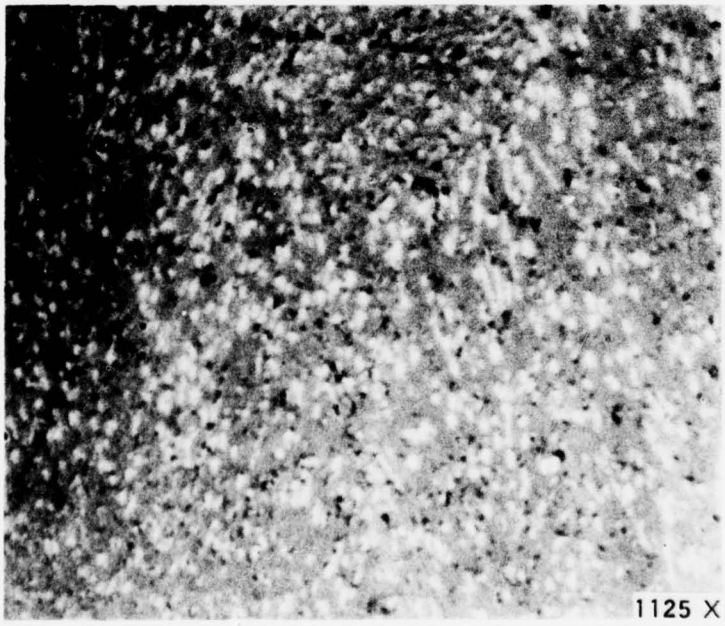

Figure 21. Run 006-10, 3000°F, Coating Microstructure.

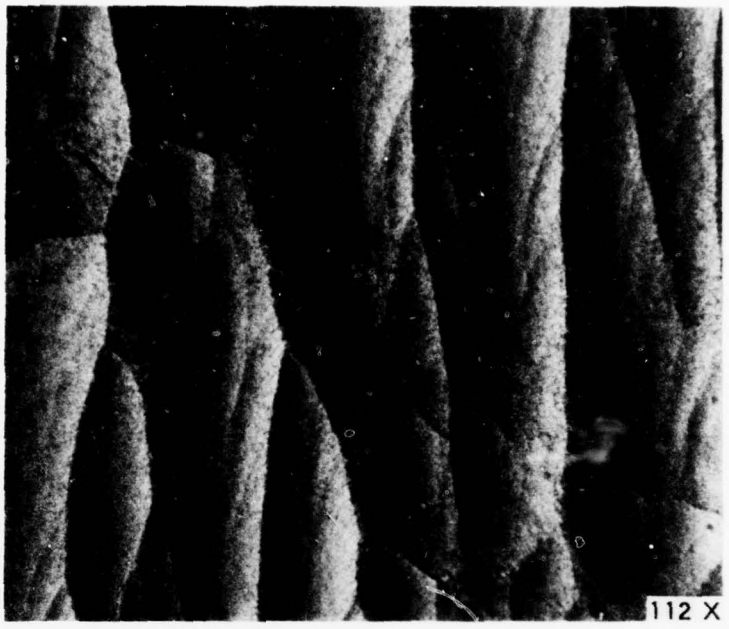

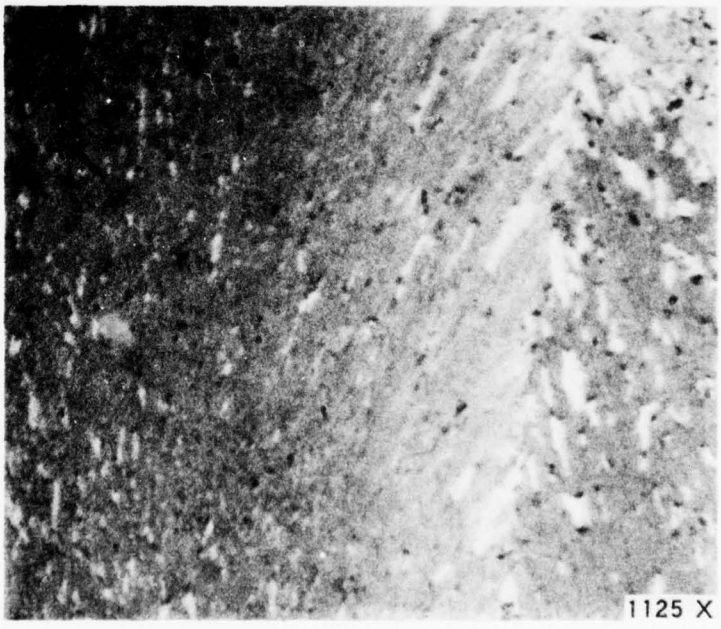

Figure 22. Run 006-10, 3200°F, Coating Microstructure.

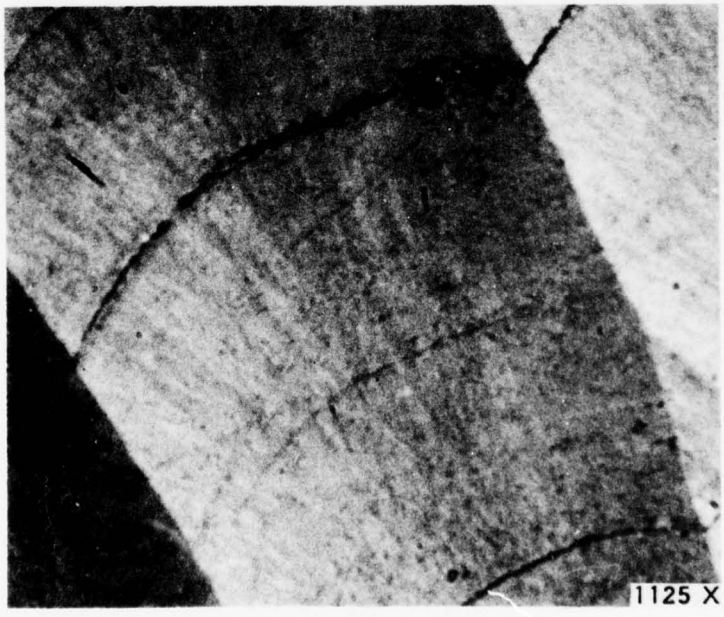

Figure 23. Run 006-10, 3400°F, Coating Microstructure.

Figure 24. Run 006-10, 3600°F, Coating Microstructure.

All of the coatings were applied to tubular HLM substrates 3.5 inches I.D. by 15.5 inches long at a nominal coating surface deposition temperature of 3,200°F. Temperature was monitored and controlled as discussed previously.

During Run 002-81 deposition temperature was monitored 13 inches from the injector. After 002-81 and prior to 006-8, the sight port orientation was modified to move the sighting area to 12 inches from the injector. This modification was made to move the internal and external sighting planes closer together.

Deposition conditions for all three runs are shown in Table 10.

Coating characterization data are shown in Tables 11, 12 and 13. Electron microprobe scans of the coatings from all three runs were conducted on samples extracted at the sight port locations. These are shown in Figures 25 through 32. Coating microstructures are shown in Figures 33 through 40.

Post-deposition examination of 002-81 showed the SiC content to decline with reduced CH_3SiCl_3 concentration as expected. It is interesting to note that the coating density in the sight port area is between 2.17 and 2.18 g/cc in Layer 3 where no SiC occurs. This PG matrix density value is much higher than would be expected (1.5 g/cc) in unalloyed pyrolytic graphite deposited at 3,200°F at atmospheric pressure. The SiC phase was visible in Layer 1 only and was classified in the Group 10 category. See Figures 33, 34 and 35.

Post-deposition examination of 006-8 showed the coating to be similar to that of 002-81. The SiC content varied with CH_3SiCl_3 concentration as in 002-81. The coating microstructure at the 12-inch position was Group 11 in Layer 1 (Figure 36). No SiC phase was visible in Layer 2 (Figure 37). The difference in microstructure between Layers 1 and 2 is believed to be directly related to SiC concentration. In general, higher concentrations result in increased SiC crystal size. At concentrations below 5 percent, the SiC phase is usually too fine and well dispersed to be visible at 1125X.

Post-deposition examination of 006-18 showed the coating layers to have consistently increased in density, SiC concentration and deposition rate with increasing CH_3SiCl_3 concentration as expected. Microscopic examination of Layer 1 (Figure 38) showed no visible SiC phase. The SiC phase was visible in Layer 2 (Figure 39) as short fine needles evenly dispersed within the PG matrix. Layer 3 (Figure 40) was similar in microstructure to Layer 2.

X-ray examination of the coating layers of 006-18 was conducted to determine the interlayer (d) spacing of the pyrolytic graphite phase. Measurements were made on the

Table 10. Deposition Conditions for Runs 002-81, 006-8 and 006-18.

Deposition Run No.	Carrier N_2 (SCFH)	Annulus N_2 (SCFH)	Total Process Gas (SCFH)	CH_4 (vol. percent)	MTS (vol. percent)	MTS/CH_4	Deposition Temperature (°F)	Deposition Time (hr)	Comments
002-81 (Layer 1)	953	15	980	1.19	0.080	0.067	3195^{+25}_{-25}	4.0	
002-81 (Layer 2)	953	15	980	1.19	0.040	0.034	3170^{+15}_{-35}	4.0	
002-81 (Layer 3)	953	15	980	1.19	0.021	0.018	3135^{+60}_{-45}	2.6	Run terminated early due to temperature recorder malfunction.
006-8 (Layer 1)	953	15	981	1.22	0.094	0.078	3190^{+30}_{-40}	5.0	
006-8 (Layer 2)	953	15	980	1.22	0.048	0.039	3190^{+25}_{-20}	5.0	Auto temperature control impossible after 4 1/2 hours. Temperature controlled manually for last 1/2 hour.
006-18 (Layer 1)	953	15	980	1.22	0.022	0.018	3195^{+15}_{-10}	5.0	
006-18 (Layer 2)	953	15	981	1.22	0.070	0.057	3200 ± 10	5.0	
006-18 (Layer 3)	953	15	981	1.22	0.120	0.098	3200^{+10}_{-05}	5.0	

Table 11. Coating Characterization Data for Run 002-81.

Inches from Injector	1	2	3	4	5	6	7	8	9	10	11	12	13	14	15
002-81 (Layer 1)															
Density (g/cc)	—	—	2.10	—	2.18	—	2.22	2.20	2.21	2.22	2.22	2.20	2.20	2.17	2.20
SiC Concentration (w/o)[a]	—	—	—	—	—	—	—	—	—	—	—	—	6	—	—
Thickness (mils)	—	—	19	—	26	—	33	37	41	44	53	50	49	48	44
Dep. Rate (mils/hr)	—	—	4.8	—	6.5	—	8.2	9.2	10.2	11.0	13.2	12.5	12.2	12.0	11.0
PG Matrix Density (g/cc)[a]	—	—	—	—	—	—	—	—	—	—	—	—	2.16	—	—
002-81 (Layer 2)															
Density (g/cc)	2.12	—	2.15	—	2.16	—	2.17	2.17	2.18	2.18	2.18	2.19	2.20	2.20	2.18
SiC Concentration (w/o)[a]	—	—	—	—	—	—	—	—	—	—	—	—	2	—	—
Thickness (mils)	11	—	18	—	25	—	35	36	36	38	41	45	45	45	47
Dep. Rate (mils/hr)	2.8	—	4.5	—	6.2	—	8.8	9.0	9.0	9.5	10.2	11.2	11.2	11.2	11.8
PG Matrix Density (g/cc)[a]	—	—	—	—	—	—	—	—	—	—	—	—	2.19	—	—
002-81 (Layer 3)															
Density (g/cc)	2.05	—	2.12	—	2.16	—	2.16	2.17	2.16	2.16	2.17	2.17	2.18	2.18	2.17
SiC Concentration (w/o)[a]	—	—	—	—	—	—	—	—	—	—	—	—	0	—	—
Thickness (mils)	6	—	12	—	16	—	20	21	25	25	28	29	30	30	28
Dep. Rate (mils/hr)	2.3	—	4.6	—	6.2	—	7.7	8.1	9.6	9.6	10.8	11.2	11.5	11.5	10.8
PG Matrix Density (g/cc)[a]	—	—	—	—	—	—	—	—	—	—	—	—	2.18	—	—

[a]Derived from electron microprobe traces.

Table 12. Coating Characterization Data for Run 006-8.

Inches from Injector	1	2	3	4	5	6	7	8	9	10	11	12	13	14
006-8 (Layer 1)														
Density (g/cc)	2.17	—	2.22	—	2.22	—	2.23	—	2.23	—	2.22	2.22	2.21	—
SiC Concentration (w/o)[a]	—	—	—	—	—	—	—	—	—	—	—	8	—	—
SiC Concentration (w/o)[b]	—	—	—	—	—	—	—	—	—	—	—	8.2	8.2	—
Thickness (mils)	17	19	24	27	32	40	45	55	58	60	63	60	59	60
Dep. Rate (mils/hr)	3.4	3.8	4.8	5.4	6.4	8.0	9.0	11.0	11.6	12.0	12.6	12.0	11.8	12.0
PG Matrix Density (g/cc)[b]	—	—	—	—	—	—	—	—	—	—	—	2.16	2.15	—
006-8 (Layer 2)														
Density (g/cc)	2.19	—	2.20	—	2.20	0	2.21	—	2.22	—	2.21	2.21	2.20	—
SiC Concentration (w/o)[a]	—	—	—	—	—	—	—	—	—	—	—	2.5	—	—
SiC Concentration (w/o)[b]	—	—	—	—	—	—	—	—	—	—	—	2.5	2.5	—
Thickness (mils)	18	18	24	30	33	42	50	58	64	65	69	68	64	60
Dep. Rate (mils/hr)	3.6	3.6	4.8	6.0	6.6	8.4	10.0	11.6	12.8	13.0	13.8	13.6	12.8	12.0
PG Matrix Density (g/cc)[b]	—	—	—	—	—	—	—	—	—	—	—	2.19	2.18	—

[a]Derived from electron microprobe traces.
[b]Derived from ashing data.

Table 13. Coating Characterization Data for Run 006-18.

Inches from Injector	0	1	2	3	4	5	6	7	8	9	10	11	12	13	14
006-18 (Layer 1)															
Density (g/cc)	—	—	—	—	2.195	2.195	2.195	2.200	2.205	2.205	2.205	2.205	2.205	2.205	2.200
SiC Concentration (w/o)[a]	—	—	—	—	—	—	—	—	—	—	—	—	0	—	—
SiC Concentration (w/o)[b]	—	—	—	—	1.5	—	1.0	—	2.0	—	2.0	—	1.2	—	2.9
Thickness (mils)	2	15	18	25	25	30	39	45	45	49	50	52	47	45	45
Dep. Rate (mils/hr)	0.4	3.0	3.6	5.0	5.0	6.0	7.8	9.0	9.0	9.8	10.0	10.4	9.4	9.0	9.0
PG Matrix Density (g/cc)[a]	—	—	—	—	—	—	—	—	—	—	—	—	2.20	—	2.18
PG Matrix Density (g/cc)[b]	—	—	—	—	2.18	—	2.18	—	2.20	—	2.19	—	2.19	—	—
006-18 (Layer 2)															
Density (g/cc)	—	—	—	2.212	2.205	2.205	2.205	2.212	2.218	2.218	2.218	2.218	2.215	2.205	2.195
SiC Concentration (w/o)[a]	—	—	—	—	—	—	—	—	—	—	—	—	6	—	—
SiC Concentration (w/o)[b]	—	—	—	—	5.8	—	6.9	—	8.8	—	9.6	—	7.8	—	5.2
Thickness (mils)	16	20	25	32	35	39	55	62	65	69	69	69	65	61	60
Dep. Rate (mils/hr)	3.2	4.0	5.0	6.4	7.0	7.8	11.0	12.4	13.0	13.8	13.8	13.8	13.0	12.2	12.0
PG Matrix Density (g/cc)[a]	—	—	—	—	—	—	—	—	—	—	—	—	2.17	—	—
PG Matrix Density (g/cc)[b]	—	—	—	—	2.16	—	2.15	—	2.15	—	2.15	—	2.16	—	2.16
006-18 (Layer 3)															
Density (g/cc)	2.312	2.310	2.295	2.255	2.245	2.245	2.262	2.275	2.295	2.285	2.285	2.272	2.255	2.255	2.212
SiC Concentration (w/o)[b]	—	—	—	—	—	—	14.9	—	15.7	—	18.7	—	11[a]	—	—
Thickness (mils)	18	22	25	30	35	45	64	66	75	78	77	75	75	70	69
Dep. Rate (mils/hr)	3.6	4.4	5.0	6.0	7.0	9.0	12.8	13.2	15.0	15.6	15.4	15.0	15.0	14.0	13.8
PG Matrix Density (g/cc)[b]	—	—	—	—	—	—	2.15	—	2.18	—	2.14	—	2.18[a]	—	—

[a]Derived from electron microprobe scans.

[b]Derived from ashing data.

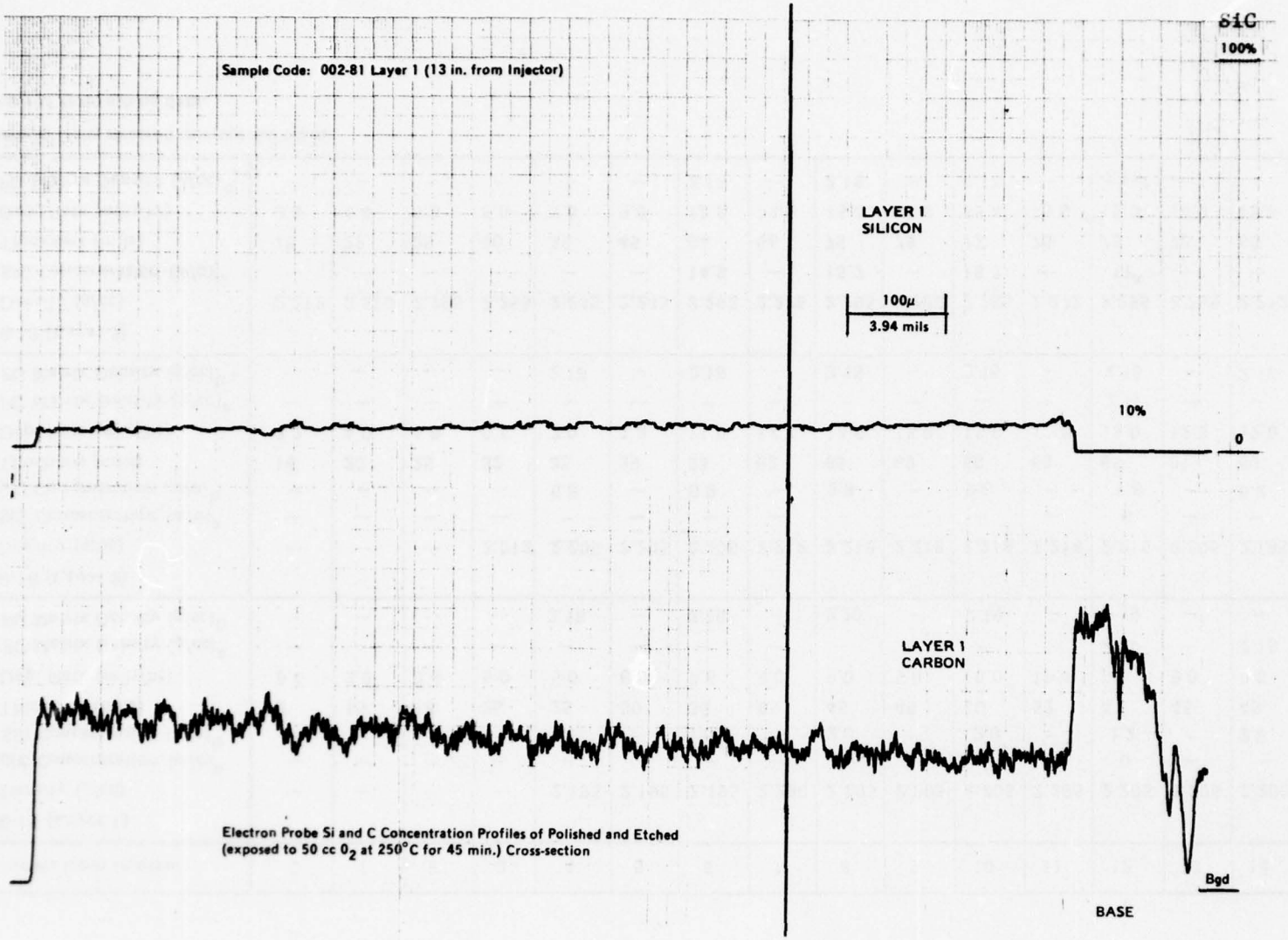

Figure 25. Electron Microprobe Scan of Coating from Run 002-81, Layer 1.

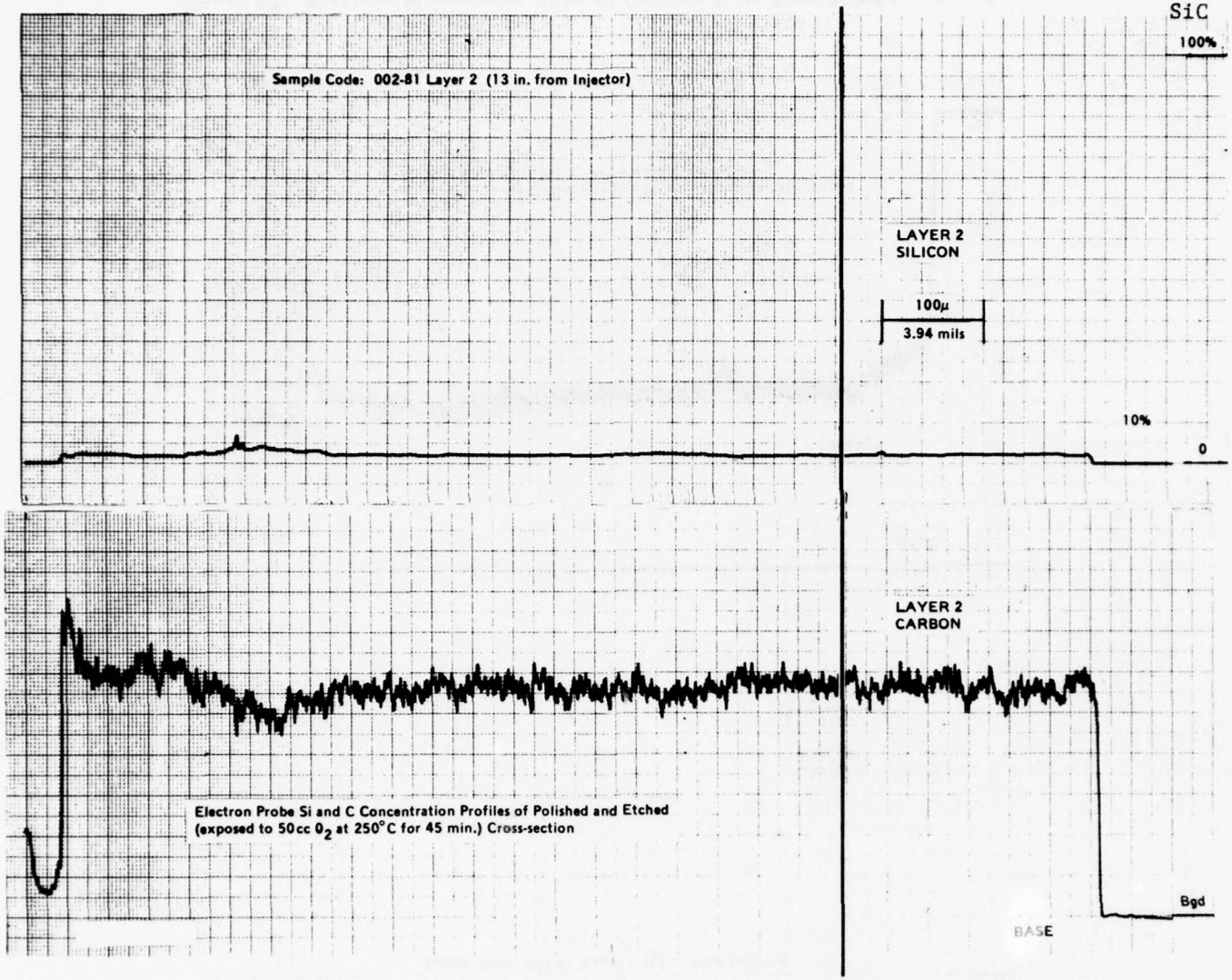

Figure 26. Electron Microprobe Scan of Coating from Run 002-81, Layer 2.

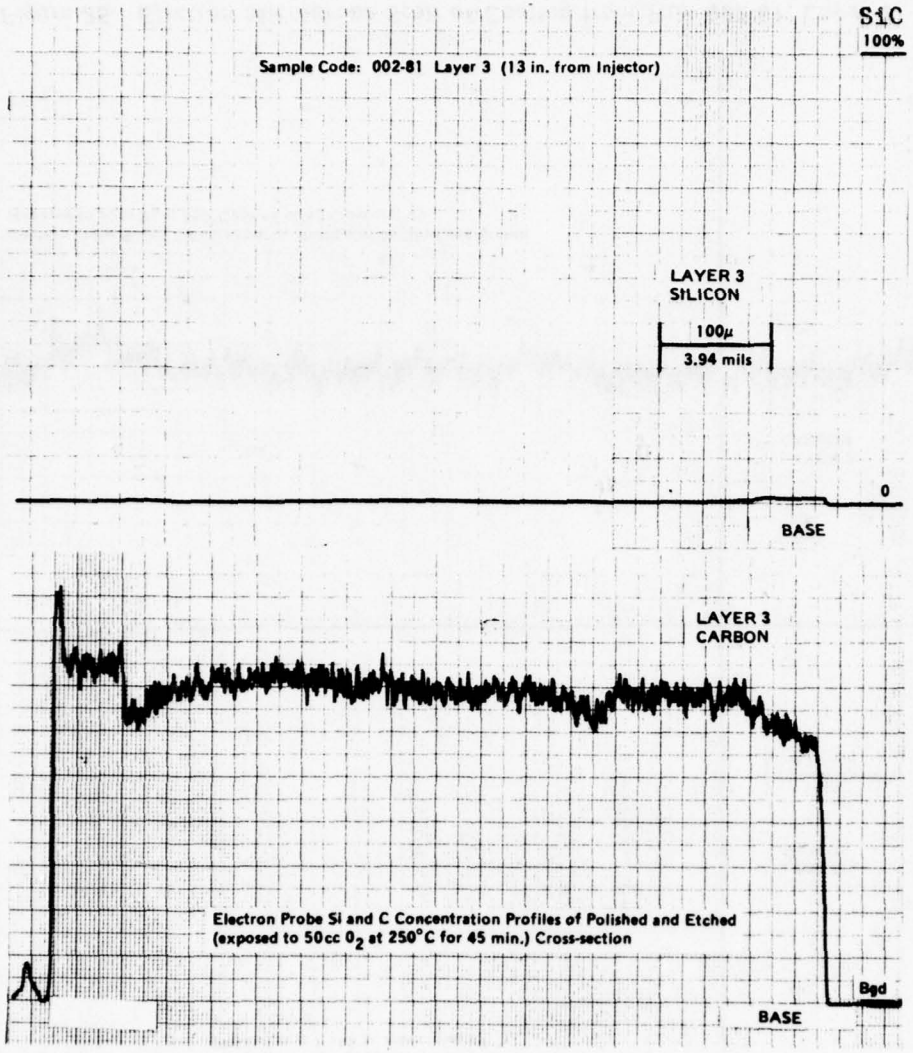

Figure 27. Electron Microprobe Scan of Coating from Run 002-81, Layer 3.

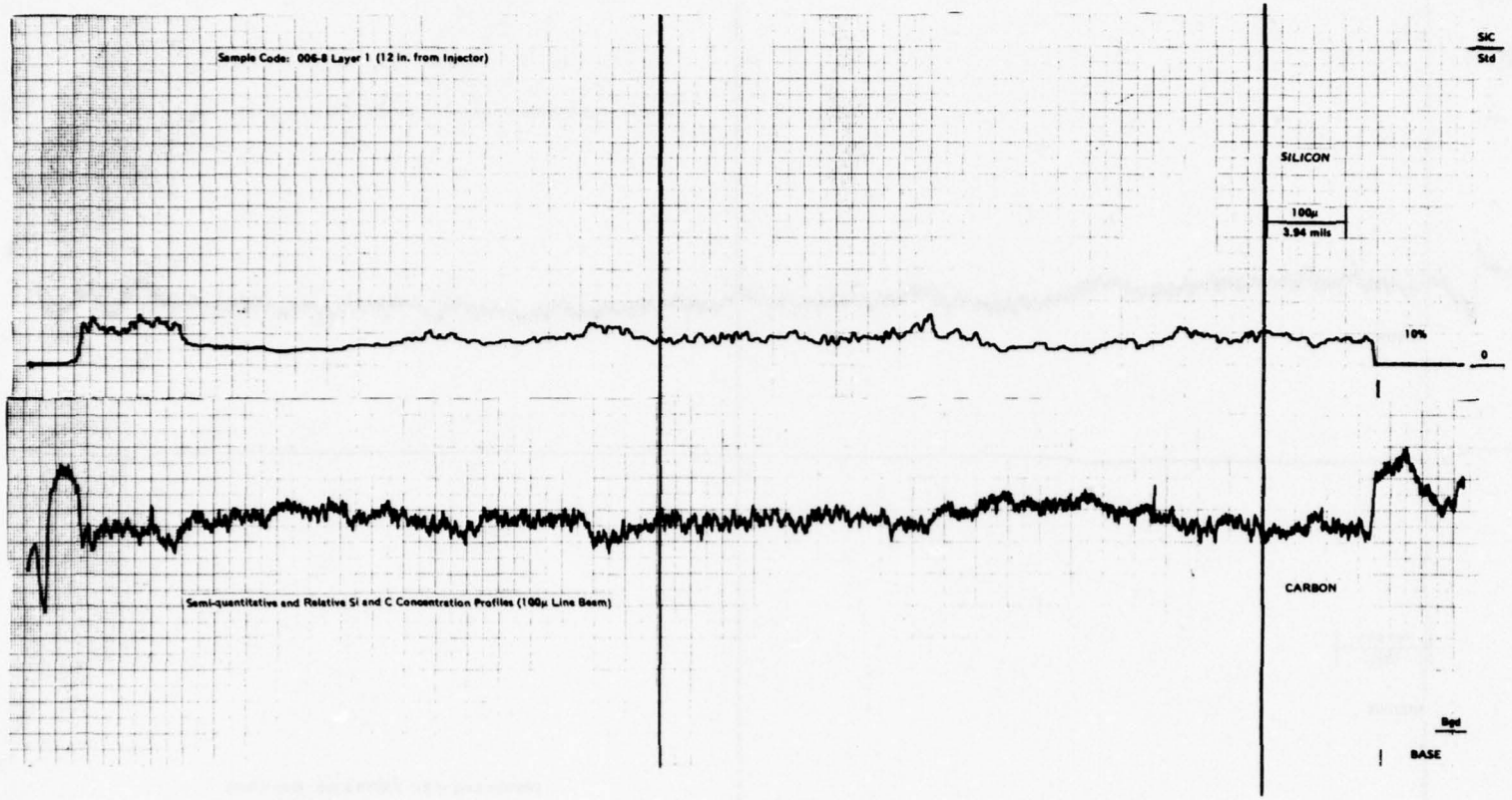

Figure 28. Electron Microprobe Scan of Coating from 006-8, Layer 1.

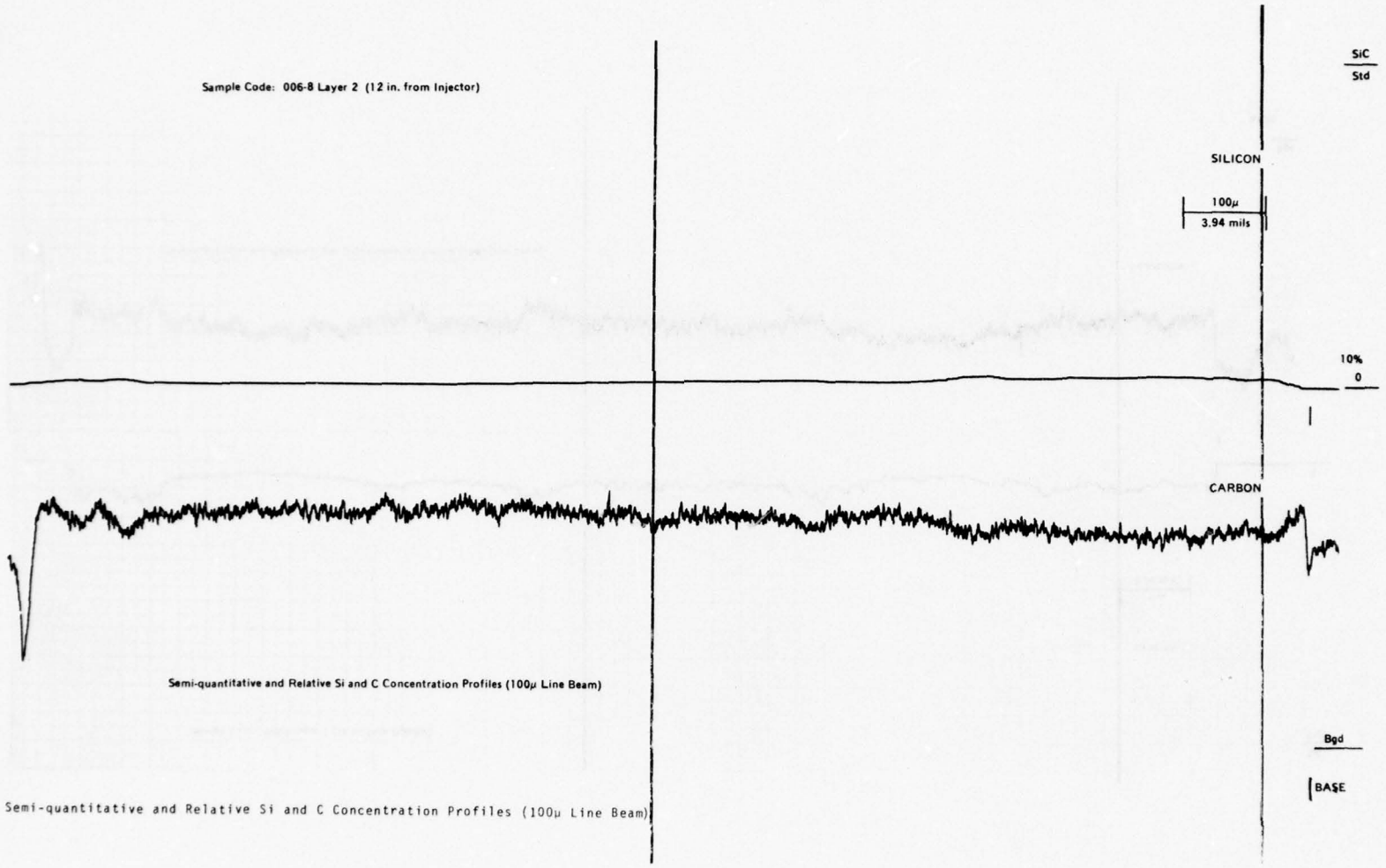

Figure 29. Electron Microprobe Scan of Coating from 006-8, Layer 2.

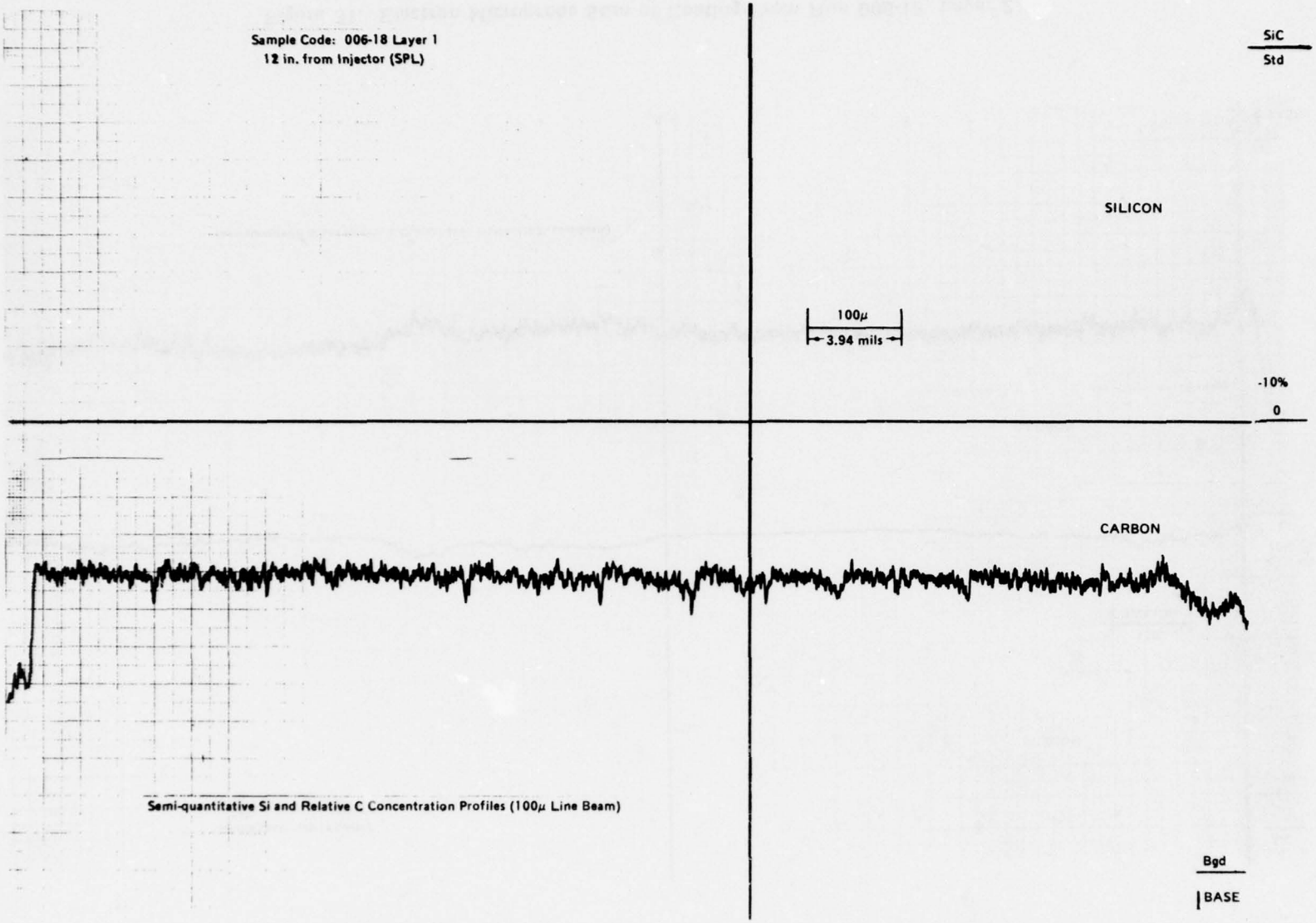

Figure 30. Electron Microprobe Scan of Coating From Run 006-18, Layer 1.

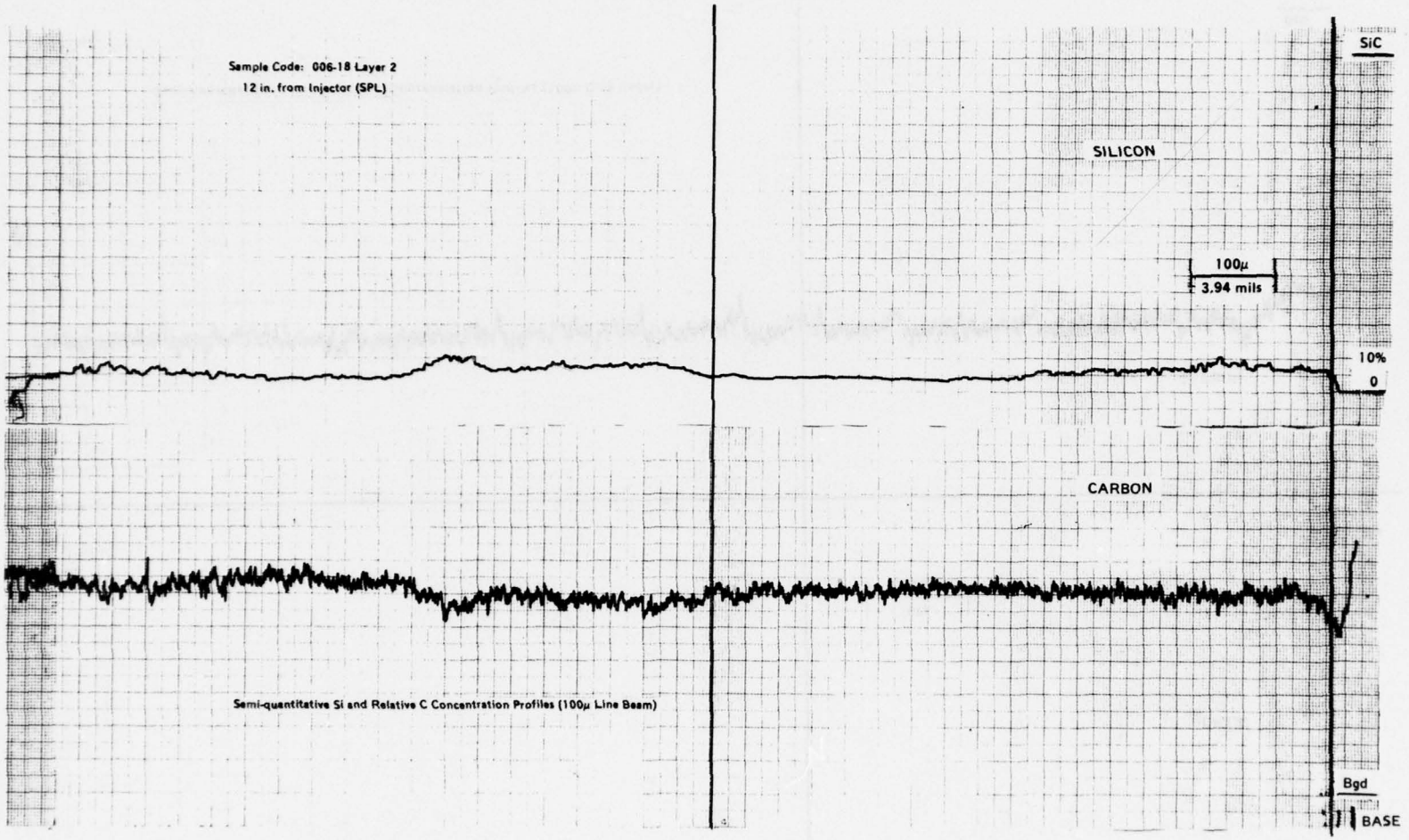

Figure 31. Electron Microprobe Scan of Coating From Run 006-18, Layer 2.

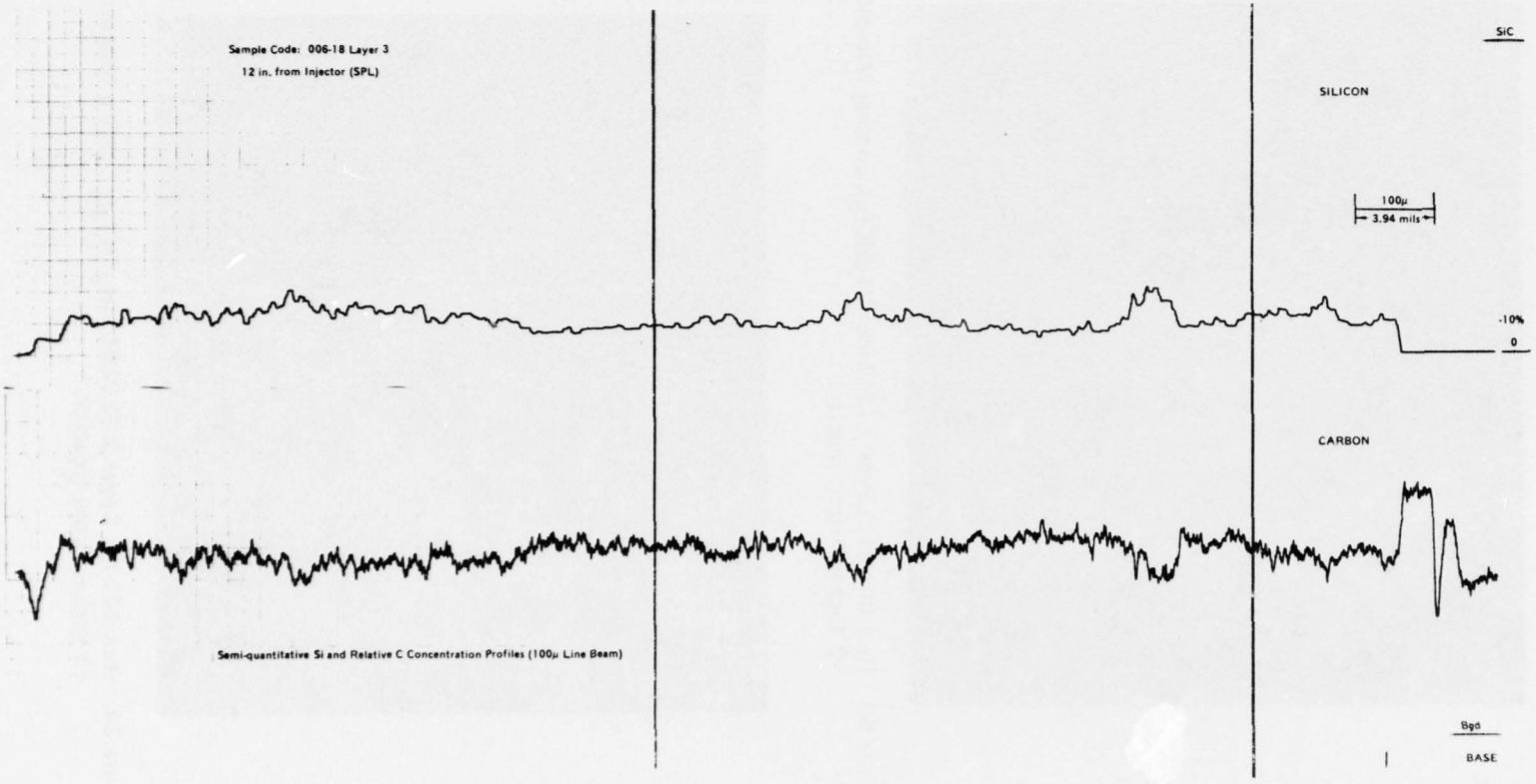

Figure 32. Electron Microprobe Scan of Coating from Run 006-18, Layer 3.

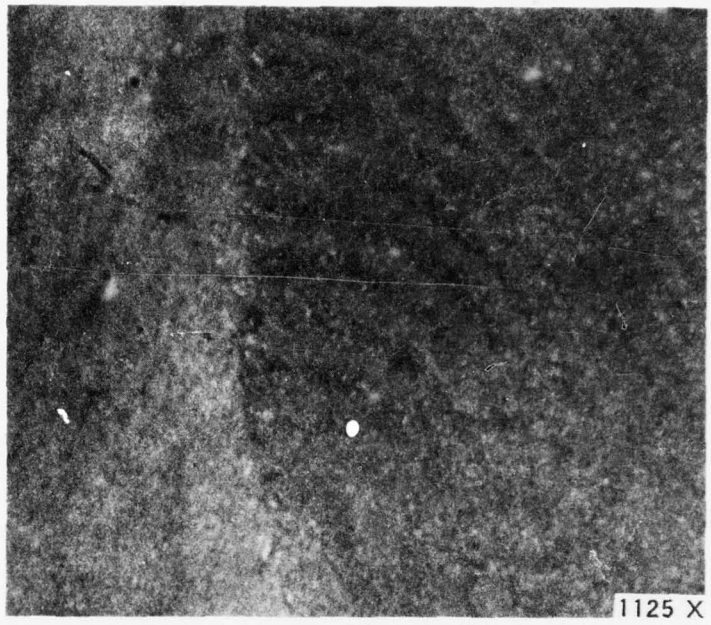

Figure 33. Run 002-81, Layer 1 (0.080% CH_3SiCl_3), Coating Microstructure 13 Inches From Injector.

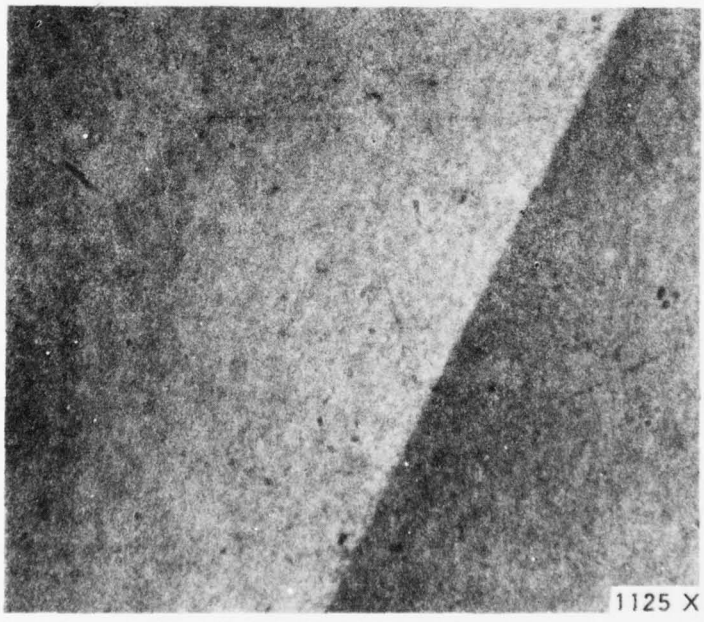

Figure 34. Run 002-81, Layer 2 (0.040% CH_3SiCl_3), Coating Microstructure 13 Inches From Injector.

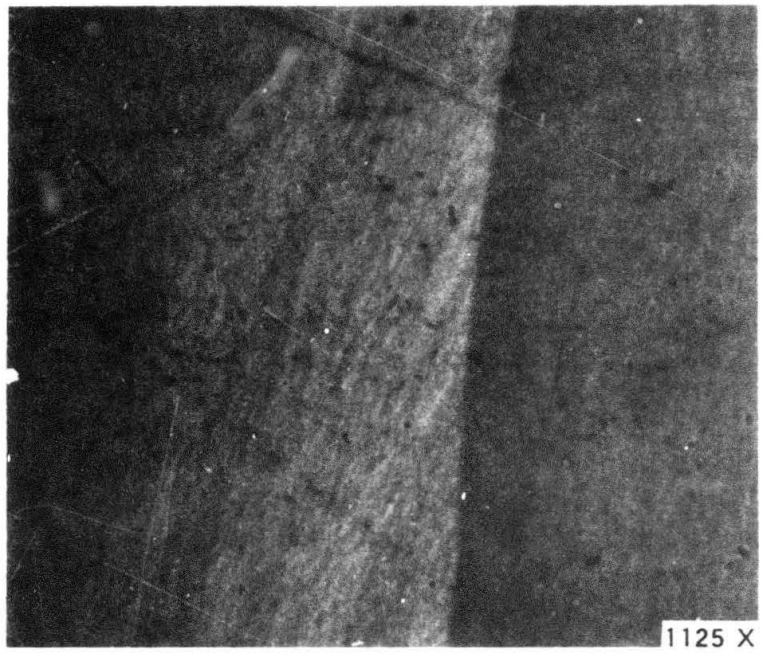

Figure 35. Run 002-81, Layer 3 (0.021% CH_3SiCl_3), Coating Microstructure 13 Inches From Injector.

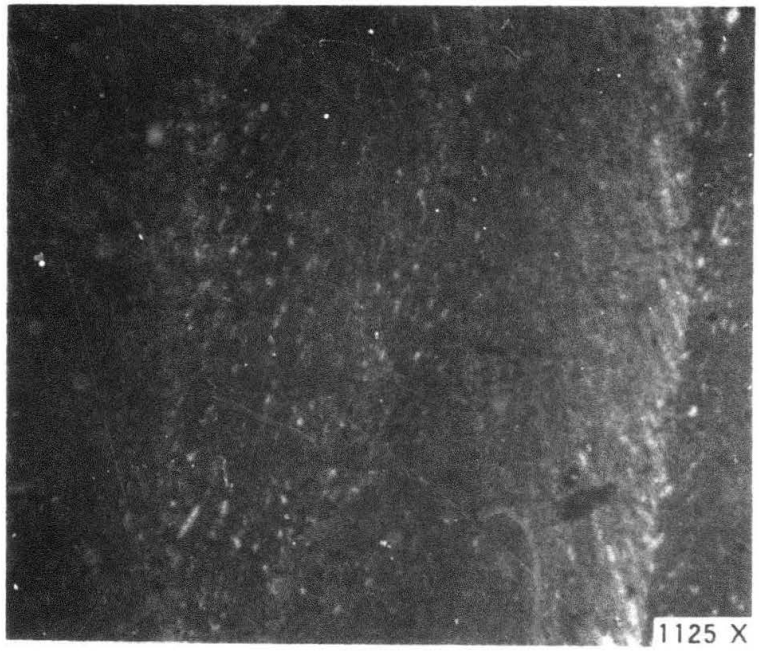

Figure 36. Run 006-8, Layer 1 (0.094% CH_3SiCl_3), Coating Microstructure 12 Inches From Injector.

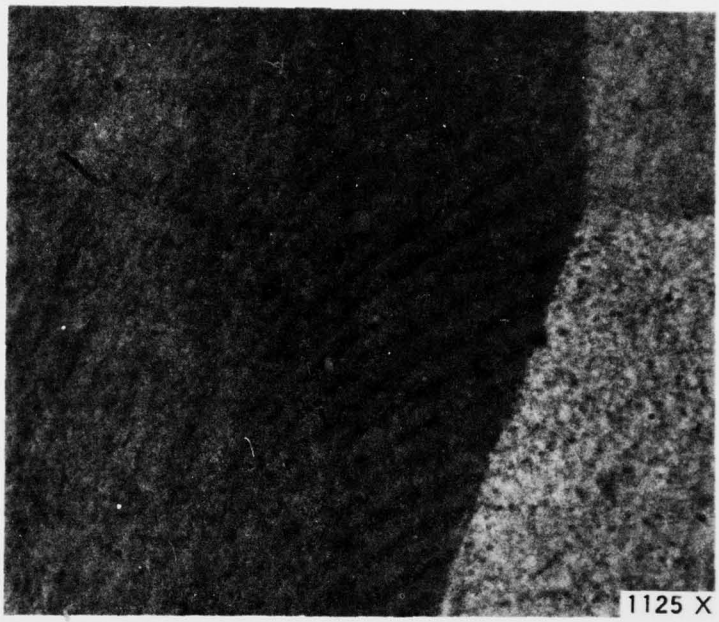

Figure 37. Run 006-8, Layer 2 (0.048% CH_3SiCl_3), Coating Microstructure 12 Inches From Injector.

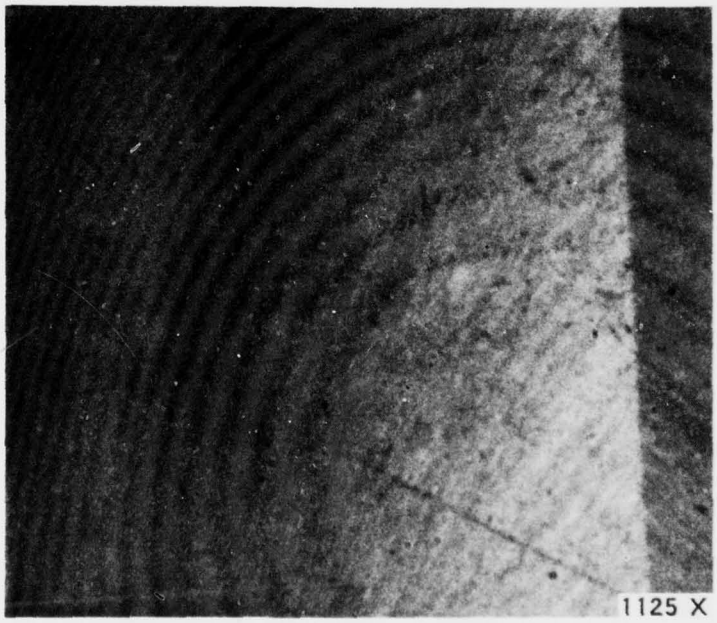

Figure 38. Run 006-18, Layer 1 (0.022% CH_3SiCl_3), Coating Microstructure 12 Inches From Injector.

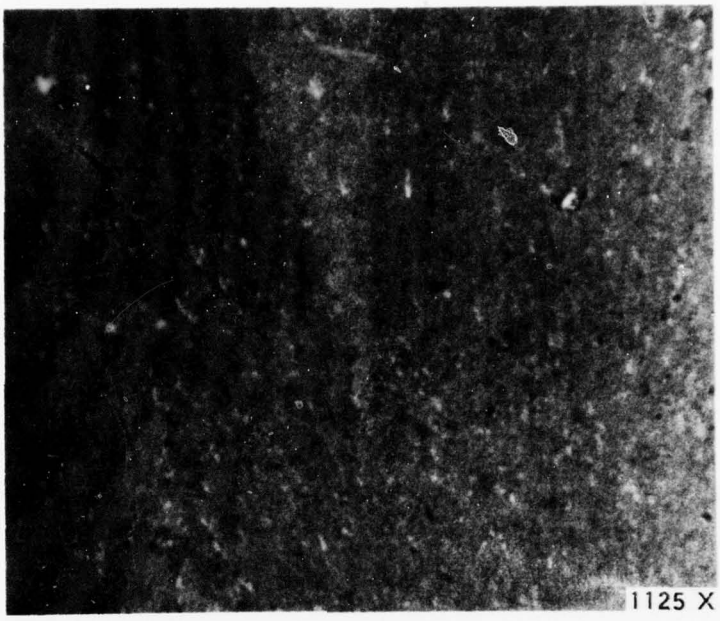

Figure 39. Run 006-18, Layer 2 (0.070% CH_3SiCl_3), Coating Microstructure 12 Inches From Injector.

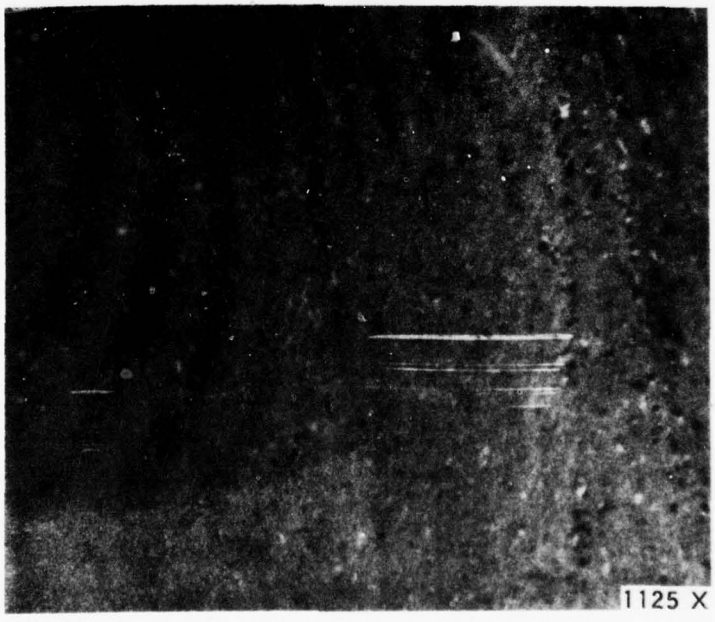

Figure 40. Run 006-18, Layer 3 (0.120% CH_3SiCl_3), Coating Microstructure 12 Inches From Injector.

first-deposited and last-deposited surfaces of each layer. These data, shown in Table 14, agree with past observations of codeposited PG/SiC/, i.e.; the first-deposited material tends to be better oriented than later-deposited material. This effect is caused by ordering which occurs during deposition of subsequent layers of coating. Because of this coating ordering phenomenon, it is difficult to separate the effect of SiC concentration on the interlayer spacing of the pyrolytic graphite matrix. It does, however, appear that the spacing increases with increasing SiC concentration.

4. ANALYSIS OF RESULTS

Correlations of coating SiC content, coating density, matrix density and deposition rate as a function of deposition temperature and gas composition were derived from the data presented above. These correlations were ultimately used to select process conditions for the fabrication of test specimens as discussed in Section IV.

The effect of deposition temperature is displayed by Figure 41. Coating SiC concentration decreases with increasing temperature. The maximum temperature at which a detectable amount of SiC deposits is ~3,400°F. The sensitivity of SiC concentration to temperature is readily apparent from this figure. The SiC content changes by approximately a factor of two as a result of a 100°F change in deposition temperature. This trend is directly related to the decomposition equilibrium of silicon carbide. At high temperatures the rate of decomposition (or sublimation) exceeds the rate of formation by pyrolysis and hence the solid SiC phase cannot deposit.

Deposition rate is seen to increase with temperature to a maximum in the vicinity of 3,600°F and then decreases with further increase in temperature. The decrease in rate results from the formation of soot in the gas phase which depletes the reacting mixture at the deposition surface. Evidence of sooting could be seen in the microstructures of the coatings formed at the high temperatures. The PG cones were coarse and broad-based, suggesting the inclusion of soot particles which had formed in the gas phase near the surface.

Coating density decreases with increasing temperature over the entire range examined. The calculated matrix density increases with deposition temperature and, of course, becomes identical with the coating density beyond the temperature at which SiC deposits. In the low temperature regime, the coating density is effected more strongly by the reduction in silicon carbide content than by the improvement in matrix density. In the high temperature regime, the density of the pure carbon phase deposited is strongly influenced by the degree of sooting. A continuing decrease in coating density with increasing temperature results. It must be mentioned that the high temperature decrease in density is not necessarily desirable and can be corrected. It results from the particular

Table 14. Interlayer Spacing of PG Phase in Coating Layers Deposited During Run 006-18.

Layer	"d" Spacing in Angstroms	
	First Deposited Surface	Last Deposited Surface
1	3.400	3.412
2	3.402	3.421
3	3.411	3.412

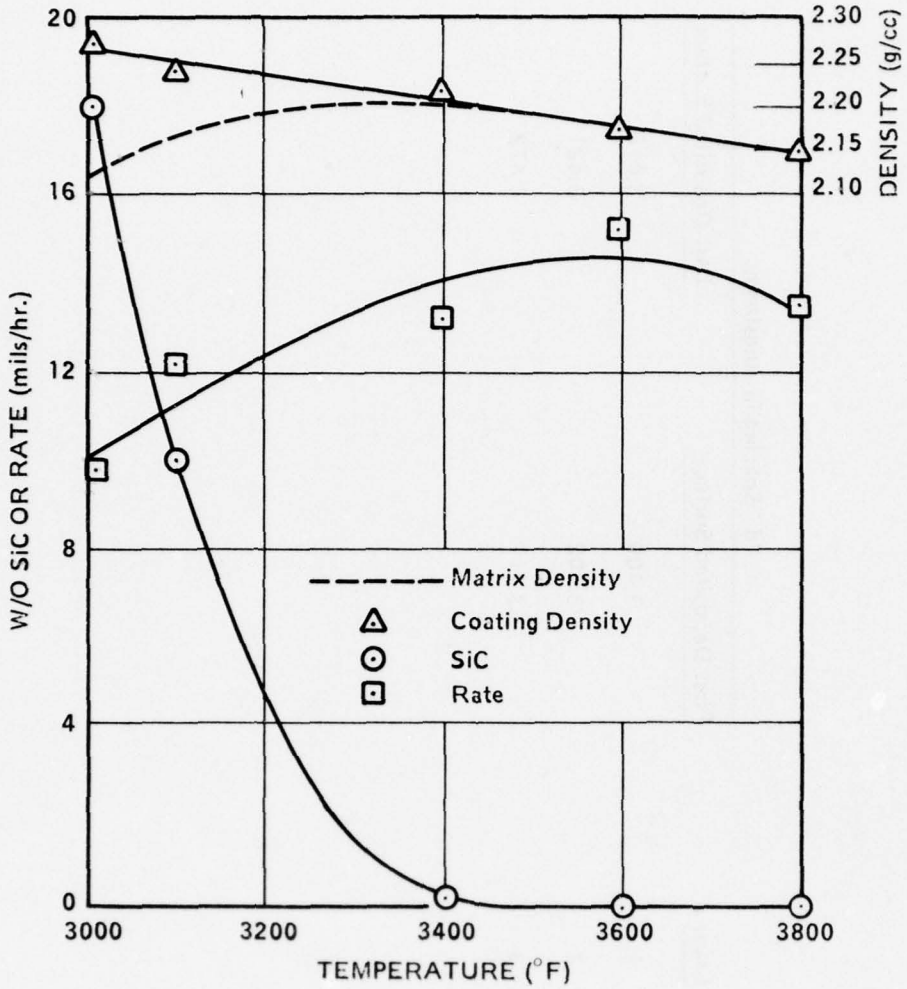

Figure 41. Effect of Temperature.

velocity and total concentration levels adopted for this run series. A higher velocity and lower total concentration would reduce the tendency to soot at high temperature and thereby increase the coating density.

Figure 42 displays the effect of CH_3SiCl_3 flow rate on coating composition, density and rate. This set of curves includes data for most of the coatings deposited at 3,200°F during this program.[1]

Within the scatter of the data, the three dependent variables shown all appear to increase linearly with increasing CH_3SiCl_3 flow rate. The data for SiC content exhibit the largest degree of scatter which reflects the sensitivity of this quantity to changes in conditions. The strong dependency on deposition temperature discussed above probably accounts for most of this scatter. There appears to be a threshold value of CH_3SiCl_3 flow rate below which an undetectable amount of SiC deposits (or no SiC deposits at all). This threshold might be related to the decomposition equilibrium of solid silicon carbide as is the high temperature limit discussed above.

The linear dependency of coating density on CH_3SiCl_3 flow rate actually reflects a linear dependency on coating composition. Such a relationship implies that the matrix density is constant, i.e., not a function of either the CH_3SiCl_3 concentration in the gas phase or the SiC content of the coating. The correlation shown by Figure 41 implies a matrix density of ~2.18 g/cc.

5. APPLICATION OF CORRELATIONS

The correlations described above were based upon experiments which were conducted with a 3.5-inch diameter cylindrical substrate and a single orifice injector, and which incorporated a given set of nitrogen and methane flow rates. They are directly applicable to selecting conditions to produce selected coatings on similar sized substrates and indeed they were successfully used for this purpose in fabricating physical property specimens as discussed in Section IV.

Application of these correlations to other substrate sizes and shapes requires the use of a scaling procedure. A simplified procedure was adopted for use in selecting conditions for the first runs to be conducted to fabricate grade coated thermal stress specimens. This procedure assumes that the process is diffusion controlled and therefore similarity in tubes of varying sizes can be achieved by maintaining constant linear velocity. Further, the jet issuing from the injector is assumed to originate from a point source and its diverging angle is independent of tube size. Based on these assumptions then, to scale from a larger to a smaller tube, the mass throughput is reduced

[1] Data from aborted or questionable runs are omitted.

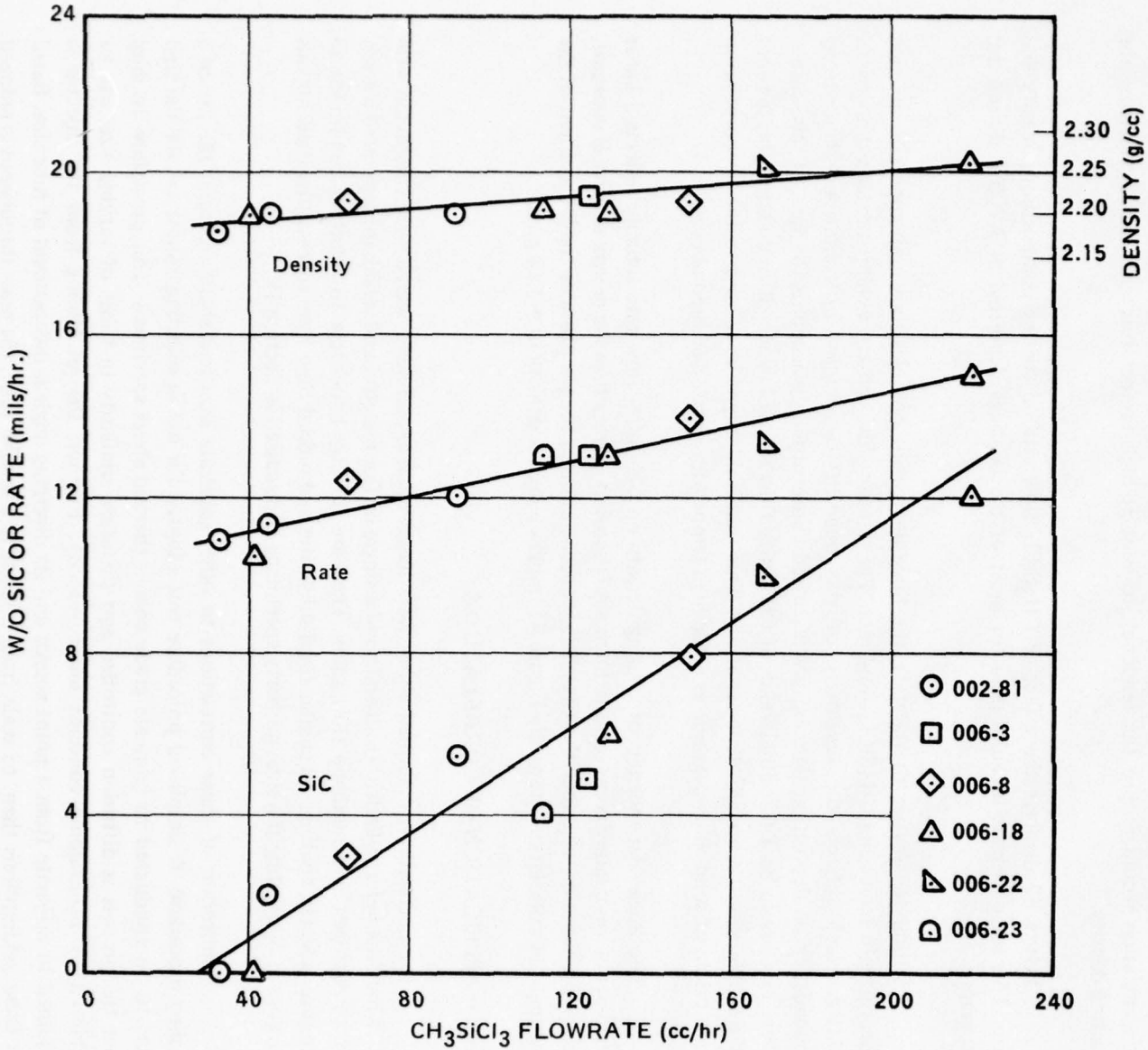

Figure 42. Effect of CH_3SiCl_3 Flowrate.

by the ratio of cross-sectional areas, the part-to-injector distance is reduced by the ratio of diameters and the inlet gas composition is the same. While this is a greatly simplified process model, it was beyond the scope of this program to develop a more rigorous model. Nonetheless, the simplified approach allowed the use of the correlations for selecting a reasonable set of conditions for the initial attempts at fabricating the graded coating thermal stress specimens for this and the AFRPL Graded Coating Programs.

SECTION IV

FABRICATION OF TEST SPECIMENS

Specimens were fabricated for use in erosion and thermal stress tests and some free-standing material was deposited for properties measurements. The erosion and thermal stress specimens were shipped for tests to be conducted elsewhere. The free-standing material was characterized both in-house and at General Atomic Company. The following sections describe the runs conducted to fabricate these specimens.

1. PHYSICAL PROPERTIES SPECIMENS

Five deposition runs, 002-86, 002-87, 006-22, 006-23 and 006-24, were conducted to fabricate homogeneous low SiC concentration, codeposited coatings from which specimens could be extracted for physical properties measurements. Only the last three coatings deposited were acceptable. Two of these were deposited at 3,200°F; one (006-22) contained ~10 w/o SiC and the other (006-23) contained ~5 w/o SiC. The third (006-24) was deposited at 3,300°F and contained ~5 w/o SiC. Consequently, properties could be determined as a function of SiC content and deposition temperature.

Coatings were applied to PG precoated 3.5-inch I.D. tubes using the deposition assembly configuration utilized during the tubular 3.5-inch experimental runs (Figure 3).

Deposition conditions are shown in Table 15 and coating characterization data are shown in Table 16.

Deposition temperature was monitored at the coating surface 13.0 and 13.5 inches from the injector in Runs 002-86 and 002-87, respectively, and 12.0 inches from the injector in Runs 006-22, 006-23 and 006-24. Temperature was controlled automatically on the deposition canister backside.

Data from the 3.5-inch experimental runs were utilized to determine the parameters for applying these coatings.

Runs 002-86 and 002-87 did not produce usable coatings due to experimental problems which occurred during deposition. Both runs were affected by the oxidation problem discussed on page 16.

Table 15. Deposition Conditions For Runs 002-86, 002-87, 006-22, 006-23 and 006-24.

Deposition Run No.	Carrier N_2 (SCFH)	Annulus N_2 (SCFH)	Total Process Gas (SCFH)	CH_4 (vol. percent)	MTS (vol. percent)	MTS/CH_4	Deposition Temperature (°F)	Deposition Time (hr)	Comments
002-86	953	15	980	1.19	0.062	0.052	*3180 $^{+40}_{-50}$	14.0	Temperature controller vibrated loose at 6 1/2 hours causing deposition temperature to rise rapidly to 3320°F. Temperature dropped to 3100°F during correction.
002-87	953	15	980	1.19	0.015	0.013	3180 $^{+40}_{-30}$	9.5	
006-22	953	15	981	1.22	0.091	0.075	3195 $^{+15}_{-25}$	16.0	
006-23	953	15	981	1.22	0.078	0.064	3200 ± 20	18.5	
006-24	953	15	981	1.22	0.116	0.095	3300 $^{+20}_{-30}$	16.0	

*Temperature range excluding excursion at 6 1/2 hours.

Table 16. Coating Characterization Data For Runs 002-86, 002-87, 006-22, 006-23 and 006-24.

Inches from Injector	0	1	2	3	4	5	6	7	8	9	10	11	12	13	14	15	Comments
002-86																	
Density (g/cc)	—	—	—	—	—	—	—	—	—	—	2.58	2.48	2.48	2.41	2.34	2.30	
Thickness (mils)	—	<1	<1	1	1	4	8	10	12	14	16	21	30	45	60	80	
Dep. Rate (mils/hr)	—	—	—	—	—	0.3	0.6	0.7	0.9	1.0	1.1	1.5	2.1	3.2	4.3	5.7	
002-87	—	—															
Density (g/cc)	—	—	2.16	2.16	2.16	2.17	2.17	2.18	2.18	2.17	2.17	2.18	2.19	2.20	2.20	2.20	Injector spacing is 1/2 inch greater than indicated by scan
Thickness (mils)	—	40	46	56	62	66	70	76	76	78	80	80	80	80	76	75	
Dep. Rate (mils/hr)	—	4.2	4.8	5.9	6.5	6.9	7.4	8.0	8.0	8.2	8.4	8.4	8.4	8.4	8.0	7.9	
006-22																	
Density (g/cc)	2.312	2.278	2.245	2.232	2.232	2.232	2.232	2.245	2.245	2.245	2.245	2.245	2.232	2.232	2.222	—	
SiC Concentration (%)[a]	—	—	—	—	—	—	—	—	—	—	(11)	—	10.1 (10)	—	(8)	—	
Thickness (mils)	31	50	63	80	100	113	139	179	204	211	216	218	213	206	191	—	
Dep. Rate (mils/hr)	1.9	3.1	3.9	5.0	6.2	7.1	8.7	11.2	12.8	13.2	13.5	13.6	13.3	12.9	11.9	—	
PG Matrix Density (g/cc)	—	—	—	—	—	—	—	—	—	—	(216)	—	2.17 (2.17)	—	(2.16)	—	
006-23																	
Density (g/cc)	—	2.232	2.232	2.232	2.218	2.212	2.205	2.205	2.215	2.215	2.215	2.215	2.205	2.205	2.200	—	
SiC Concentration (%)[a]	—	—	—	—	—	—	—	—	—	—	—	—	6.1 (4)	—	3.9	—	
Thickness (mils)	—	60	105	106	122	138	184	213	244	248	248	248	254	242	215	—	
Dep. Rate (mils/hr)	—	3.2	5.7	5.7	6.6	7.5	9.9	11.5	13.2	13.4	13.4	13.4	13.7	13.1	11.6	—	
PG Matrix Density (g/cc)	—	—	—	—	—	—	—	—	—	—	—	—	2.16 (2.18)	—	2.17	—	
Microstructure (Grp.)	—	—	—	—	—	—	10	—	11/21	—	11/21	—	11/21	11/21	11/21	—	
006-24																	
Density (g/cc)	—	2.255	2.245	2.232	2.205	2.195	2.195	2.195	2.195	2.205	2.205	2.205	2.200	2.195	2.195	2.190	
SiC Concentration (%)[a]	—	—	—	—	—	—	—	—	—	—	—	—	(6)	—	—	—	
Thickness (mils)	—	45	64	81	92	109	135	166	213	246	255	255	249	242	210	201	
Dep Rate (mils/hr)	—	2.8	4.0	5.1	5.8	6.8	8.4	10.4	13.3	15.4	15.9	15.9	15.6	15.1	13.1	12.6	
PG Matrix Density (g/cc)	—	—	—	—	—	—	—	—	—	—	—	—	(2.16)	—	—	—	
Microstructure (Grp.)	—	—	—	—	—	—	11/21	—	11/21	—	11/21	—	21	—	21	—	

[a]Derived from ashing data except for values in parenthese which were derived from microprobe scans

Run 006-22 was conducted after the furnace problem had been corrected and the following several other deposition runs. The target coating thickness was 200 mils and target SiC content was 10 w/o.

Post-deposition examination showed the coating to be approximately 200 mils thick for the last 8 inches of the substrate tube. The SiC concentration averaged 10 percent as desired.

Microscopic examination of polished coating samples was conducted at the 6-, 9- and 12-inch positions. At the 6-inch position the SiC phase was visible as fine, well dispersed needles within the PG cones and much larger needles in the cone boundaries. The overall microstructure classification was within the Group 11/21 range. At the 9- and 12-inch positions the SiC phase was visible as needles somewhat concentrated within the PG cone boundaries, and the overall microstructure classification was again Group 11/21. Coating microstructures for the 6-, 9- and 12-inch positions are shown in Figures 43, 44 and 45.

Samples from the 10-, 12- and 14-inch positions were subjected to electron microprobe examination. The resultant traces are shown in Figures 46, 47 and 48.

A "c" direction density profile was made at the 13-inch position by splitting the coating into thin layers and determining the individual densities of these layers. These data are compared with the electron microprobe data in Table 17. The correlation between SiC content and density is discussed in Section V.

Run 006-23 was conducted to fabricate a 5 w/o SiC containing coating with a nominal thickness of 200 mils. Deposition temperature was monitored at the deposition surface, 12 inches from the injector, and maintained at 3,200°F.

Post-deposition examination showed the coating thickness to be 200 mils or greater for the last 8 inches of the tube. Coating microstructures at the 12- and 14-inch positions are shown in Figures 49 and 50. In this area the SiC phase was visible as fine, well-dispersed, acicular needles. The overall classification of the microstructure was within the Group 11 range. Some concentration of more massive needles could be seen in the PG cone boundaries. In these areas the SiC phase was within the Group 21 range. Ashing determinations showed the SiC concentration to be 6.1 w/o 12 inches from the injector and 3.9 w/o 14 inches from the injector.

An electron microprobe trace (Figure 51) was taken at the 12-inch position and showed the SiC concentration to average 5 w/o for the first deposited 61% of the coating thickness and 3 w/o for the remainder.

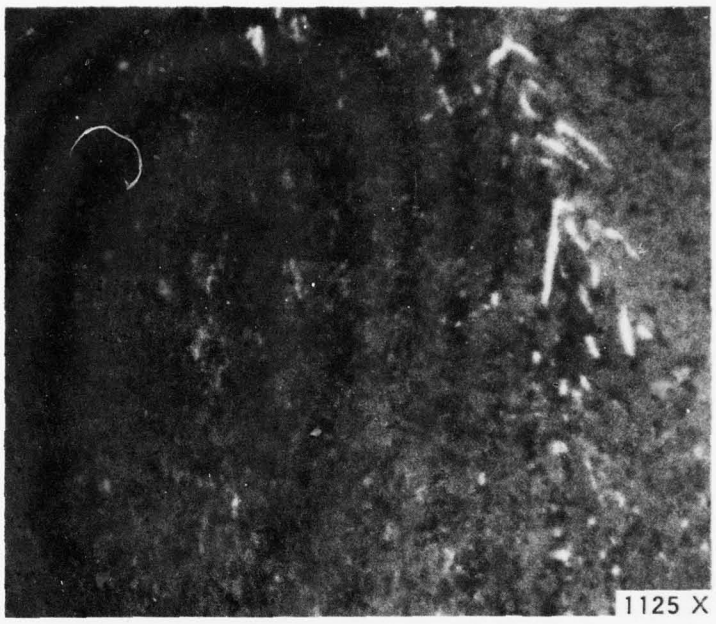

Figure 43. Run 006-22 Coating Microstructure 6 Inches From Injector.

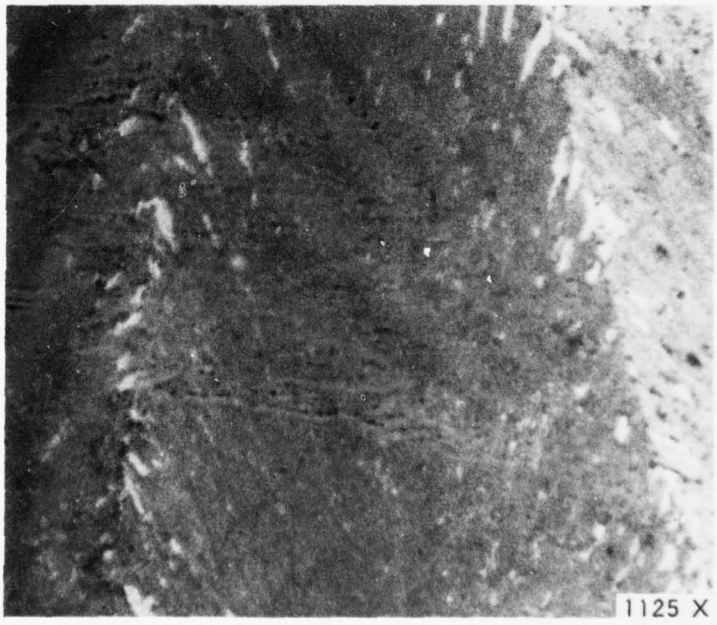

Figure 44. Run 006-22 Coating Microstructure 9 Inches From Injector.

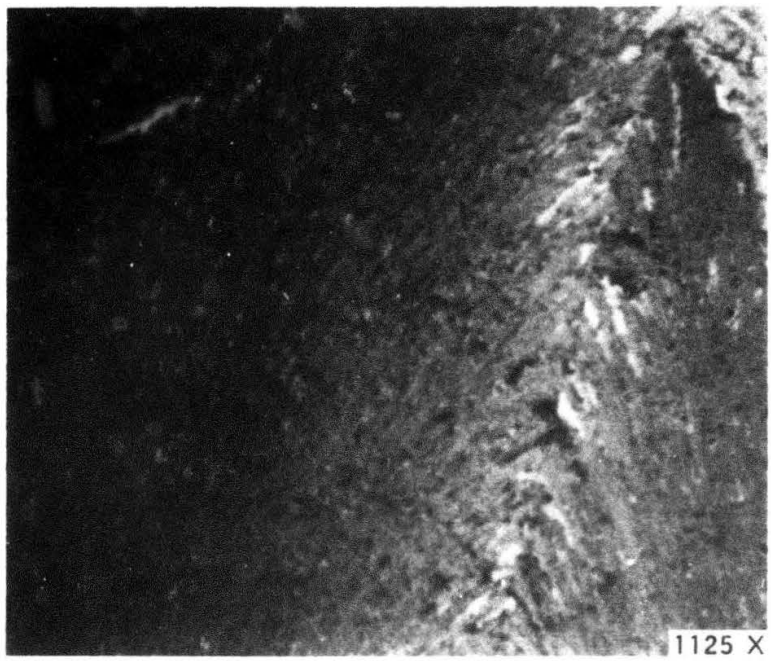

Figure 45. Run 006-22 Coating Microstructure 12 Inches From Injector.

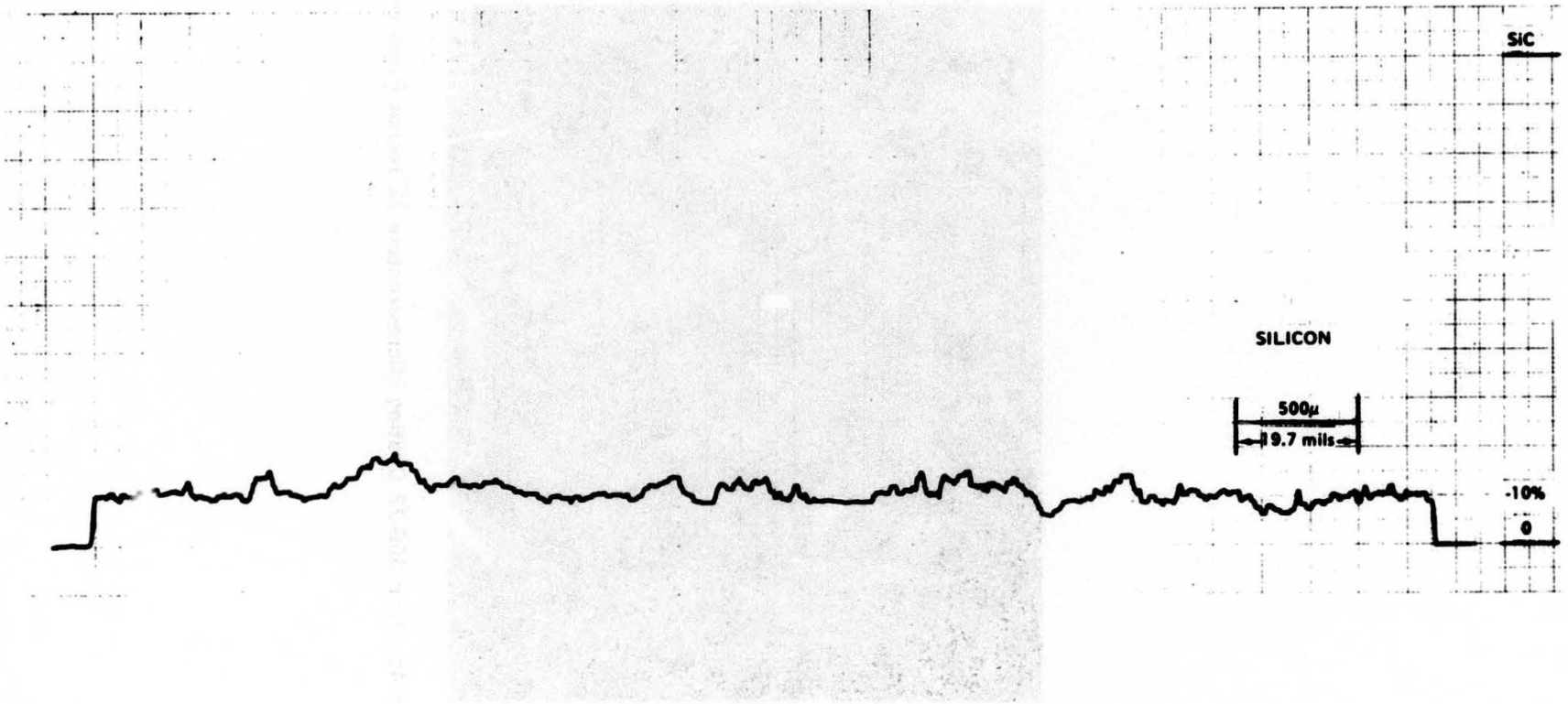

Figure 46. Electron Microprobe Scan of Coating From Run 006-22, 10 Inches From Injector.

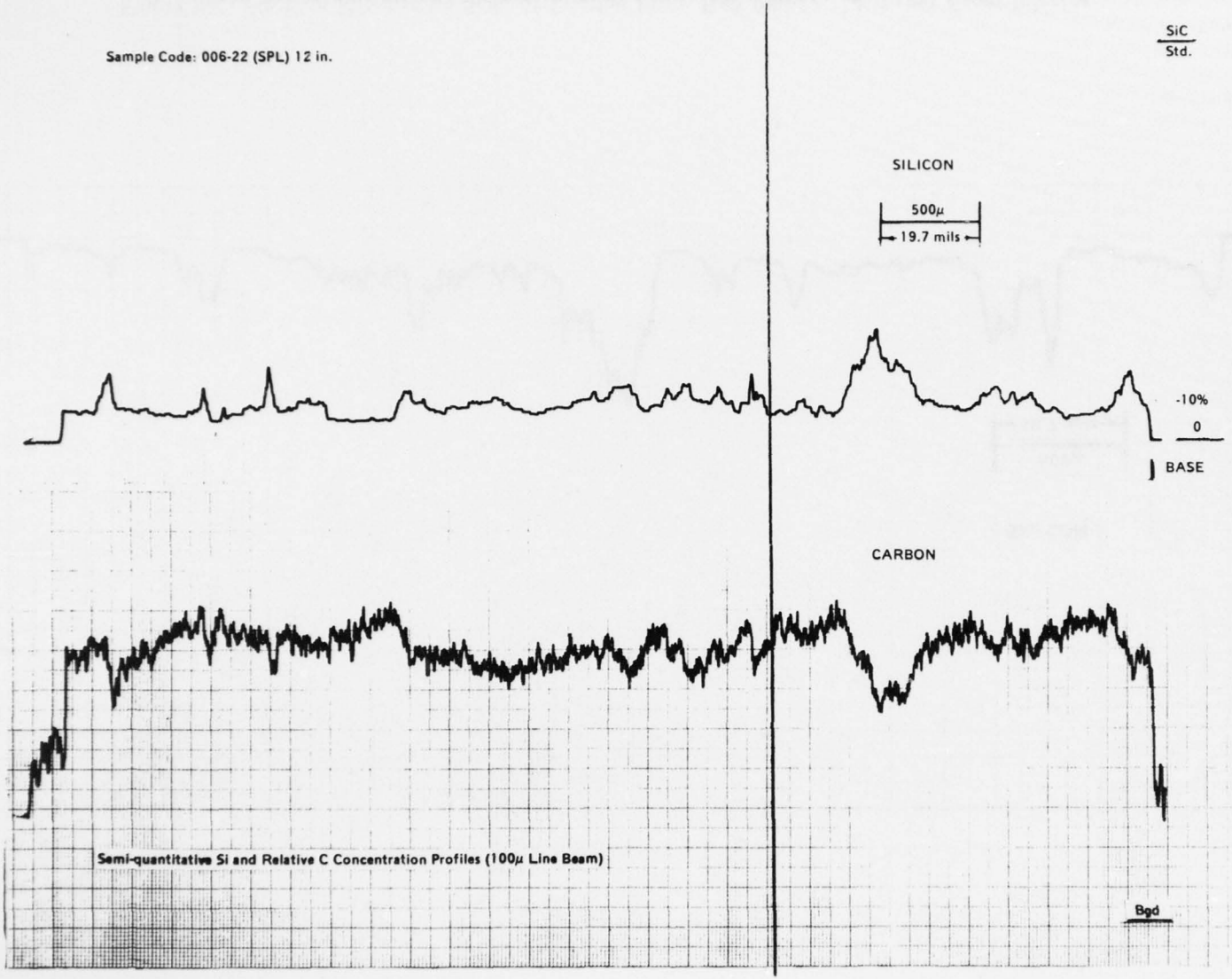

Figure 47. Electron Microprobe Scan of Coating From Run 006-22, 12 Inches From Injector.

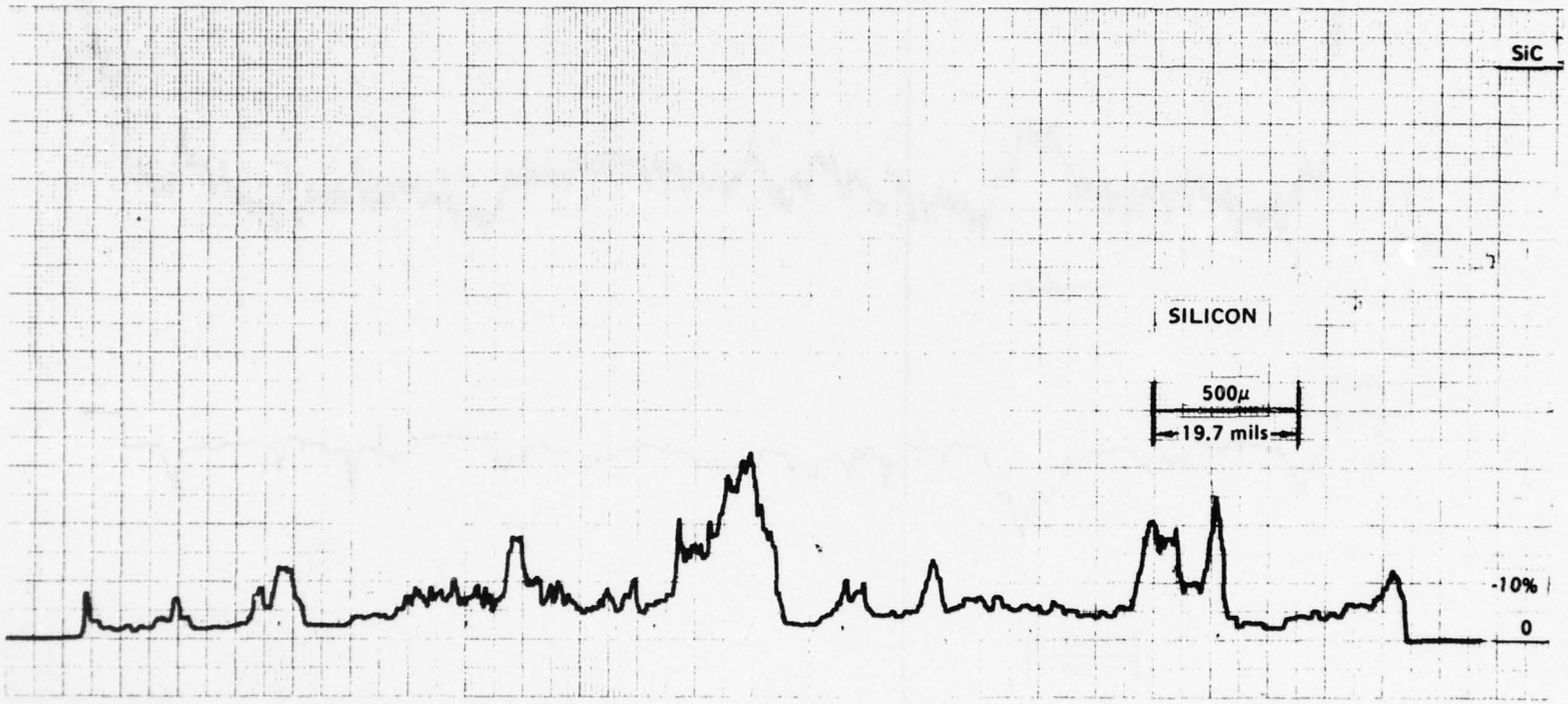

Figure 48. Electron Microprobe Scan of Coating From Run 006-22, 14 Inches From Injector.

Table 17. "C" Direction Density and SiC Concentration Profile of Coating From Run 006-22 at 13 Inches From Injector.

Distance from Substrate (mils)	Density (g/cc)	Average SiC Concentration[a] (w/o)
0-30	2.222	8
30-55	2.222	12
55-80	2.232	8
80-107	2.232	12
107-132	2.220	9
132-156	2.220	7
156-206	2.212	6

[a]Average between electron microprobe traces taken at 12 and 14 inch positions.

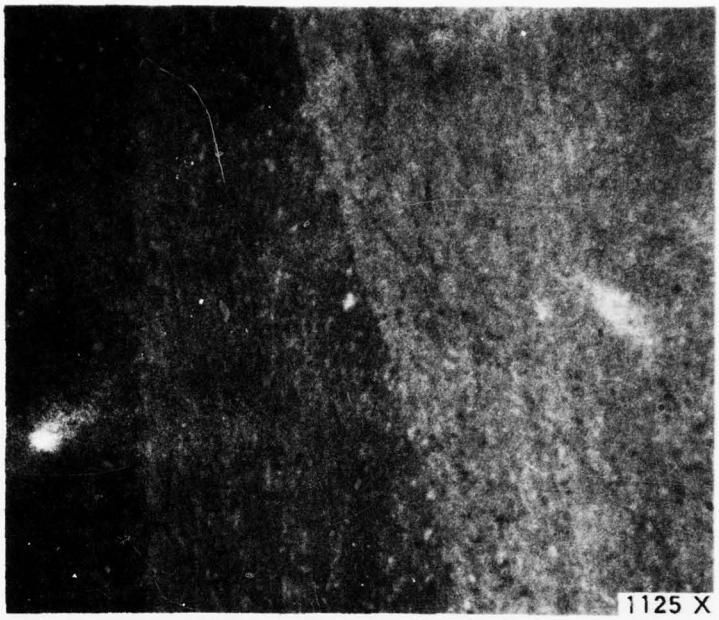

Figure 49. Run 006-23 Coating Microstructure 12 Inches From Injector.

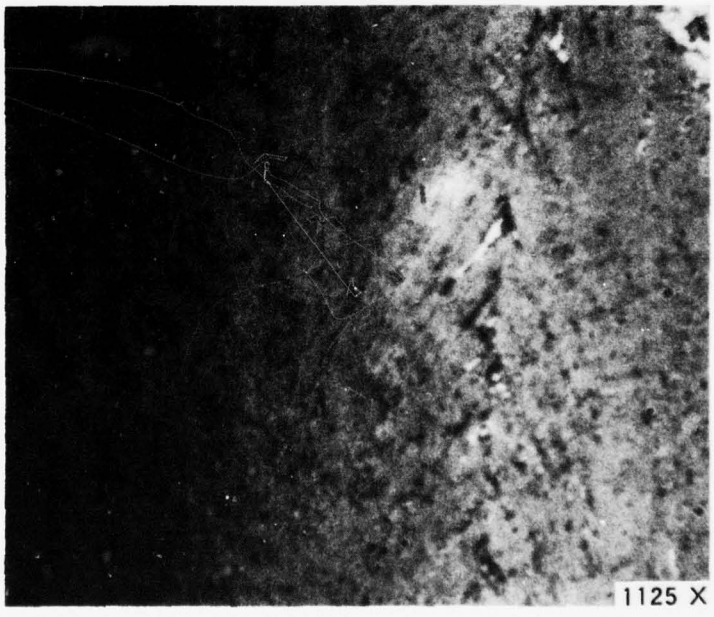

Figure 50. Run 006-23 Coating Microstructure 14 Inches From Injector.

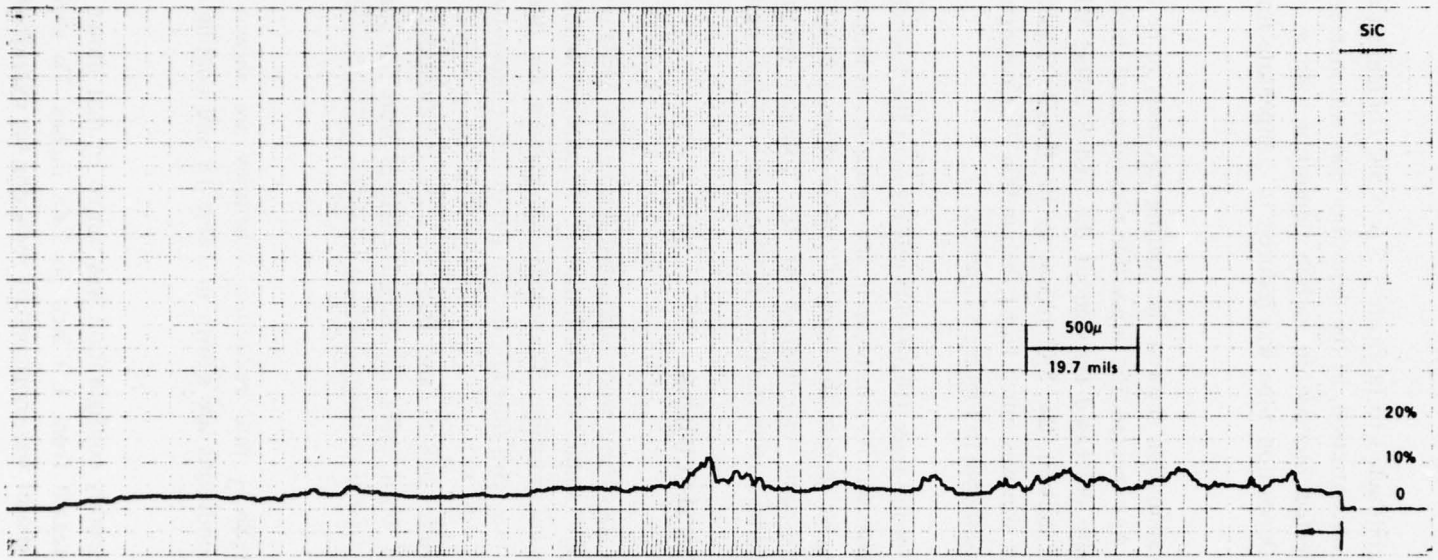

Figure 51. Electron Microprobe Scan of Coating From Run 006-23, 12 Inches From Injector.

Run 006-24 was conducted to fabricate a 5 w/o SiC containing coating, 200 mils thick at 3,300°F. The CH_3SiCl_3 concentration, in the deposition gas, was increased from that of 006-23 to compensate for the expected increase in carbon deposition rate as a result of the increased deposition temperature. Deposition time was reduced to compensate for the expected increase in deposition rate.

Post-deposition examination showed the coating thickness to be 200 mils or greater for the last 7 inches of the tube. As expected, the deposition rate increased throughout the last 7 inches of the tube. However, the rate decreased throughout the first 8 inches which was not anticipated. Microscopic examination showed the SiC phase to be heavily concentrated in the PG cone boundaries and the crystal size was much larger than in 006-23. Coating microstructures 12 and 14 inches from the injector are shown in Figures 52 and 53.

An electron microprobe trace (Figure 54) was taken at the 12-inch position and showed the SiC concentration to average 6%. As can be seen, the variations in indicated SiC concentration are much more severe than those seen in the trace of 006-23 (Figure 51). This agrees with the visual observations during microscopic examination of the polished coatings during which heavy concentrations of SiC could be seen in the PG cone boundaries of the coating fabricated at 3,300°F.

2. THERMAL STRESS SPECIMENS

Six thermal stress specimens were fabricated during the AFRPL Graded Coating Program. The graded coatings were made by continuously increasing deposition temperature while maintaining constant gas composition. The coatings deposited for this program were made by decreasing CH_3SiCl_3 flow rate with time at constant deposition temperature.

Two deposition runs, 008-11 and 008-23, were conducted to fabricate specimens for thermal stress testing. In both cases the target coatings were 80 mils thick. The target SiC concentration was 15 w/o at the coating/substrate interface graded linearly to 0 w/o at the coating surface.

The nominal CH_3SiCl_3 rate reduction schedules are shown in Figures 55 and 56. Nonvariable deposition conditions are shown in Table 18 and coating characterization data are shown in Table 19.

The deposition assembly configuration was similar to that shown in Figure 4, page 9. The substrate length was increased from 1.0 inch to 2.65 inches. To accommodate the increased substrate length, the exit spacer was shortened by removing the cylindrical upstream portion so the

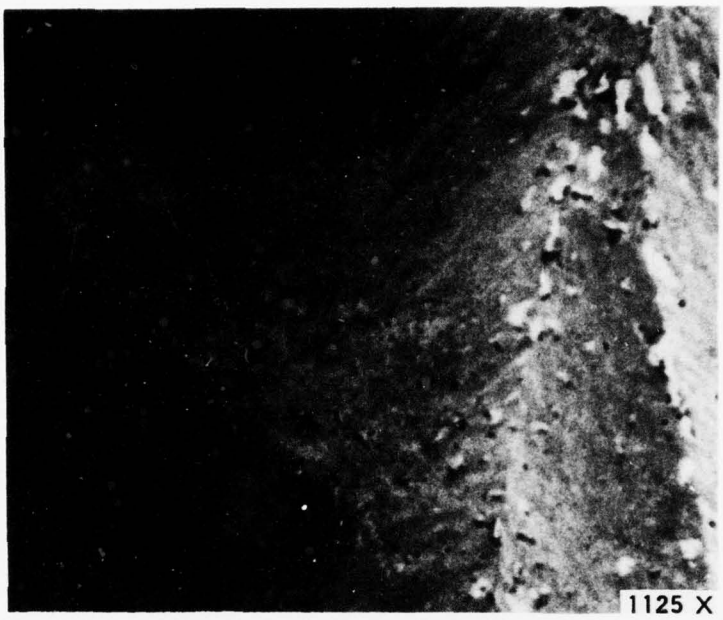

Figure 52. Run 006-24 Coating Microstructure 12 Inches From Injector.

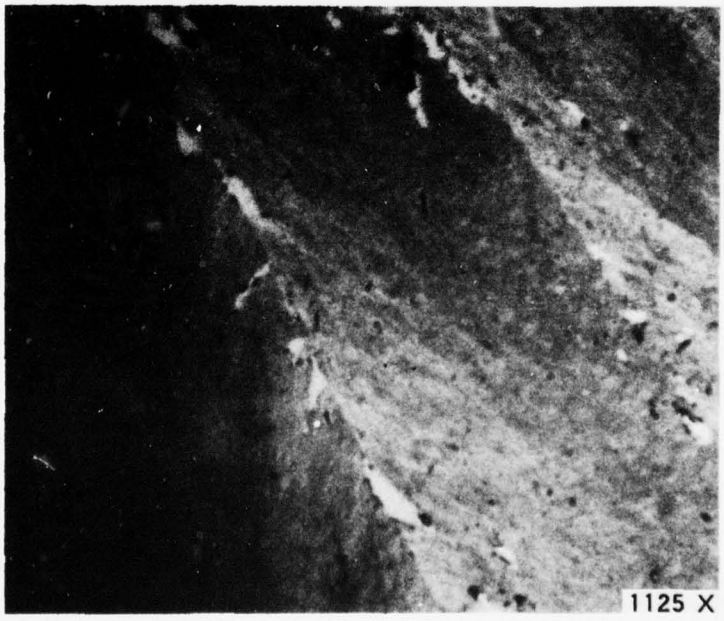

Figure 53. Run 006-24 Coating Microstructure 14 Inches From Injector.

Figure 54. Electron Microprobe Scan of Coating From Run 006-24, 12 Inches From Injector.

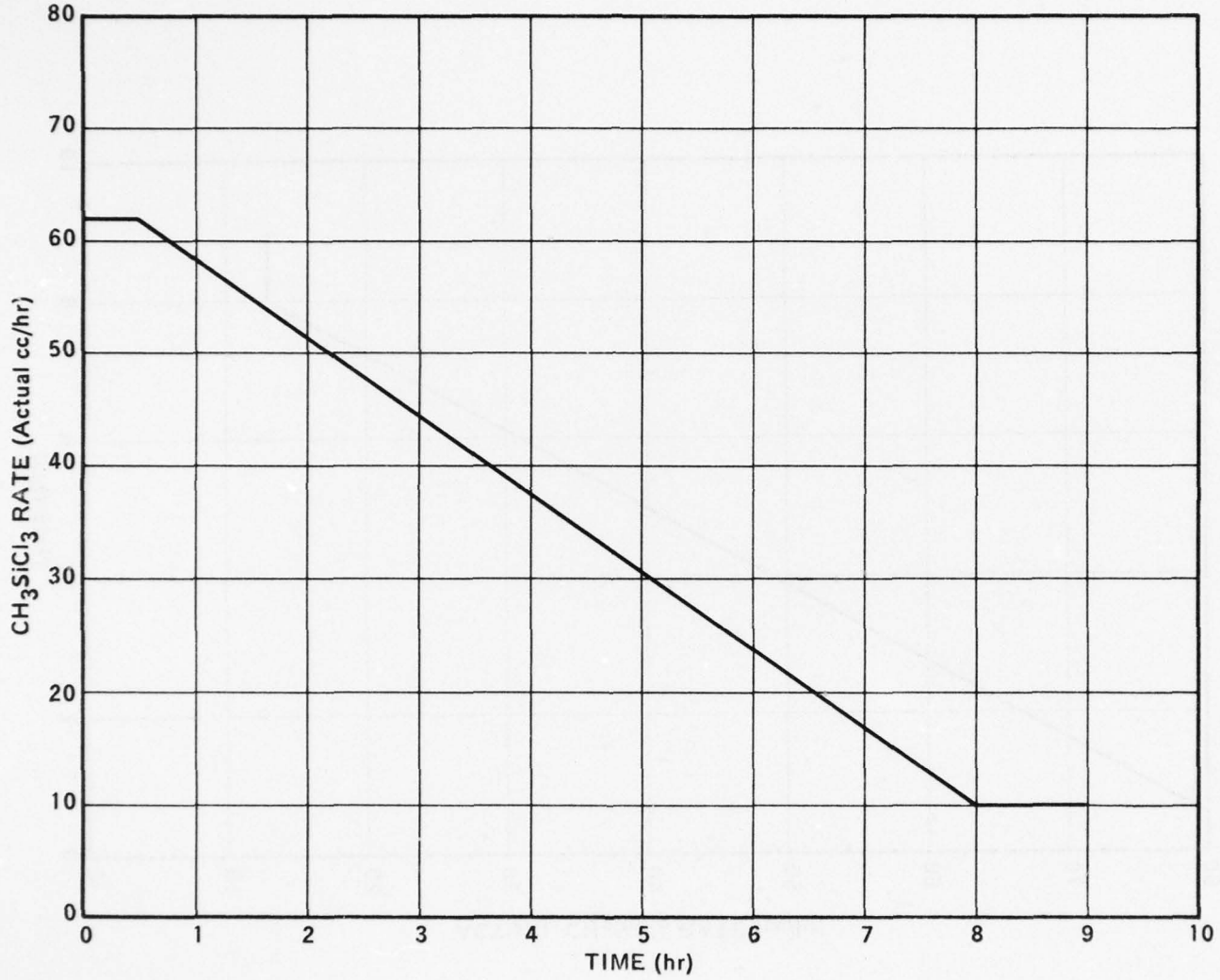

Figure 55. Nominal CH_3SiCl_3 Rate vs. Time for Run No. 008-11.

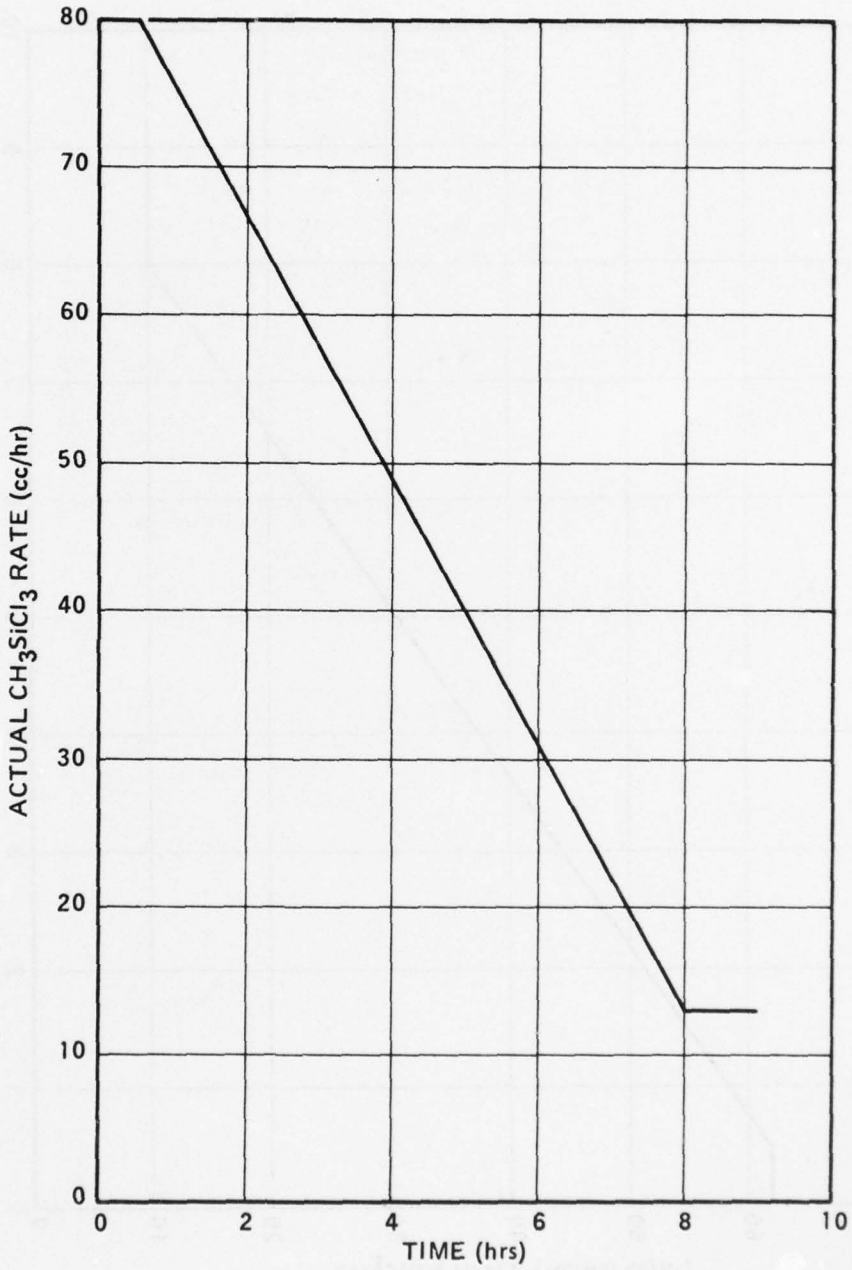

Figure 56. Nominal CH_3SiCl_3 Rate vs. Time for Run No. 008-23.

Table 18. Deposition Conditions for Thermal Stress Specimen Coating Runs.

Deposition Run No.	Carrier N_2 (SCFH)	Annulus N_2 (SCFH)	Total Process Gas (SCFH)	CH_4 (vol. percent)	MTS (vol. percent)	MTS/CH_4	Deposition Temperature (°F)	Deposition Time (hr)
008-11	296	15	315	1.14	0.132/0	0.116/0	3195^{+15}_{-15}	9
008-23	450	15	471	1.17	0.134/0.021	0.115/0.018	3200^{+30}_{-45}	9

Table 19. Coating Characterization Data for Therma Stress Specimens.

Run No.	Coating Thickness (mils)		Thickness of SiC Containing Zone (mils)[a]		Coating Appearance
	Entr. End	Exit End	Entr End	Exit End	
008-11	81	78	59	45	Entr. End - SiC visible mostly in cone boundaries as string-like growths and acicular needles. Unalloyed zone contains many intraconical delaminations.
					Exit End - Similar to entrance except SiC dispersion somewhat better.
008-23	108	99	88	45	Entr. End - Coating contains one major delamination 6-mils from substrate and extending for 350°, circumferentially. SiC phase in Group 11 category where visible. Dispersion is much better than in 008-11. However, concentration appears to be lower. Unalloyed zone contains many intraconical delaminations.
					Exit End - Coating contains one short discontinuous delamination 6-mils from substrate and extending for 30° circumferentially. Microstructure similar to entrance end.

[a]Determined by examining polished coating ends microscopically at 800X.

short, tapered section was adjacent to the substrate. This accommodated 1.0 inch of the additional substrate length. The remaining 0.65 inch was accommodated by shortening the entrance spacer. The injector was positioned 6 1/4 inches from the substrate entrance end. Deposition temperature was recorded on the coating surface approximately 1.0 inch from the substrate upstream end.

At the beginning of the deposition cycle, 008-11 was conducted using the same deposition gas flow rates as 006-10. The CH_3SiCl_3 rate reduction was started after 1/2 hour of deposition and continued until 8 hours into the cycle when it reached zero. No CH_3SiCl_3 was introduced for the last hour of the deposition cycle.

Post-deposition examination of the polished coating ends showed the SiC phase to be heavily concentrated in the cone boundaries. At 1125X the SiC phase appeared to be absent in the last 20 to 30 mils of the coating thickness. In this area there were many intraconical delaminations which increased in frequency with increasing coating thickness. No extensive cracks or delaminations were present. Photomicrographs of the coating ends are shown in Figures 57 through 64.

Run 008-23 was conducted utilizing approximately 50 percent higher carrier and precursor gas flow rates. The higher overall rates were expected to reduce preheating of the deposition gas. In the past, this procedure has improved the quality and dispersion of the SiC phase in the coating. The CH_3SiCl_3 rate was never reduced to zero in an attempt to maintain a slight amount of SiC in the coating.

Post-deposition examination of the polished coating ends showed both to contain extensive delaminations near the coating/substrate interface. The increased gas flow rates produced the desired coating microstructure, but the SiC concentration appeared to be lower than that of the previous run. The increased gas flow rates also increased the average deposition rate by 30 percent. Photomicrographs of the coating ends are shown in Figures 65 through 72.

3. EROSION TEST SPECIMENS

Five deposition runs, 008-9, 008-12, 008-20, 008-22 were conducted to fabricate homogeneous, low SiC content coatings for erosion testing.

The target coated specimen configuration, shown in Figure 73, utilized ATJ graphite as the substrate material.

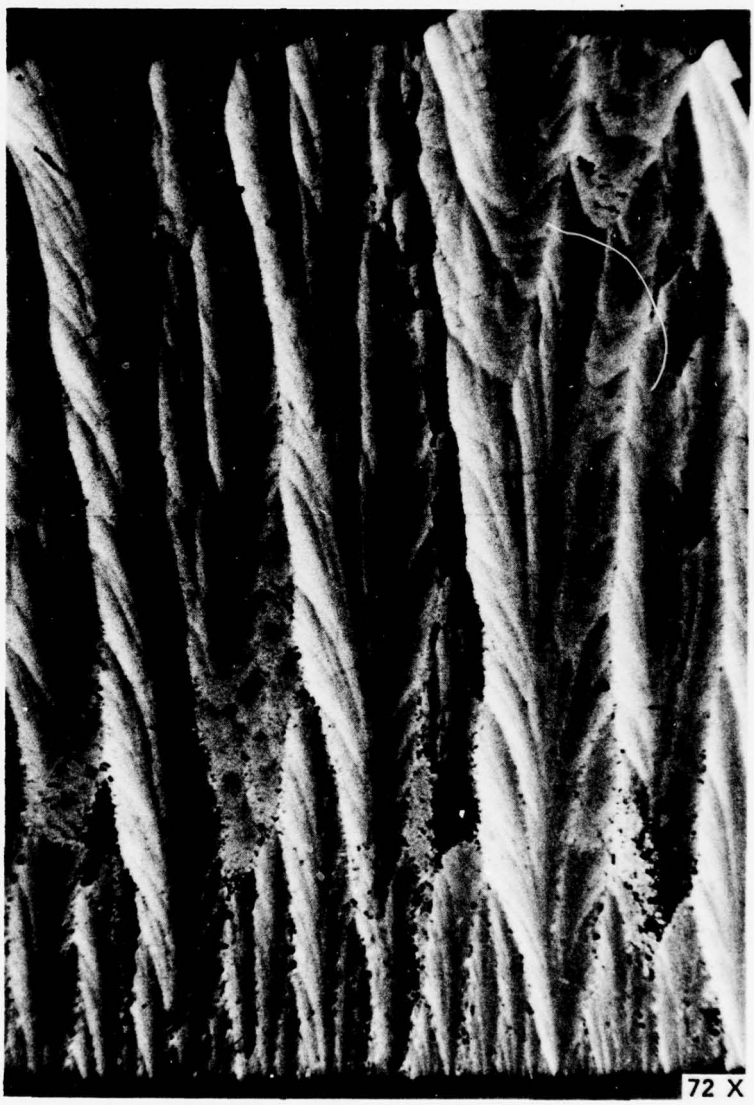

Figure 57. Run 008-11, Entrance End, Coating Microstructure (Full Thickness).

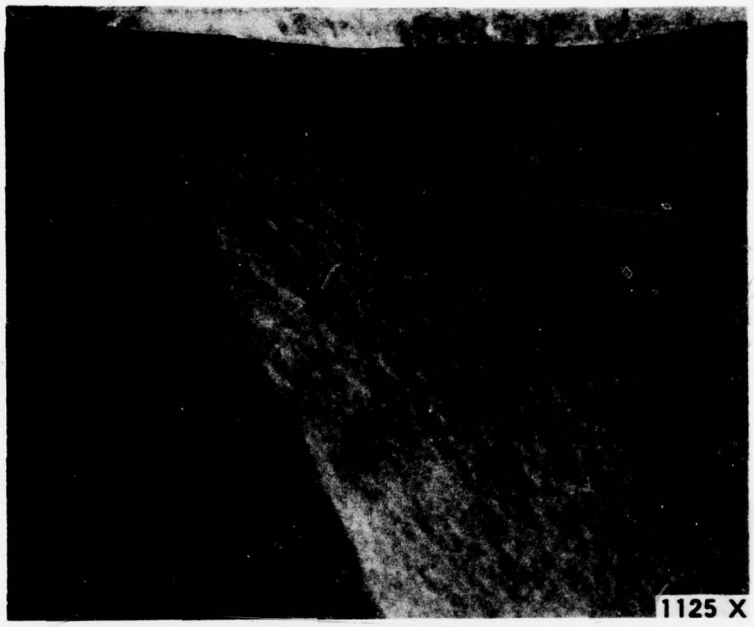

Figure 58. Run 008-11, Entrance End, Coating Microstructure Near Coating Surface.

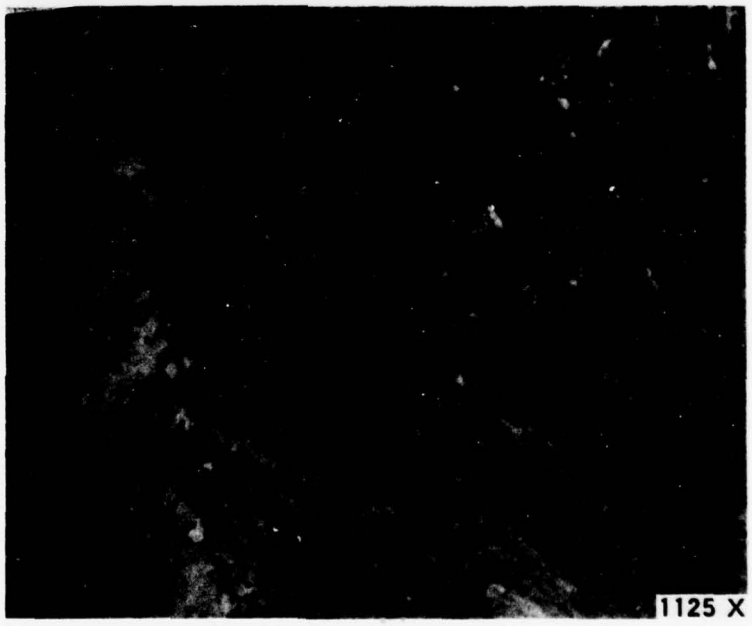

Figure 59. Run 008-11, Entrance End, Coating Microstructure At Coating Mid-Thickness.

Figure 60. Run 008-11, Entrance End, Coating Microstructure Near Substrate.

Figure 61. Run 008-11, Exit End, Coating Microstructure (Full Thickness).

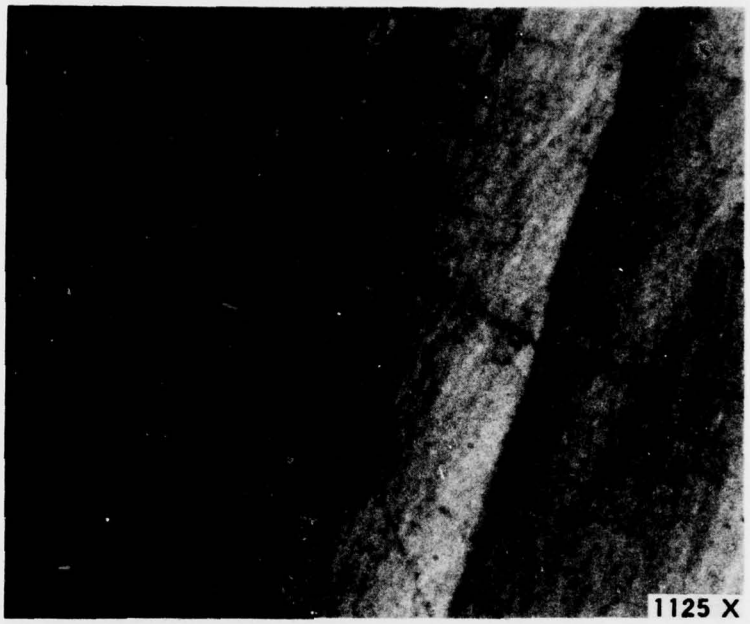

Figure 62. Run 008-11, Exit End, Coating Microstructure Near Coating Surface.

Figure 63. Run 008-11, Exit End, Coating Microstructure At Coating Mid-Thickness.

Figure 64. Run 008-11, Exit End, Coating Microstructure Near Substrate.

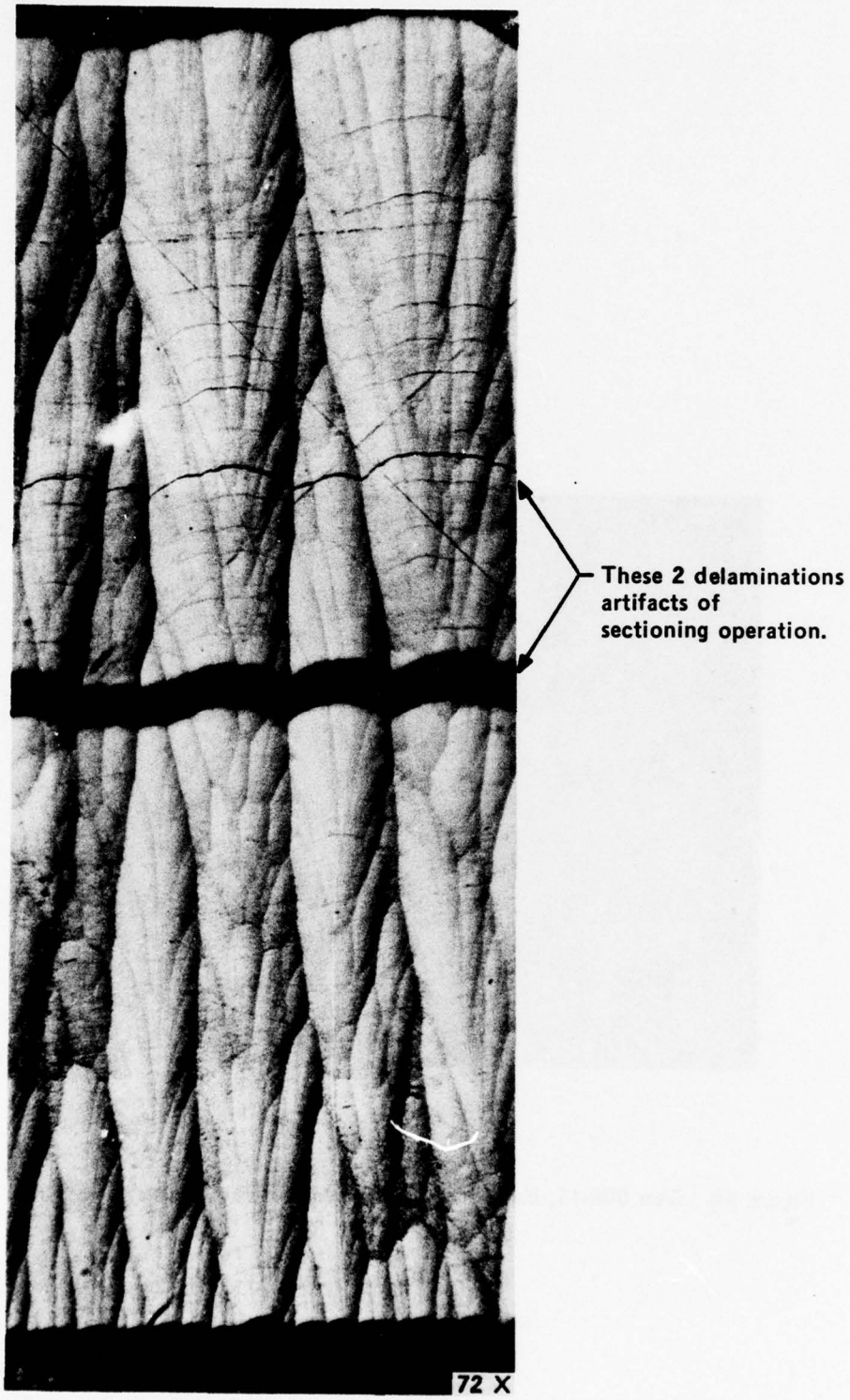

Figure 65. Run 008-23, Entrance End, Coating Microstructure (Full Thickness).

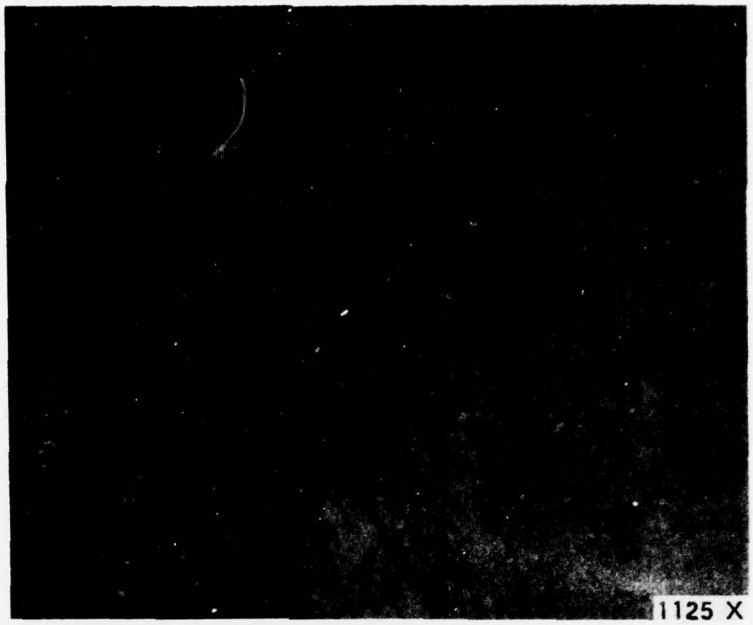

Figure 66. Run 008-23, Entrance End, Coating Microstructure Near Coating Surface.

Figure 67. Run 008-23, Entrance End, Coating Microstructure At Coating Mid-Thickness.

Figure 68. Run 008-23, Entrance End, Coating Microstructure Near Substrate.

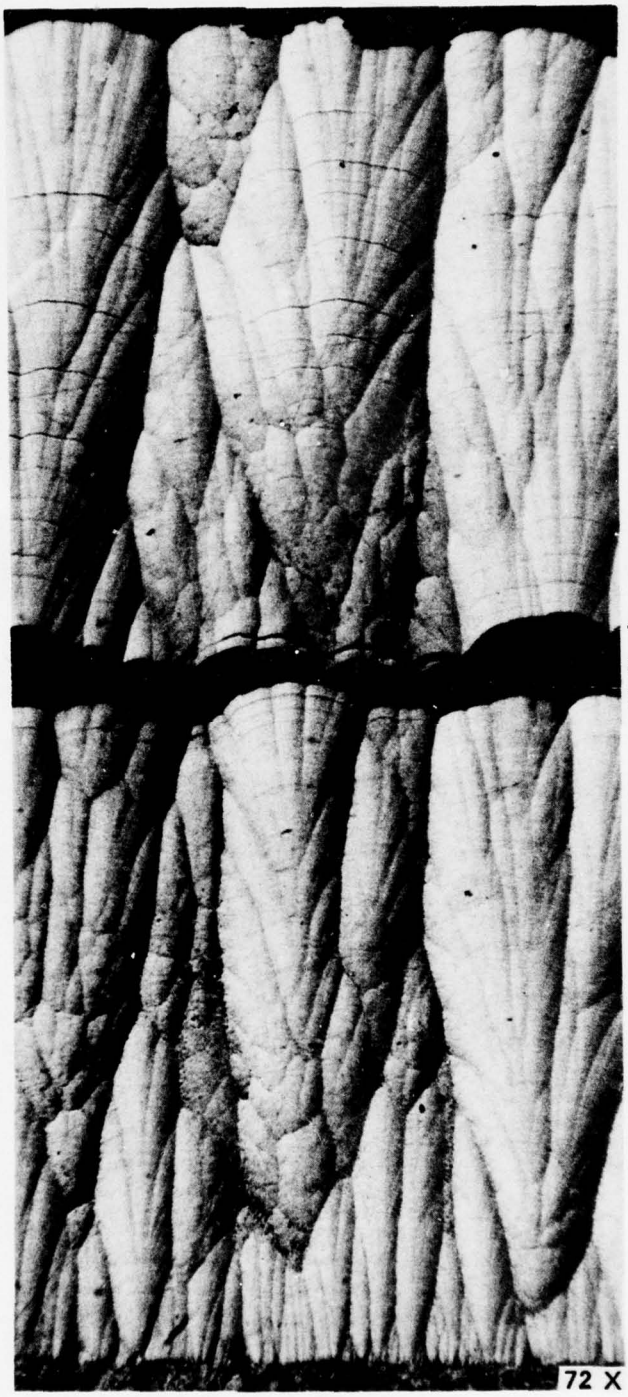

Figure 69. Run 008-23, Exit End, Coating Microstructure (Full Thickness).

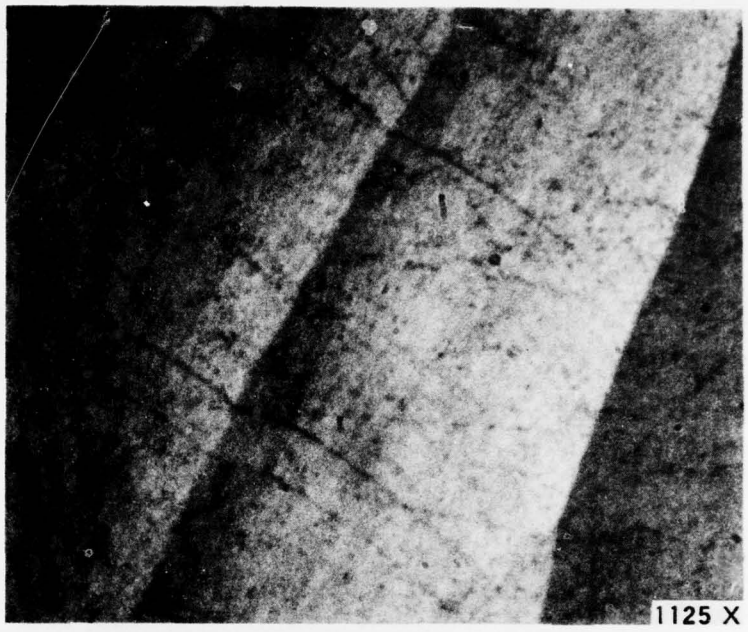

Figure 70. Run 008-23, Exit End, Coating Microstructure Near Coating Surface.

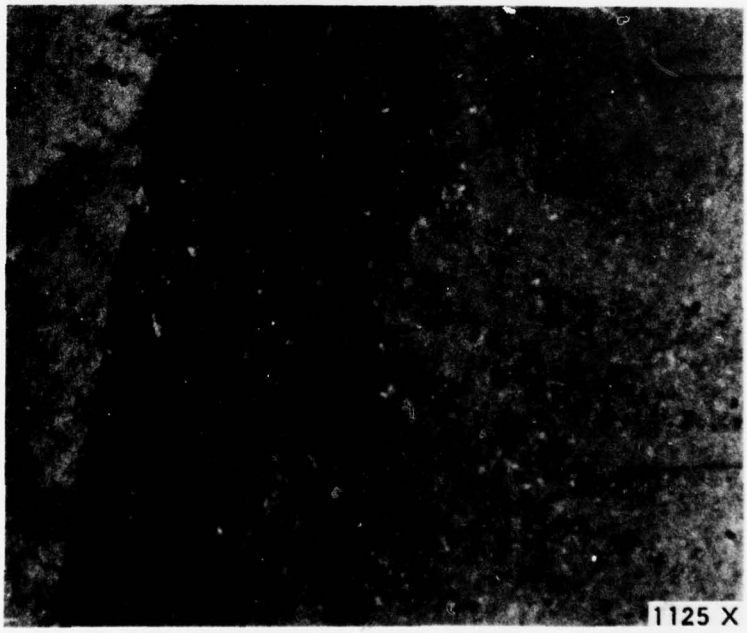

Figure 71. Run 008-23, Exit End, Coating Microstructure at Coating Mid-Thickness.

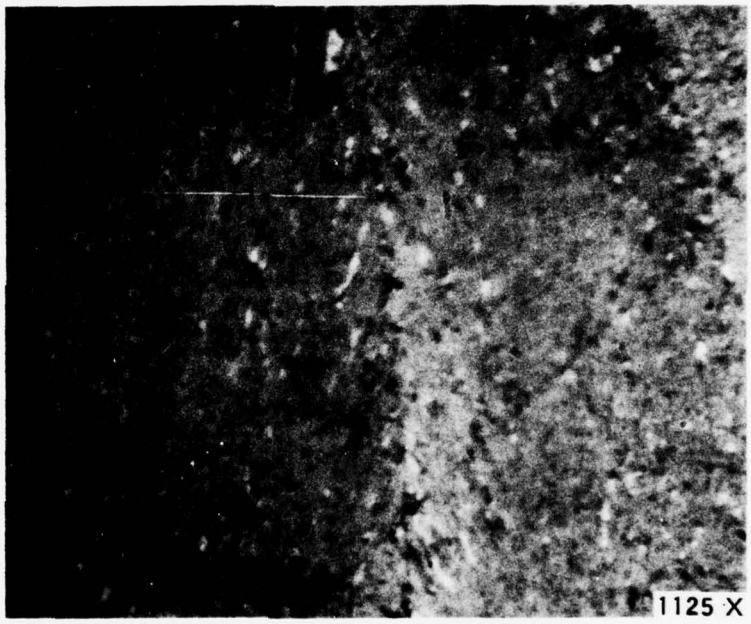

Figure 72. Run 008-23, Exit End, Coating Microstructure Near Substrate.

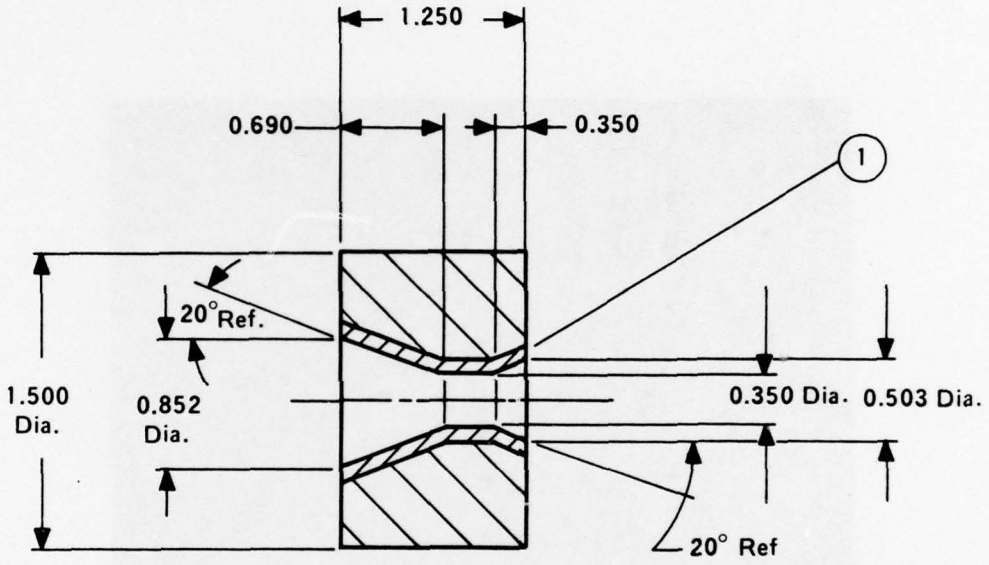

(1) 15 percent SiC Modified Pyrolytic Graphite

Figure 73. Coated Erosion Test Specimen Configuration.

Coating deposition conditions are shown in Table 20 and coating characterization data are shown in Table 21.

Four substrates were coated simultaneously in each run. This was accomplished by mounting the four parts in holes drilled on a 2.5-inch bolt circle in a graphite plate. This plate was held in a 4.5-inch diameter tubular graphite chamber and spaced 13 3/4 inches from the injector. The injector configuration was the same as that used in the 3.5-inch tubular deposition runs.

Coating characterization was conducted by axially sectioning one part from each run and removing samples for sink/float density measurements and by polishing and examining microscopically a polished axial cross section of the coating at magnifications up to 1772X.

The first two runs, 008-9 and 008-12, were conducted with a target coating thickness of 100+ mils and a target SiC concentration of 6 to 8 w/o.

The nominal deposition temperature measured on the substrate holding plate backside was 3,200°F. Post-deposition density measurements of the coating fabricated during Run 008-9 indicated that the SiC concentration was approximately twice as high as desired. The coating microstructures achieved are shown in Figures 74, 75 and 76 and are considered to be typical of PG/SiC deposited at a temperature of 3,200°F. The SiC concentration appears to be much higher at the entrance end than at the throat and exit areas. Additionally, the SiC crystals are considerably more massive at the entrance end.

The next run, 008-12, was conducted at a CH_3SiCl_3 concentration half that of 008-9.

Post-deposition examination of the coating from 008-12 showed a definite reduction in density indicating a reduction in SiC concentration had occurred. A reduction in SiC concentration was also apparent when examining the polished ends of the coating microscopically. Photomicrographs of the coating, shown in Figures 77, 78 and 79, show the SiC phase to be smaller in crystal size and more evenly dispersed than in the previous run. The reduced CH_3SiCl_3 rate also caused a reduction of 18 percent in the average coating deposition rate and reduced the size of the SiC crystals. The reduction in SiC concentration apparently modified the CTE of the coating so that the coating/substrate CTE mismatch was now high enough to induce excessive stresses in the coating as evidenced by two coating delaminations which occurred.

The last three deposition runs, 008-20, 008-21 and 008-22, were conducted with a target coating thickness of 40 mils to lower the stresses within the coating and reduce the likelihood of delaminating.

Table 20. Coating Deposition Conditions for Erosion Test Specimen Deposition Runs.

Deposition Run No.	Carrier N_2 (SCFH)	Annulus N_2 (SCFH)	Total Process Gas (SCFH)	CH_4 (vol. percent)	MTS (vol. percent)	MTS/CH_4	Deposition Temperature (°F)	Deposition Time (hr)	Comments
008-9	953	15	981	1.22	0.078	0.064	*3190 $^{+30}_{-35}$	10	Momentary power loss at 7 1/2 hours caused temperature fall to 3120°F, briefly.
008-12	953	15	980	1.22	0.039	0.032	3195 $^{+15}_{-20}$	10	
008-20	953	15	980	1.22	0.031	0.025	3200 $^{+30}_{-30}$	4	
008-21	953	15	980	1.22	0.039	0.032	3300 $^{+25}_{-30}$	4	
008-22	953	15	980	1.22	0.039	0.032	3305 $^{+30}_{-25}$	4	

*Excluding temperature drop during momentary power loss.

Table 21. Coating Characterization Data for Erosion Test Specimens.

Deposition Run No.	Average Coating Thickness (mils)			Coating Density (g/cc)[a]			Coating Microscopic Appearance
	Entr.	Throat	Exit	Exit	Throat	Exit	
008-9	142	143	85	2.25	2.23	2.18	No visible cracks or delaminations. In entrance area SiC phase visible as medium sized acicular needles, well dispersed, with a slight tendency to cluster in cone boundaries (Group 21). At throat area and exit end SiC Group 11 with dispersion much poorer with most visible SiC phase in cone boundaries.
008-12	112	121	70	2.225	2.210	2.200	Coating contains two delaminations visible in axial cross-section; one very near substrate and other in mid-thickness. SiC phase fine and evenly dispersed (Group 10).
008-20	23	39	28	2.220	2.215	2.210	Coating contains one delamination visible in axial cross-section very near substrate and extending from forward end of throat to exit end of specimen. SiC phase fine and evenly dispersed (Group 5), throughout.
008-21	38	52	30	2.185	—	2.175	Coating debonded from substrate at radius in aft end of throat. No other cracks or delaminations. SiC phase fine and evenly dispersed (Group 5) throughout.
008-22	34	49	32	2.222	—	2.210	Same as 008-21.

[a]One specimen from each run sampled.

Figure 74. Run 008-9 Coating Microstructure At Entrance End.

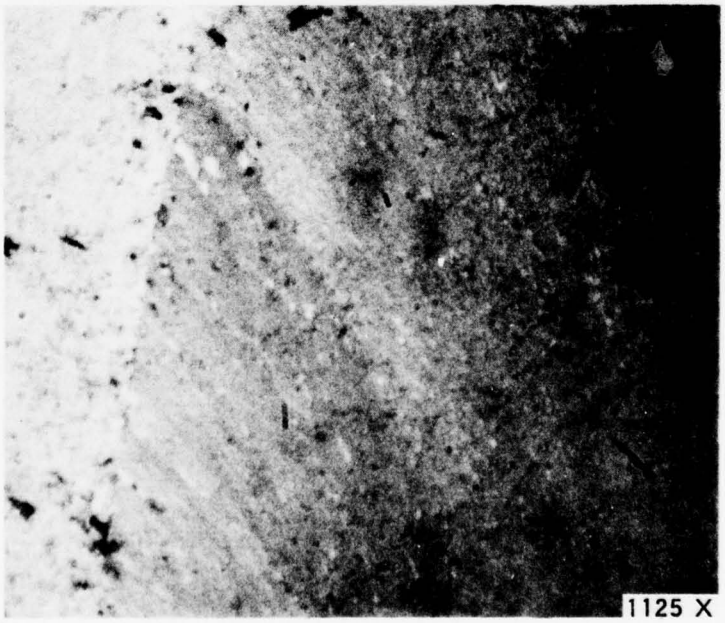

Figure 75. Run 008-9 Coating Microstructure At Throat.

Figure 76. Run 008-9 Coating Microstructure At Exit End.

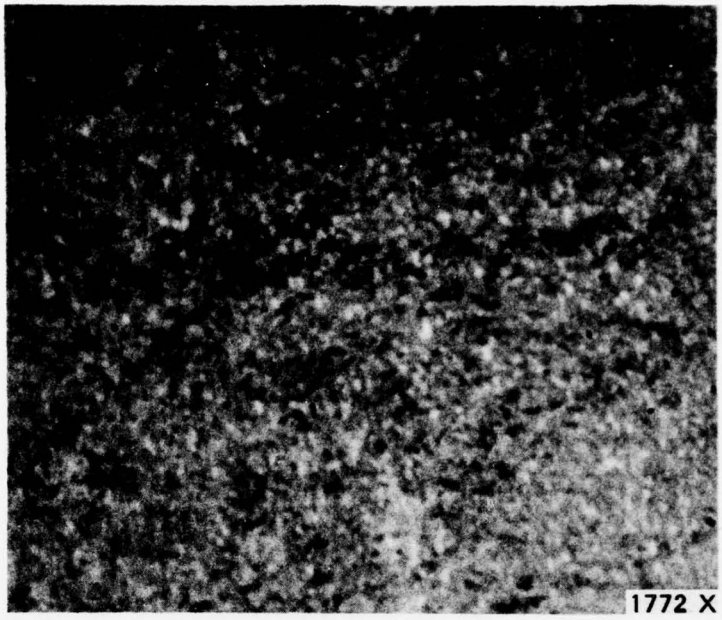

Figure 77. Run 008-12 Coating Microstructure At Entrance End.

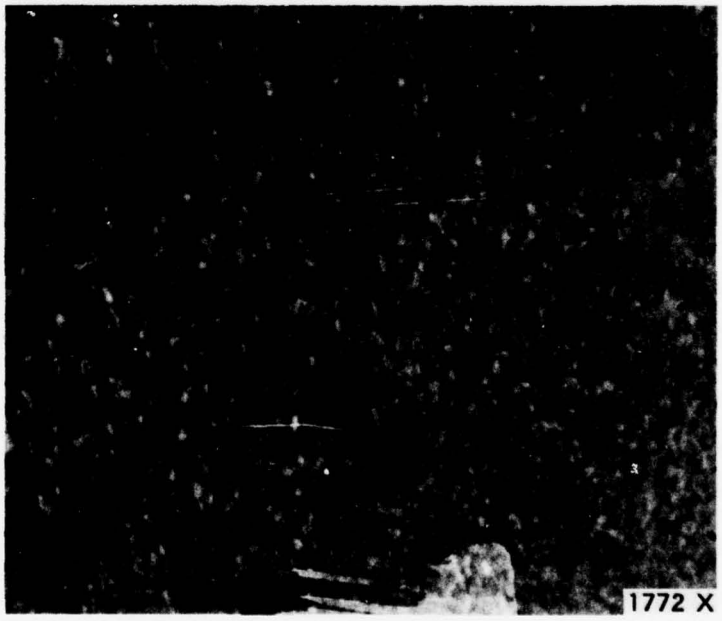

Figure 78. Run 008-12 Coating Microstructure At Throat.

Figure 79. Run 008-12 Coating Microstructure At Exit End.

Run 008-20 was conducted at a slightly lower CH_3SiCl_3 rate than 008-12 to reduce the SiC concentration further; otherwise, the deposition conditions were similar.

Post-deposition examination indicated that the coating from 008-20 was of a lower SiC concentration than that of 008-12, as expected. The coating microstructure, shown in Figures 80, 81 and 82, was similar to that of 008-12 and, again, the coating delaminated. The microstructures achieved in both Runs 008-12 and 008-20 were indicative of a deposition temperature lower than the desired 3,200°F. In both cases, the SiC phase was extremely fine and well dispersed and showed no tendency to cluster in the PG cone boundaries as in the first coating of this series deposited during Run 008-9. Steps were taken in the last two deposition runs of this series to assure that a coating deposition temperature of 3,200°F was achieved.

Runs 008-21 and 008-22 were both conducted using the deposition gas flow rates of Run 008-12. Prior to introducing the precursor gases, the temperature of the substrate exit end was monitored through the furnace exhaust gas tube. When the substrate holding plate temperature was held at 3,300°F, the substrate exit end temperature was 3,220°F. Since the previous deposition runs were made at a holding plate temperature of 3,200°F, it is likely that the substrate exit end temperature was close to 3,120°F. The substrate throat and entrance ends would have been somewhat less than 3,120°F. Apparently, the sight port was viewing the substrate holding plate between the heated furnace walls and the specimen location. In this area the temperature was 80°F higher than at the substrate. This strongly indicated that Run 008-20 was conducted at a lower coating surface deposition temperature than desired. Rather than try to realign the sight port, the nominal deposition control temperature was increased from 3,200 to 3,300°F for these last two runs. With the addition of the reaction endotherm, when the precursor gases are introduced, this temperature would yield a coating surface deposition temperature very close to 3,200°F.

Post-deposition examination of the coating microstructures from 008-21 and 008-22, Figures 83 through 86, showed them to be similar to those from Runs 008-12 and 008-20. Although no effect of increasing the deposition temperature could be seen in the coating microstructure no serious delaminations occurred, indicating that the coating was more compatible with the substrate than in 008-12 and 008-20. A short debond was visible between the coating and the substrate at the radius where the throat breaks into the tapered conical exit section of the substrate. However, it is likely that this was an artifact of the sectioning operation rather than an inherent defect. The increased coating/substrate compatibility probably represents a change in the PG matrix properties rather than any change in the SiC phase.

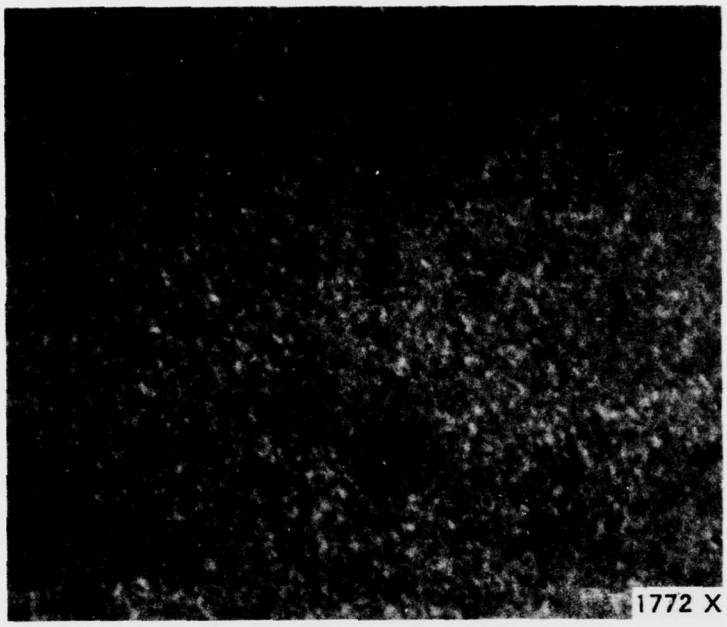

Figure 80. Run 008-20 Coating Microstructure At Entrance End.

Figure 81. Run 008-20 Coating Microstructure At Throat.

Figure 82. Run 008-20 Coating Microstructure At Exit End.

Figure 83. Run 008-21 Coating Microstructure At Entrance End.

Figure 84. Run 008-21 Coating Microstructure At Exit End.

Figure 85. Run 008-22 Coating Microstructure At Entrance End.

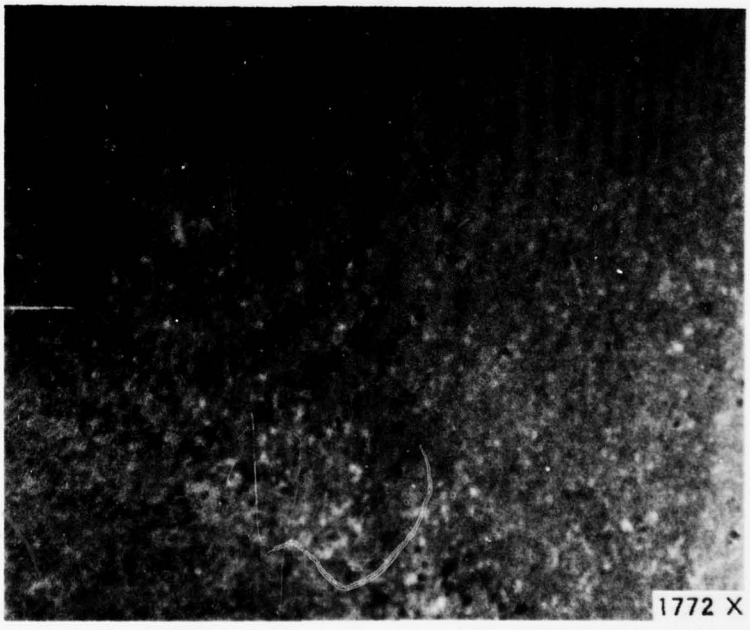

Figure 86. Run 008-22 Coating Microstructure At Exit End.

SECTION V

MATERIALS CHARACTERIZATION PROCEDURES

The coatings deposited during this program were routinely characterized with respect to density, morphology, and SiC content. In additon selected thermal/mechanical properties were determined using material specifically deposited for this purpose. The following sections discuss the characterization techniques employed and describe the results of the properties measurements.

1. PHYSICAL PROPERTIES

a. Density

Coating bulk density was determined using the sink/float technique on small coating samples extracted at the desired position. The density fluids were supplied by Cargille Laboratories, Inc., and were calibrated by suspending skin/float standards, also supplied by Cargille, in the fluids. With extreme care density could be determined within ±0.005 g/cc. However, in most cases, accuracy within ±0.01 g/cc was considered to be adequate.

b. Morphology

Coating microstructures were examined by potting and micropolishing "c" direction coating specimens extracted from the desired location. The specimens were first ground on a series of silicon carbide abrasive papers. Grit No. 240, 320, 400 and 600 were normally used. Water was used to carry away removed material and to lubricate the grinding surface. After grinding, the insert was diamond polished. Oil and/or water was used as a lubricant during the polishing process. A 6-micron diamond final polish was usually sufficient to provide clear microscopic observation. This polish was often improved by use of a 1-micron diamond paste.

The polished specimens were examined on a Zeiss inverted standard metallurgical microscope at magnifications of up to 1772X. A light polarizer was used to enhance contrast between the PG matrix and the SiC crystals. Determination of SiC crystal diameters and lengths were made by the use of a linear reticule placed in the microscope optics which superimposes the scale on the observed material.

A cataloging system was utilized to identify and group the various types of microstructures encountered in the program. This system, which is shown in Table 22, is based on

Table 22. Description of Various PG/SiC Coating Microstructural Groups.

Group 5	SiC phase very fine, evenly dispersed, acicular needles less than 0.010 mil diameter with an L/D ratio greater than 3/1.
Group 6	Similar to Group 5 with SiC phase showing a tendency to cluster in the PG cone boundaries.
Group 10	SiC phase fine, evenly dispersed, acicular needles to 0.010 to 0.035 mil diameter with an L/D ratio greater than 3/1.
Group 11	Similar to Group 10 with SiC phase showing a tendency to cluster in the PG cone boundaries.
Group 20	SiC phase medium sized, evenly dispersed, acicular needles 0.035 mil to 0.105 mil diameter with an L/D ratio greater than 3/1.
Group 21	Similar to Group 20 with SiC phase showing a tendency to cluster in the PG cone boundaries.
Group 30	SiC phase coarse, moderatley well dispersed, acicular needles greater than 0.105 mil diameter with an L/D ratio greater than 3/1. PG growth cones usually contain occasional, intraconical, delaminations and strain lines.
Group 40	SiC phase fine, well dispersed, granules less than 0.035 mil diameter.
Group 70	SiC phase has no definite structure. Usually consists of coarse string-like growths surrounding unalloyed PG cones. PG cones contain many delaminations and strain lines.

SiC crystal size, L/D ratio, and degree of dispersion. Groups 5 and 6 are similar to 10 and 11, respectively, except finer, so as to be almost beyond the resolution of the microscope. Groups 5, 10, 20 and 30 all contain acicular SiC crystallites of similar length-to-diameter ratio with the size increasing with increasing group number. Photomicrographs of typical microstrucures of each group are shown in Figures 87 through 95.

c. Composition

Three techniques were evaluated for determining the SiC content of codeposits. These were: (1) use of a correlation between bulk coating density and SiC content, (2) ashing, and (3) electron microprobe analysis.

(1) Density Correlation

At one time, an empirically derived correlation between SiC content and density was routinely used to determine coating composition. As more information became available about the properties of the coatings and as more data became available from other analytic techniques, it was apparent that density is not a reliable indicator of composition.

The major source of error is the variability of PG matrix density. As discussed in pages 60 through 63, the matrix density is a function of deposition temperature. Hence, the bulk density is a function of both SiC content and deposition conditions. Figure 96 demonstrates the sensitivity of bulk density to matrix density and SiC content.

(2) Ashing

A technique was developed to determine SiC concentration by ashing coating samples in air to remove the free carbon phase and convert the SiC phase to SiO_2. Using the original sample weight and the ashed (SiO_2) weight, the SiC concentration can be calculated using the formula:

$$\frac{\text{weight ashed}}{\text{weight original X 1.5}} \text{X100} = \%\text{SiC}$$

The principal difficulty in using this method was that of oxidizing the SiC phase to completion and the time required. Initially, the specimens were pulverized in a mortar and pestle to increase the surface area and, therefore, increase the oxidation rate. This was found to be unnecessary, and later coating samples were simply split along the a-b plane into 5- to 10-mil-thick

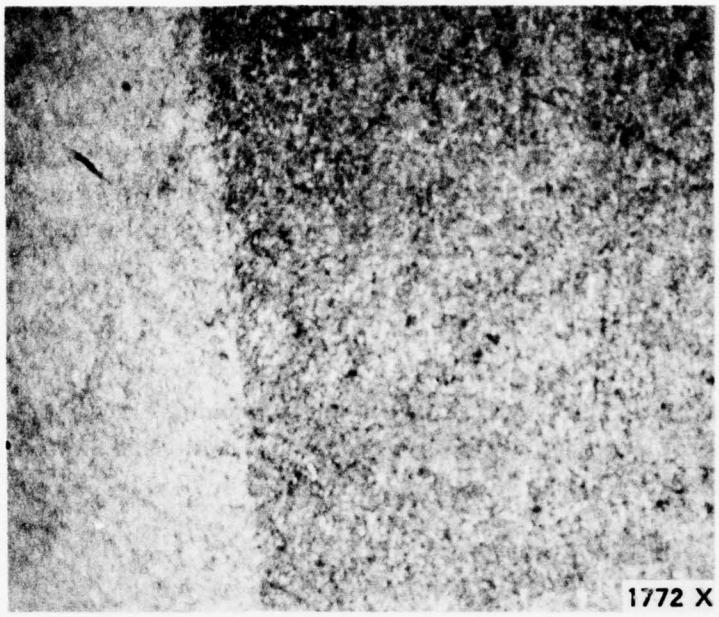

Figure 87. Typical Group 5 PG/SiC Microstructure.

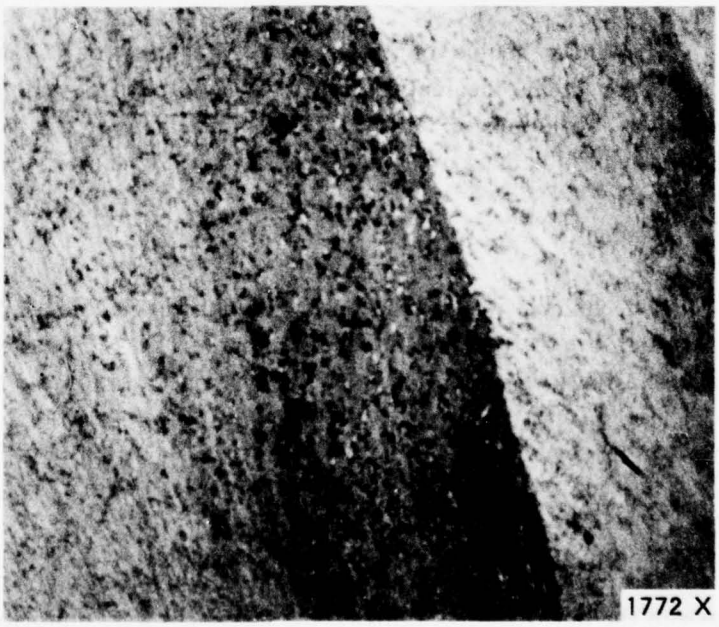

Figure 88. Typical Group 6 PG/SiC Microstructure.

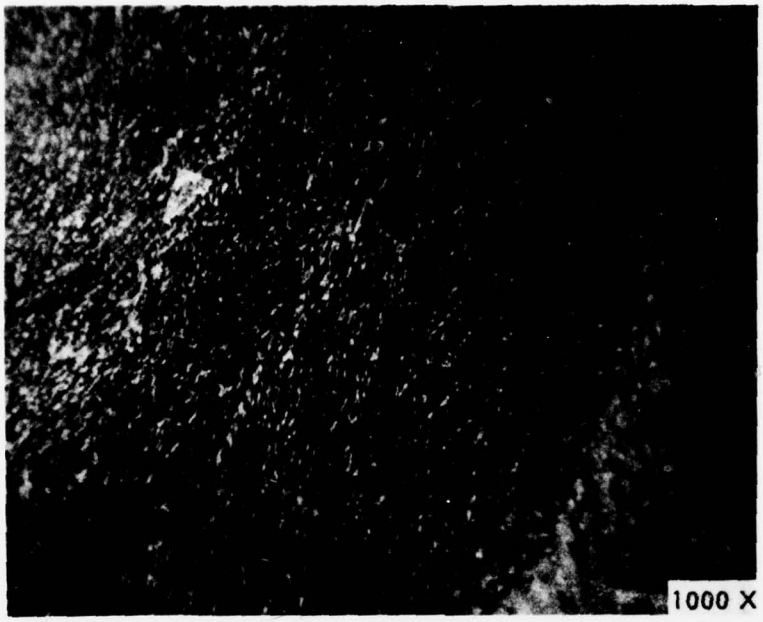

Figure 89. Typical Group 10 PG/SiC Microstructure.

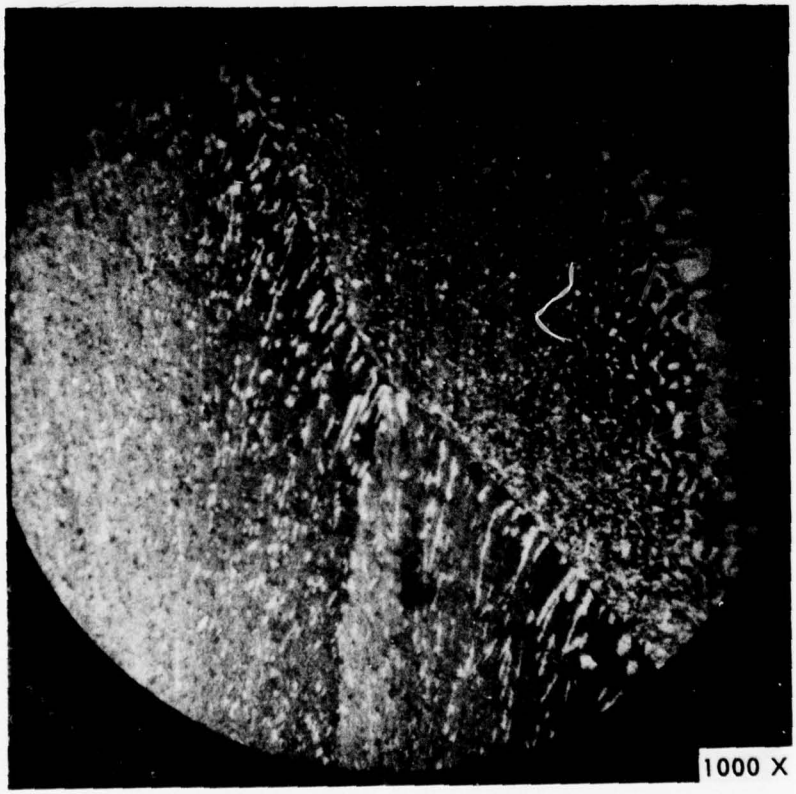

Figure 90. Typical Group 11 PG/SiC Microstructure.

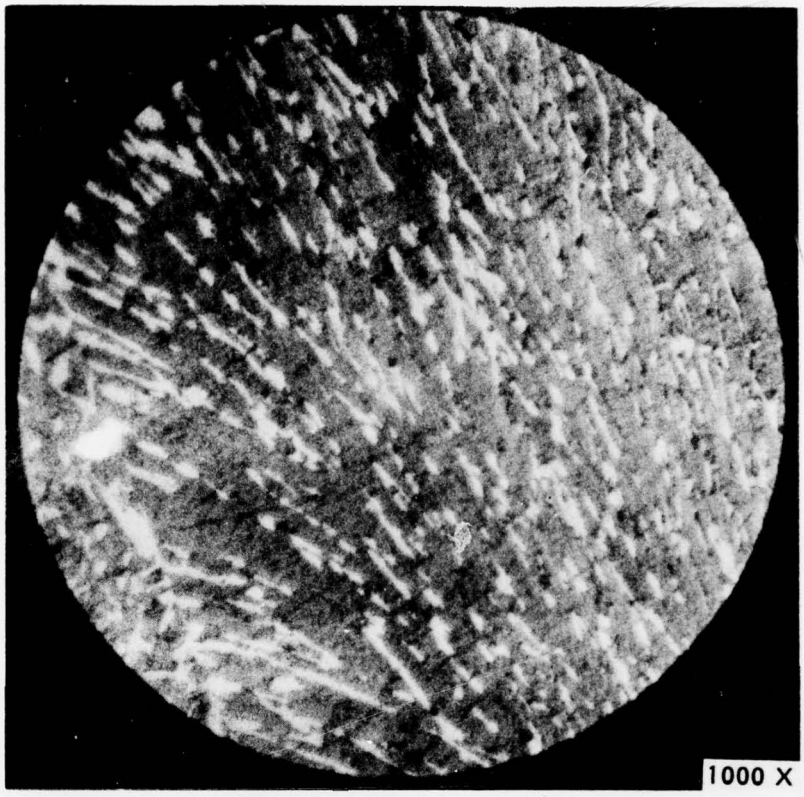

Figure 91. Typical Group 20 PG/SiC Microstructure.

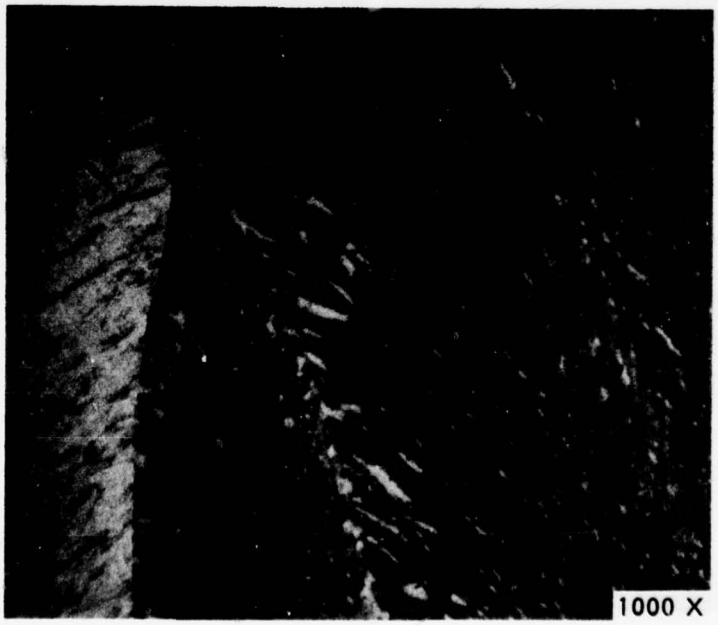

Figure 92. Typical Group 21 PG/SiC Microstructure.

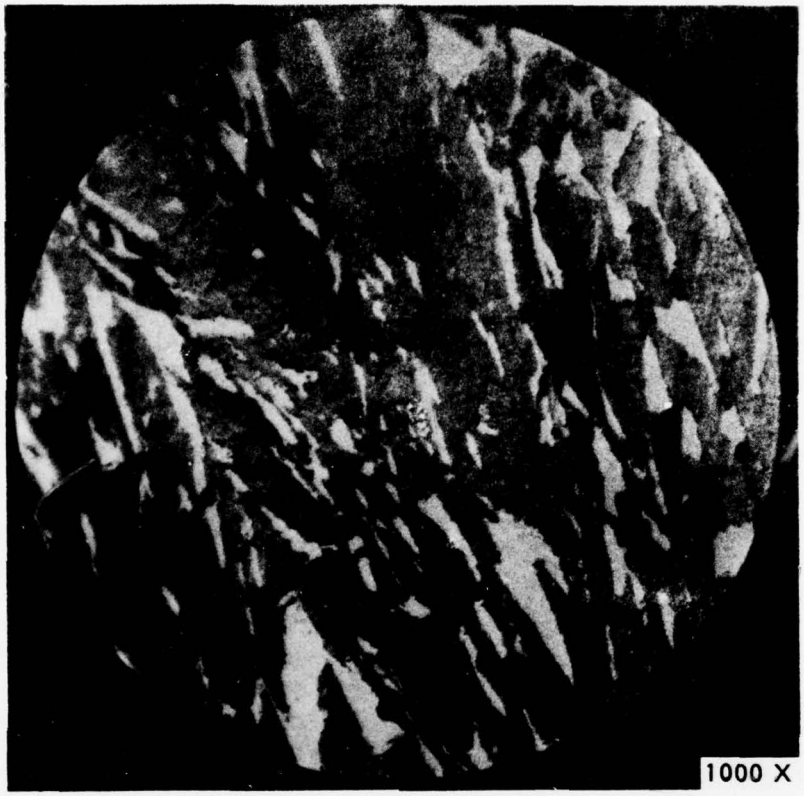

Figure 93. Typical Group 30 PG/SiC Microstructure.

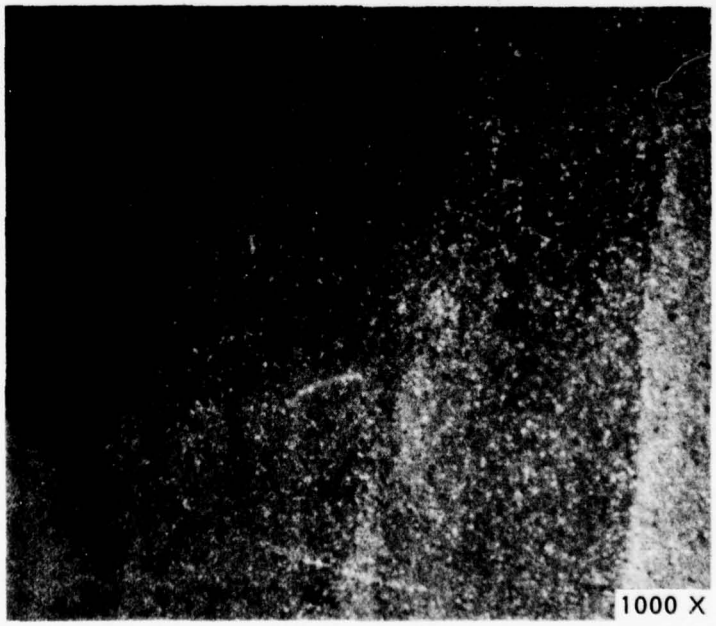

Figure 94. Typical Group 40 PG/SiC Microstructure.

Figure 95. Typical Group 70 PG/SiC Microstructure.

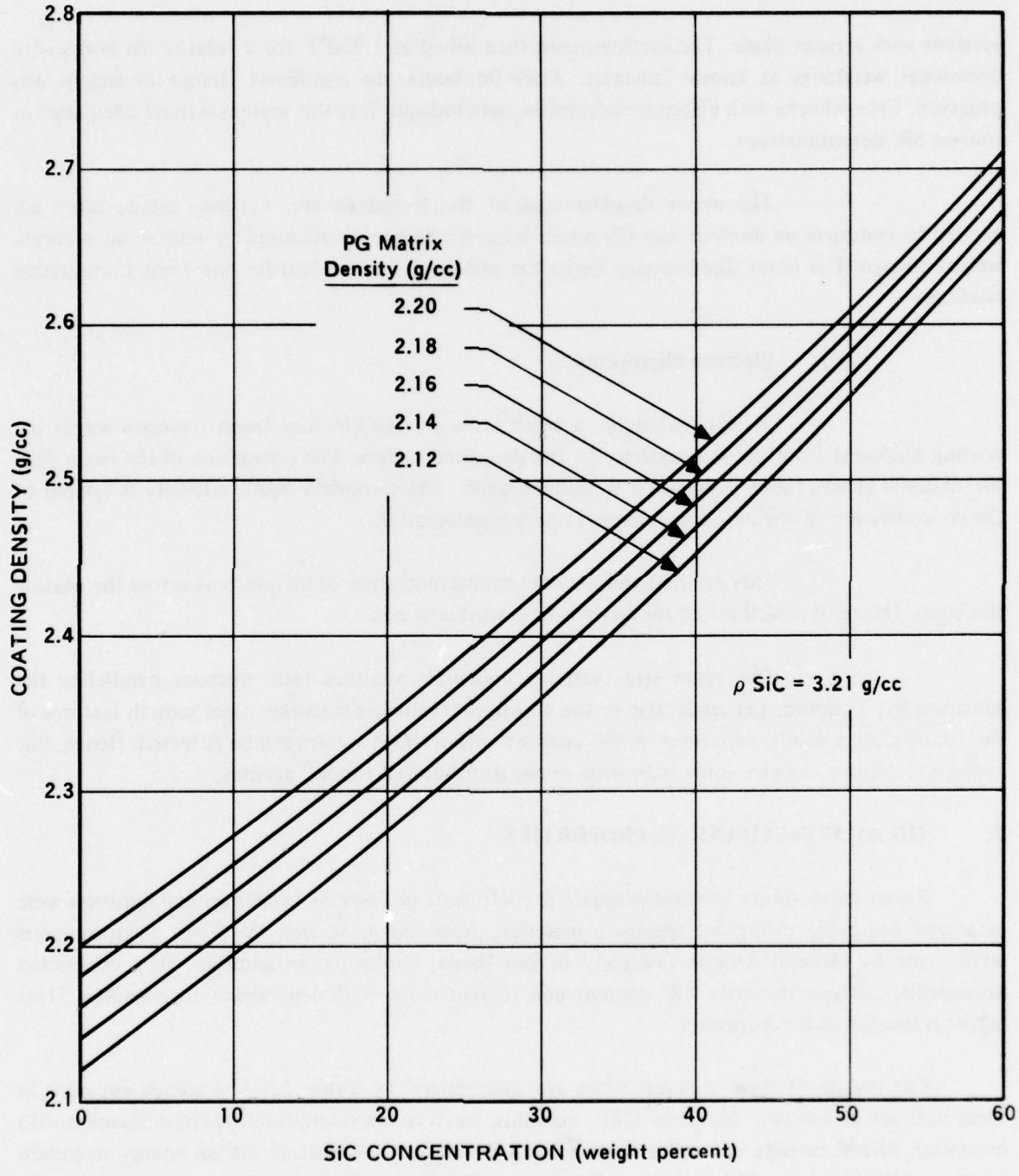

Figure 96. Relationship Between Coating Density, SiC Concentration And Pyrolytic Graphite Matrix Density.

sections with a razor blade. The sections were then ashed at 1,950°F for a total of 96 hours with occasional weighings at known intervals. After 96 hours, no significant change in weight was observed. Cross-checks with electron microprobe data indicate that this system is quite adequate for routine SiC determinations.

The major disadvantages of the technique are: (1) long ashing times are needed to complete an analysis and (2) rather large specimens are required to achieve an accurate weight change. The latter disadvantage limits the utility of this method for analyzing thin, graded coatings.

(3) Electron Microprobe

In this technique, a small cross section electron beam traverses across the coating thickness from the substrate to the last deposited surface. The interaction of the beam with the material causes the emission of a secondary beam. The secondary beam intensity is related to the concentration of the particular element under consideration.

This method yields a continuous indication of SiC content across the coating thickness. Hence, it is well suited for analysis of graded coatings.

The beam size used for codeposit analyses (100 microns parallel to the substrate by 2 microns perpendicular to the substrate) is smaller than the major growth features of the coating. As a result, variations in SiC content within the PG cones can be detected. Hence, this analysis technique can give some indication of the dispersion of the SiC needles.

2. THERMAL/MECHANICAL PROPERTIES

Room temperature flexural properties, coefficient of thermal expansion and hardness were measured using the properties specimen materials described in Section IV. These measurements were made by General Atomic Company in San Diego, California. In addition, they conducted microprobe analysis to verify SiC content and measured the bulk densities of the samples. Their report is located in the Appendix.

The results of these measurements are summarized by Table 23. The trends apparent in these data are as follows: hardness, CTE, modulus, fracture stress and fracture strain increase with increasing silicon carbide content and decreasing deposition temperature. Strain energy to failure increases with decreasing SiC content and increasing deposition temperature.

Table 23. Summary of General Atomic Results.

Sample No.	Deposition Temp, °F	Average Weight Percent Silicon	Density, g/cc	CTE 10^{-6} °C^{-1}	Mechanical Properties*				Average Hardness DPH
					Elastic Modulus 10^6 psi	Fracture Stress 10^4 psi	Fracture Strain 10^{-2} in/in	Strain Energy to Failure lb-in/in^3	
006-22	3200	∿ 5	2.24	3.24	2.049	2.479	1.206	91.2	65
006-23	3200	∿ 3	2.21	3.21	1.814	2.048	1.120	115.9	55
006-24	3300	∿ 3	2.20	2.98	1.661	1.733	1.039	150.6	45

*4-point bending, room temperature

SECTION VI

CONCLUSIONS AND RECOMMENDATIONS

The following conclusions are drawn from the results of this program:

(1) The silicon carbide content of a codeposit coating can be varied by adjustment of either deposition temperature or MTS flow rate.

(2) Graded coatings can be deposited by independently varying either parameter.

(3) Neither single-variable method produces the most desired SiC microstructure (well dispersed, high aspect ratio aciculae) throughout the coating thickness. This microstructure occurs in the first deposited material but gradually changes to a less acicular structure.

(4) The density of the PG matrix in a PG/SiC codeposit is a function of deposition temperature. The data suggest that the matrix density is independent of both SiC content and MTS flow rate. However, the considerable scatter in the data may obscure such relationships if they exist.

(5) In general, the PG matrix density is much higher in the codeposited material than in unalloyed pyrolytic graphite deposited at 3,000 – 3,400°F. Additionally, the d-spacing is lower than would be expected in unalloyed low temperature pyrolytic graphite. These phenomena indicate that the CH_3SiCl_3 precursor has a profound effect on the carbon phase deposition process.

Based on the results of this program, the following recommendations are made:

(1) The effects of other variables on coating morphology should be determined. Improvements in cone structure, surface condition and SiC structure should be achieved particularly at the higher deposition temperatures. Such improvements might be expected at higher flow rates and lower concentrations.

(2) Process methods involving simultaneous variation of more than one parameter should be investigated as a means of improving coating microstructure.

(3) Material characterization should be extended to include a study of crystallographic parameters and their relationship to properties and process conditions.

APPENDIX

General Atomic Report

GENERAL ATOMIC

GA-C13425

CHARACTERIZATION STUDIES OF THREE HOMOGENEOUS, SILICON-ALLOYED, PYROLYTIC GRAPHITE ROCKET NOZZLE MATERIALS

by

Hong Shim

Prepared under
Purchase Order No. 98974
(Prime Contract F33615-74-C-5103)
for
Atlantic Research Corporation
5390 Cherokee Avenue
Alexandria, Virginia 22314

General Atomic Project 0920

April 1, 1975

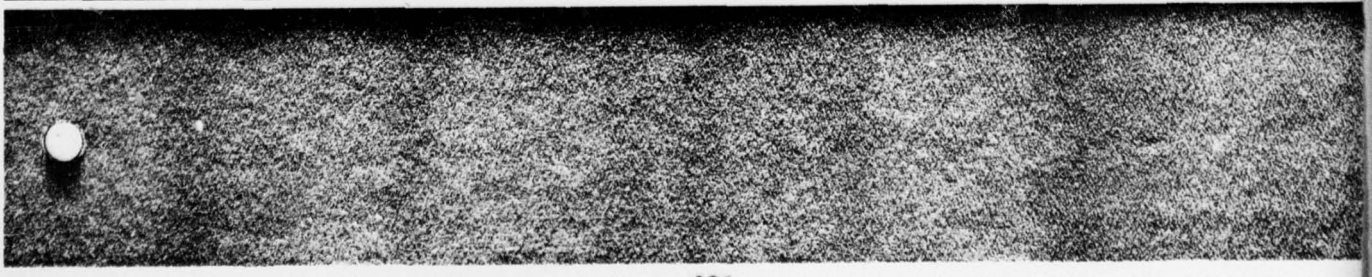

CHARACTERIZATION STUDIES OF THREE HOMOGENEOUS, SILICON-ALLOYED, PYROLYTIC GRAPHITE ROCKET NOZZLE MATERIALS

(H. SHIM)

Pursuant to Atlantic Research Corporation's purchase order number 98974, Contract F33615-74-C-5103, General Atomic has characterized properties of three homogeneous PG/SiC specimens supplied by Atlantic Research Corporation. The work statement for the study is:

> The Seller shall make available and employ his facilities and personnel at the level of effort specified in the paragraph entitled LEVEL OF EFFORT, provide the necessary materials and use his best efforts to perform the following characterization analysis of Buyer furnished PG/SiC coated specimens.
>
> 1. Microprobe - for SiC concentration distribution across the thickness of the coating. (Total of five)
>
> 2. Thermal Expansion Curve ($\Delta\ell/\ell$) from room temperature to 1000°C for one location in the coating specimen (θ-Zplane). (Total of five)
>
> 3. Microflexural stress-strain curve to failure. Sufficient number of measurements to establish statistical significance of flexural strength (θ-Z plane). (Approximately eight of each for total of forty)
>
> 4. Microhardness (DPH) across the thickness of the coating.(Total of five)
>
> 5. Preferred orientation at one location in the coating specimen. (Total of three)
>
> 6. Submit a written report for each lot of specimens provided. The report shall include all the data obtained and include a discussion of measurement accuracy. Camera-ready copy of the reports are required.

The work statement was later modified (March 6, 1975) and they are:

> Item 5, preferred orientation analysis, is deleted in its entirety.
>
> Item 7, authorizing travel for 2 men to Washington, D.C., on October 9 and 10, 1974 is added.

Out of five specimens, three homogeneous, silicon-alloyed, PG/SiC materials were received on the 13th of February, 1975. The identification number were 006-22, 006-23 and 006-24.

1.0 MICROHARDNESS

Diamond Pyramid hardness (DPH) numbers were measured on a surface oriented perpendicular to the stubstrate surface along lines parallel to the direction of deposition (Fig. 1). In order to obtain more representative values, two traces were made. A 50 g load was used in making the indentations. Because of the recovery of the indentation mark made by the indenter of a microhardness tester, a thin organic film was applied to the surface of interest prior to the test, and hardness was measured from the size of the impression left in the layer. Starting from the substrate side, indentations were made at 0.006–0.007 inches intervals. The DPH numbers measured as a function of distance from the substrate are plotted in Fig. 2. The average hardness is about 65 DPH for 006-22 material, 55 DPH for 006-23 material and 45 DPH for 006-24 material.

2.0 DENSITY MEASUREMENT

A sink-float method that uses a column of mixture of bromoform and methanol was employed to measure the density of PG/SiC materials. The apparent bulk density is about 2.24 g/cc for 006-22 material, 2.21 g/cc for 006-23 material and 2.20 g/cc for 006-24 material.

3.0 X-RAY MICROPROBE

The sketch in Fig. 3 shows the position where microprobe traverses were made.

The first traverse was made at constant speed automatically controlled by the machine and the second traverse was made at faster speed by hand-cranking the x-ray beam. Only, results from the first traverse are reported (Fig. 4). A beam of about 300μ wide was used. The silicon concentration (wt.%) was obtained by calibrating x-ray intensity with a pure silicon standard specimen. The silicon concentration is about 5% except for the middle portion of the coating thickness for 006-22 material, 3% for 006-23 material and 3 to 2% for 006-24 material. X-ray scanning photographs show the heterogeneity with higher silicon concentration at boundaries (Fig. 5).

4.0 MECHANICAL PROPERTIES

The positions from which specimens for mechanical testings were cut is depicted in Fig. 6. The major plane of all specimens was parallel with the substrate surface its long dimension was parallel with the axis of the nozzle. All surfaces of every specimen were polished through 0.5μ diamond grits. Final dimensions were about 0.040 (width) x 0.015 (thickness) x 1.000 (length) inches. Tests were conducted in a 4-point bending fixture whose outer and inner knife edge spacings were 0.2969 and 0.1484 inches, respectively, and with the crosshead speed of 0.020 inch/min. in an Instron machine. The load was applied parallel to crystallographic C-direction of the deposit. The data obtained in the tests were analyzed using a computer program valid for large deflection expressions including corrections for frictional effects between the knife edges and specimen. The results are summarized in Table I.

5.0 COEFFICIENT OF THERMAL EXPANSIVITY (CTE)

Fig. 7 describes specimen orientation and direction of measurement for CTE study. A bar with edges of about 0.160 inches and 0.650 inches long was the specimen, and CTE was measured in the direction of length. The mean CTE was measured in the temperature range of 22 - 1000°C. A typical elongation - temperature curve is shown in Fig. 8. The curve in the figure starts to level off at about 700°C. It was found that, above 700°C, a grayish-colored film, whose nature is not known, was deposited on the Quartz tube of the CTE apparatus. The thermal expansivity is about $3.24 \times 10^{-6}\ °C^{-1}$ for 006-22 material, $3.21 \times 10^{-6}\ °C^{-1}$ for 006-23 material and $2.98 \times 10^{-6}\ °C^{-1}$ for 006-24 material.

TABLE I MECHANICAL PROPERTIES* OF PG/SIC MATERIALS
MEASURED IN 4-POINT BENDING

Specimen Identification Number	No. of Specimen Tested	Fracture Stress ($x10^4$ psi)		Elastic Modulus ($x10^6$ psi)		Strain Energy to Fracture (lb-in/in^3)		Fracture Strain ($x10^{-2}$ in/in)	
		Avg.	Std. Dev.	Avg.	Std. Dev.	Avg.	Std. Dev.	Avg.	Std. Dev.
006-22	11	2.479	0.366	2.049	0.157	91.2	25.9	1.206	0.232
006-23**	9	2.048	0.330	1.814	0.081	115.9	36.4	1.120	0.193
006-24	10	1.733	0.258	1.661	0.081	150.6	47.2	1.039	0.160

* - It should be remembered that the testing specimens were prepared from the middle portion of the coating thickness whose silicon concentration is not necessarily representative of the average concentration of the materials.

** - Originally twelve specimens were prepared, but, in the test, three of them failed in a interlaminar shear mode at lower loads. Therefore, only results for nine specimens are reported here.

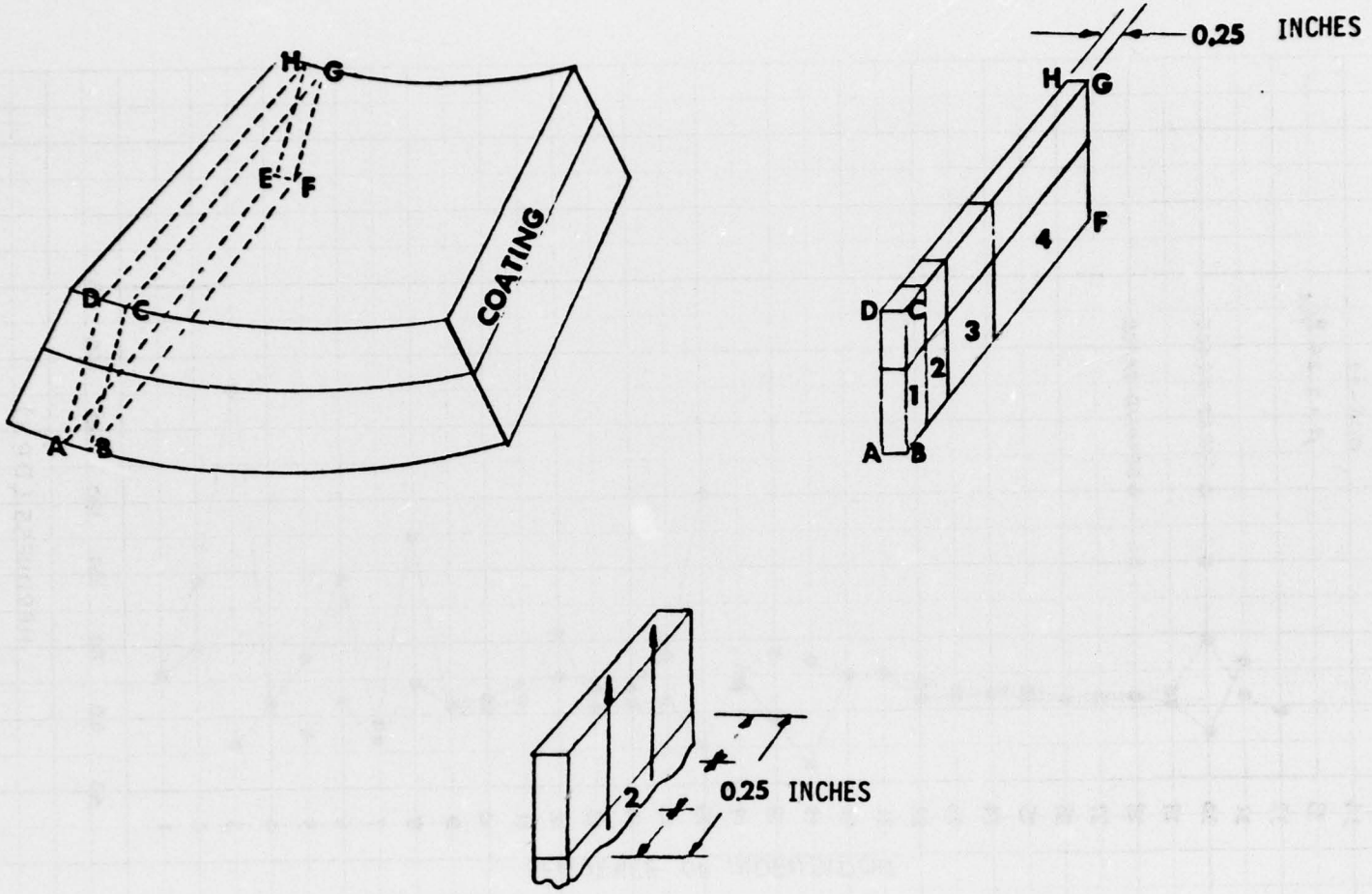

FIG. 1 SCHEMATIC DIAGRAMS SHOWING POSITIONS AT WHICH DPH NUMBERS WERE MEASURED. INDENTATIONS WERE MADE ALONG LINES INDICATED AS ARROW.

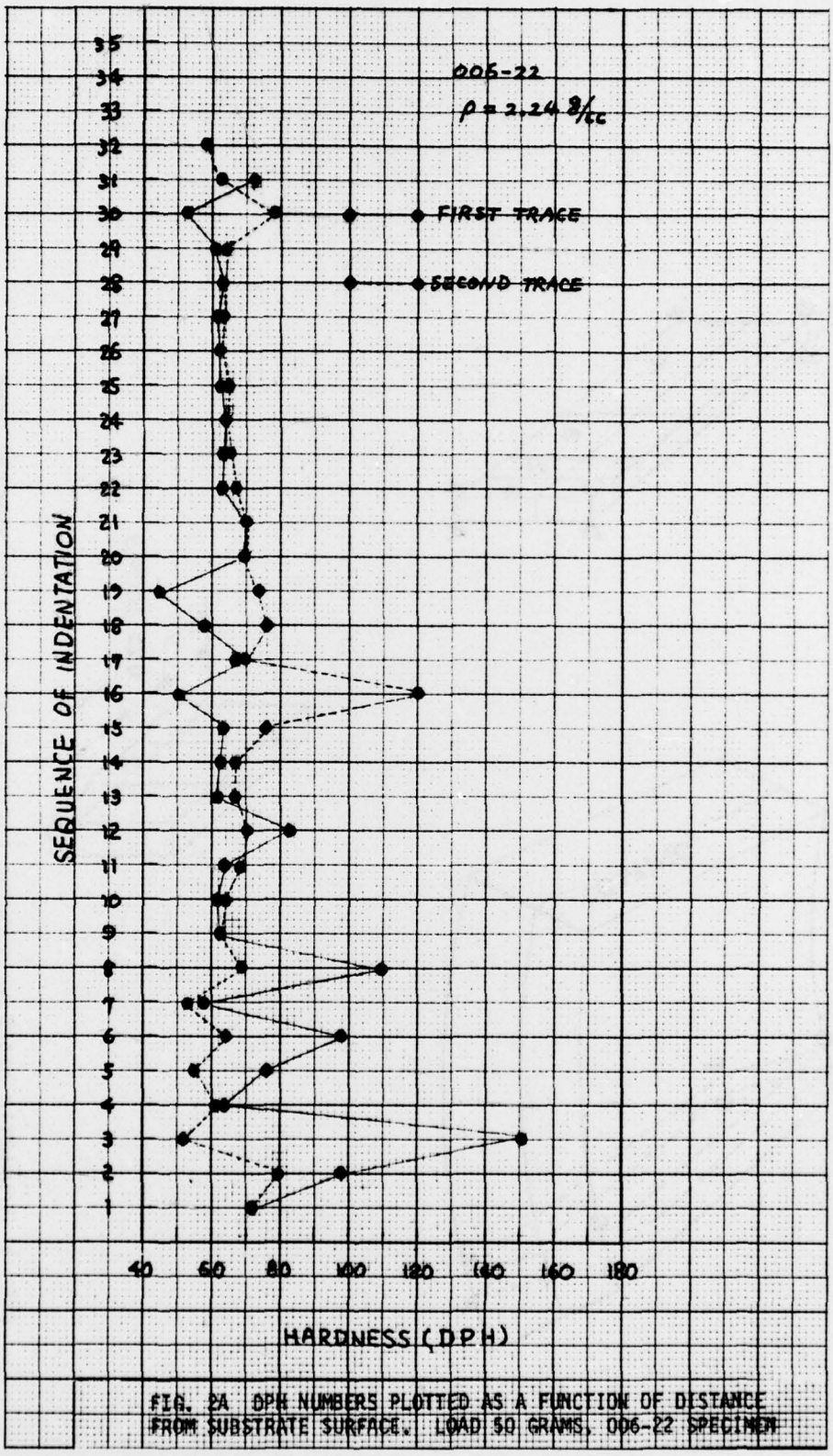

FIG. 2A DPH NUMBERS PLOTTED AS A FUNCTION OF DISTANCE FROM SUBSTRATE SURFACE. LOAD 50 GRAMS, 006-22 SPECIMEN

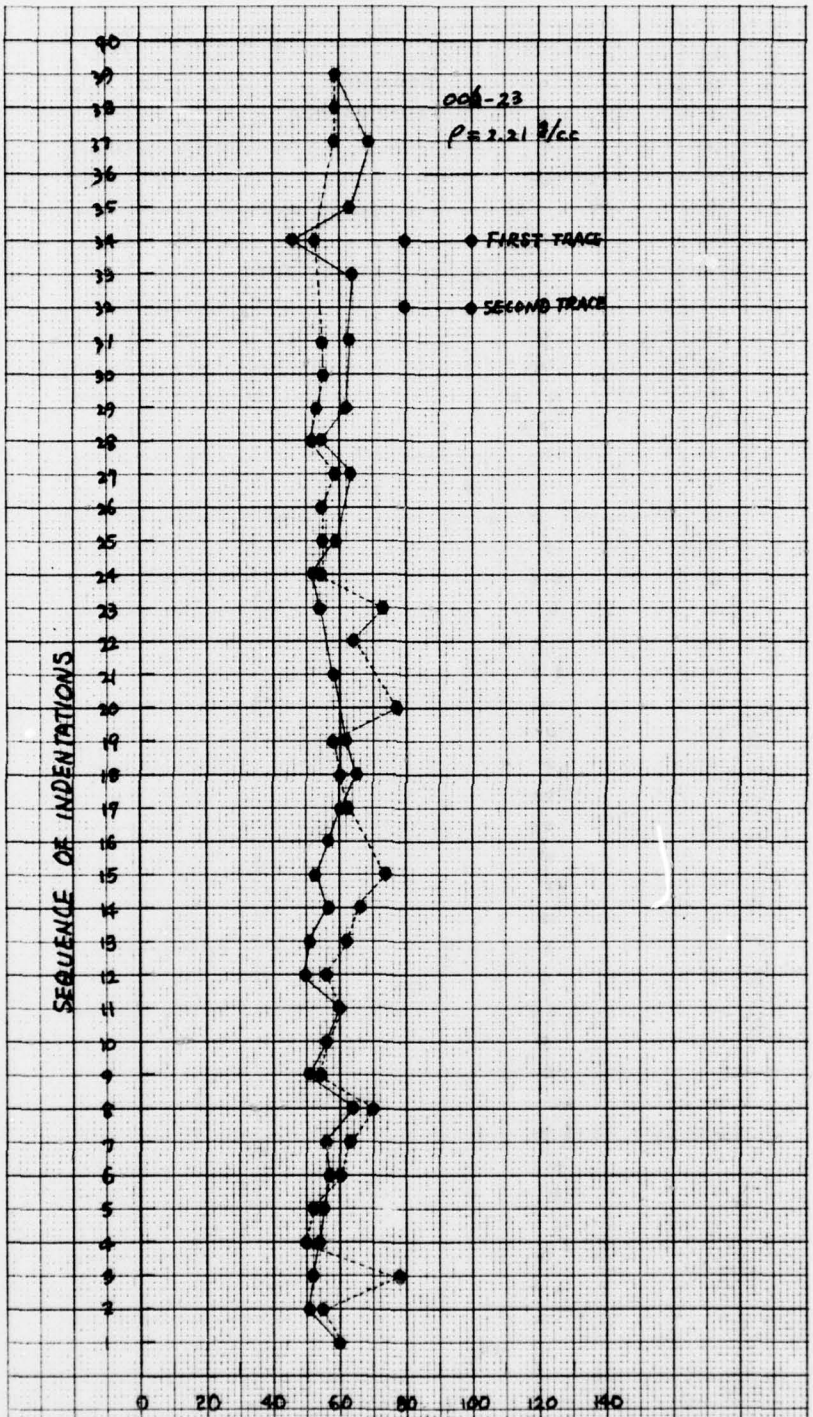

FIG. 28 DPH NUMBERS PLOTTED AS A FUNCTION OF DISTANCE FROM SUBSTRATE SURFACE. LOAD 50 GRAMS. 006-23 SPECIMEN

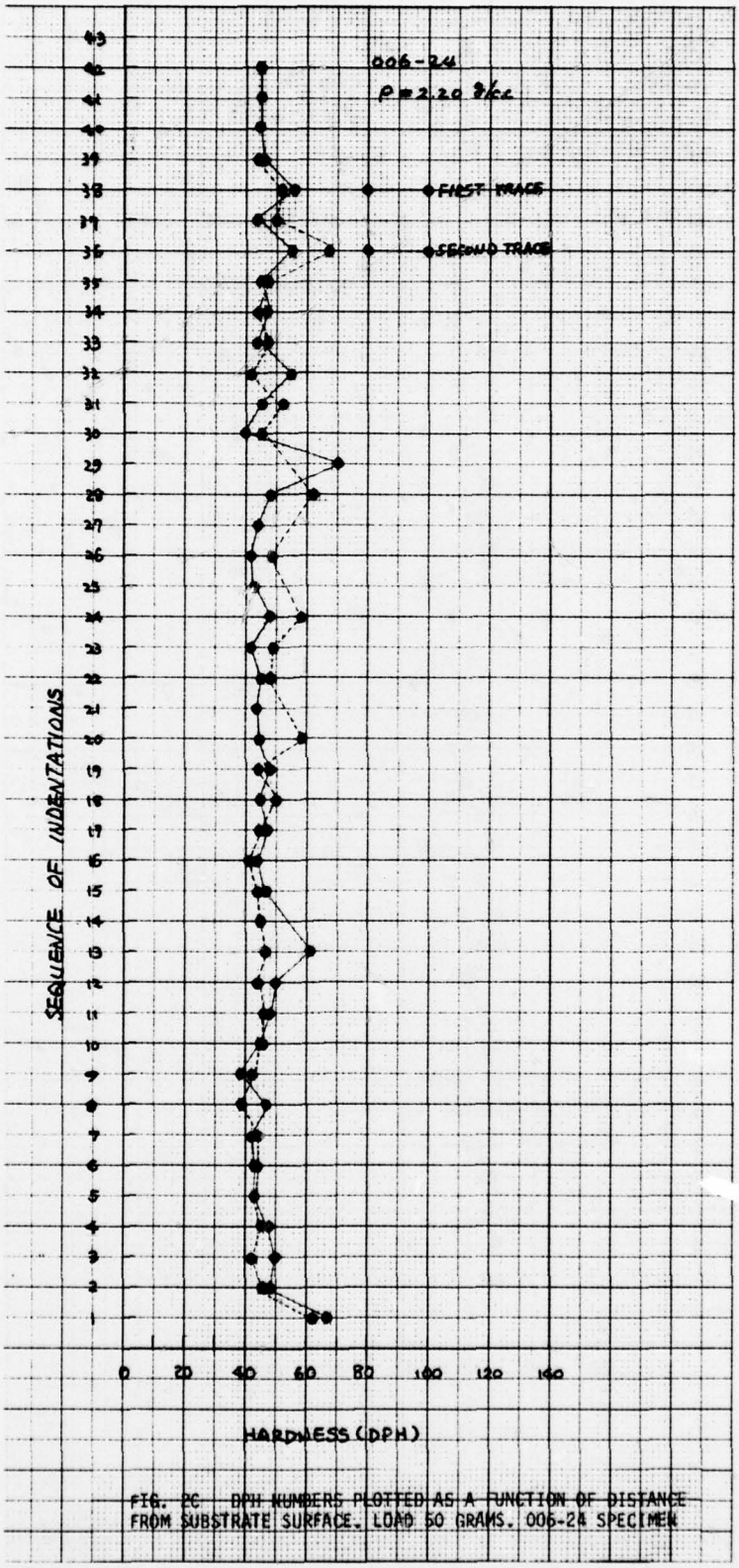

FIG. 2C DPH NUMBERS PLOTTED AS A FUNCTION OF DISTANCE FROM SUBSTRATE SURFACE. LOAD 50 GRAMS. 006-24 SPECIMEN

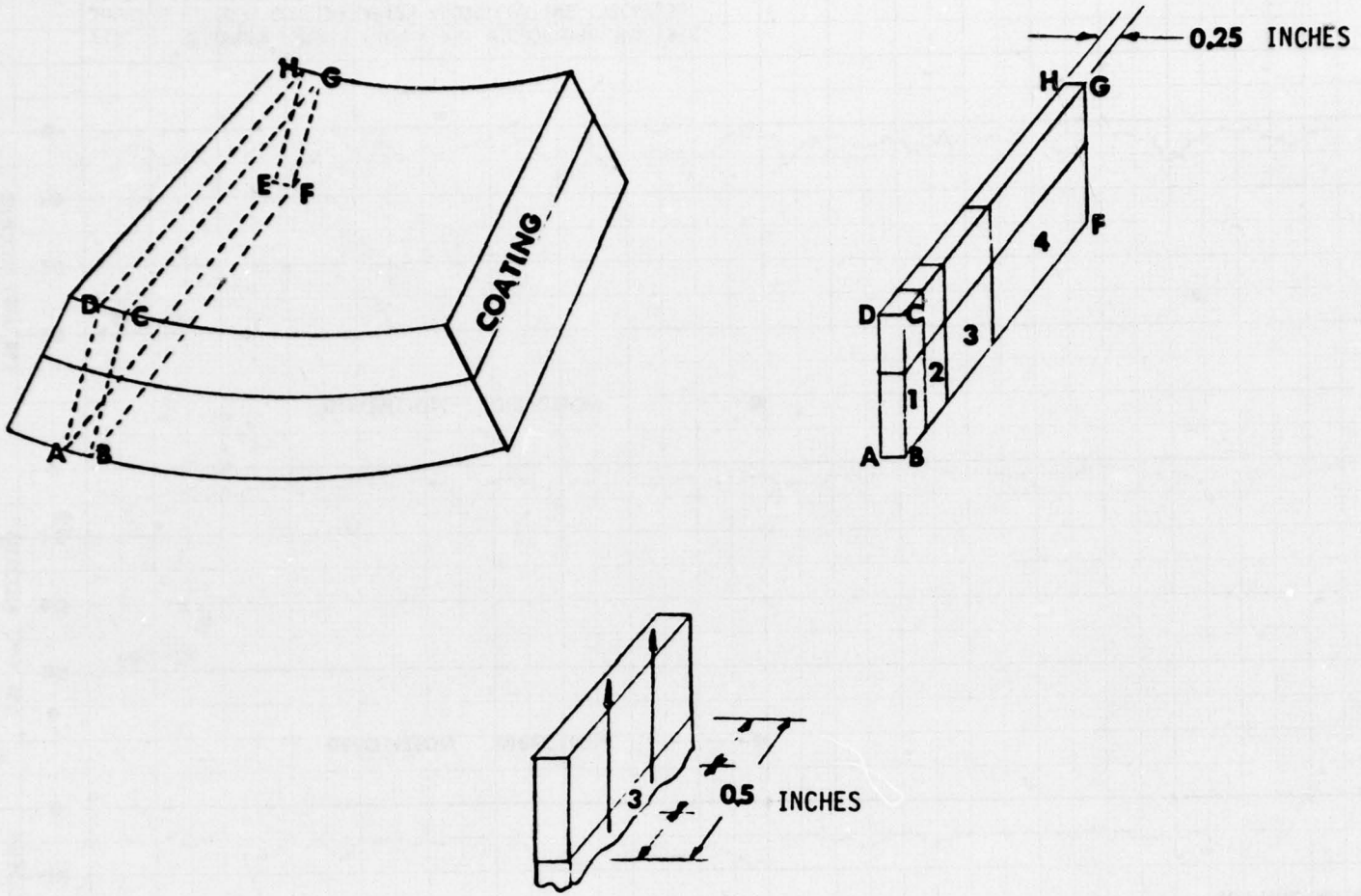

FIG. 3 SCHEMATIC DIAGRAMS SHOWING POSITIONS AT WHICH TRAVERSES MADE BY THE MICROPROBE ALONG THE LINES INDICATED AS ARROW.

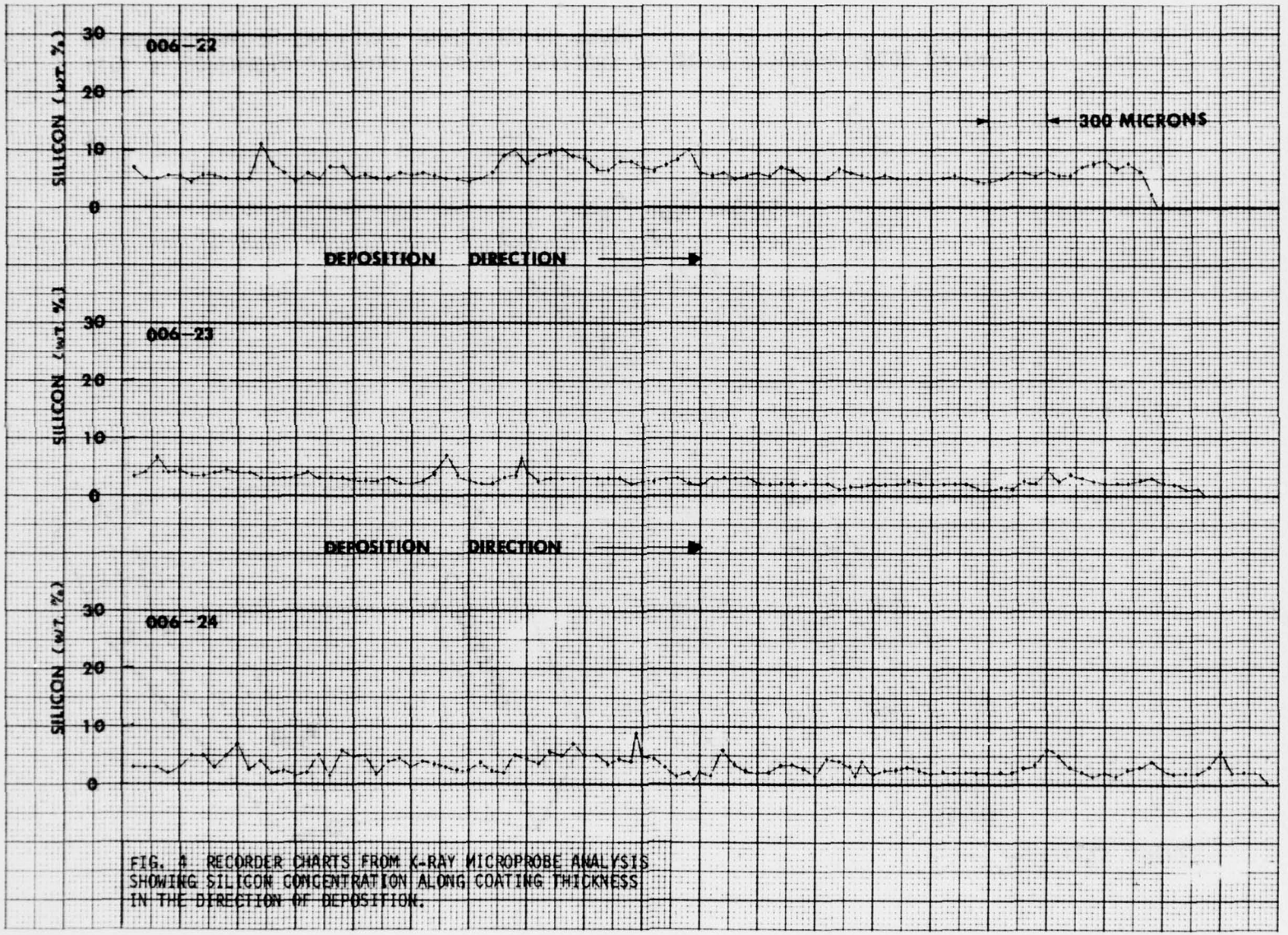

FIG. 4 RECORDER CHARTS FROM X-RAY MICROPROBE ANALYSIS SHOWING SILICON CONCENTRATION ALONG COATING THICKNESS IN THE DIRECTION OF DEPOSITION.

FIG. 5A X-RAY SCANNING PHOTOGRAPH. SILICON IS REPRESENTED AS WHITE AREA. HIGH SILICON CONCENTRATION OCCURS AT BOUNDARIES.

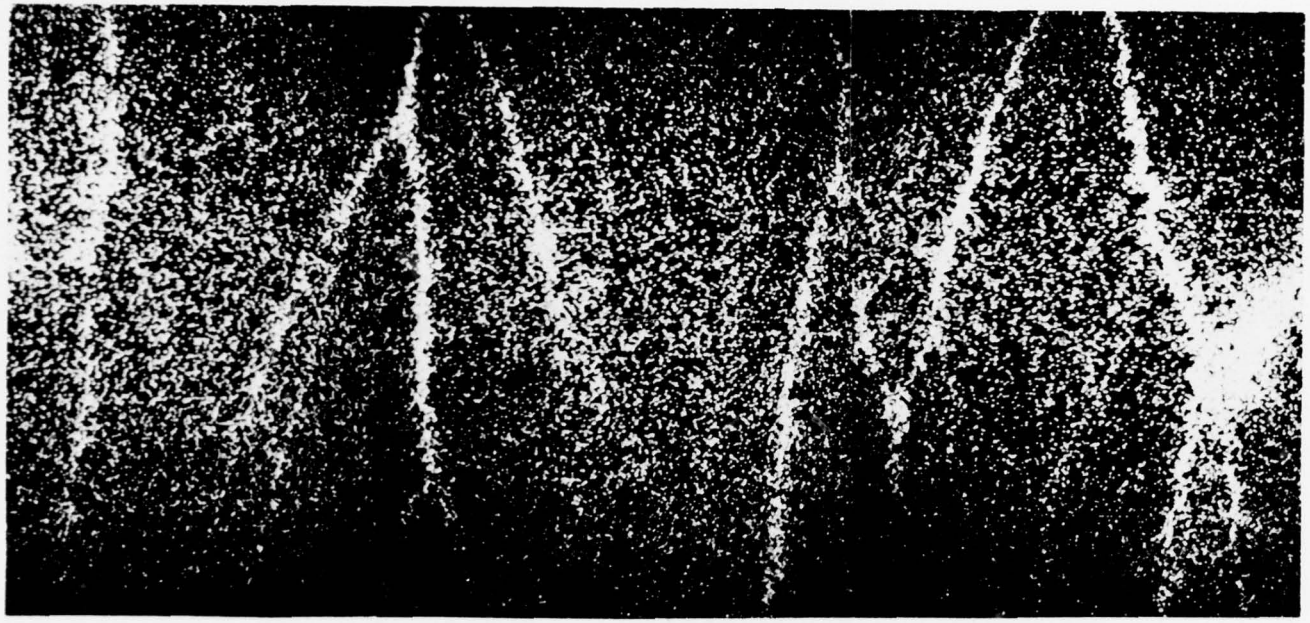

FIG. 5B X-RAY SCANNING PHOTOGRAPH. SILICON IS REPRESENTED AS WHITE AREA. HIGH SILICON CONCENTRATION OCCURS AT BOUNDARIES.

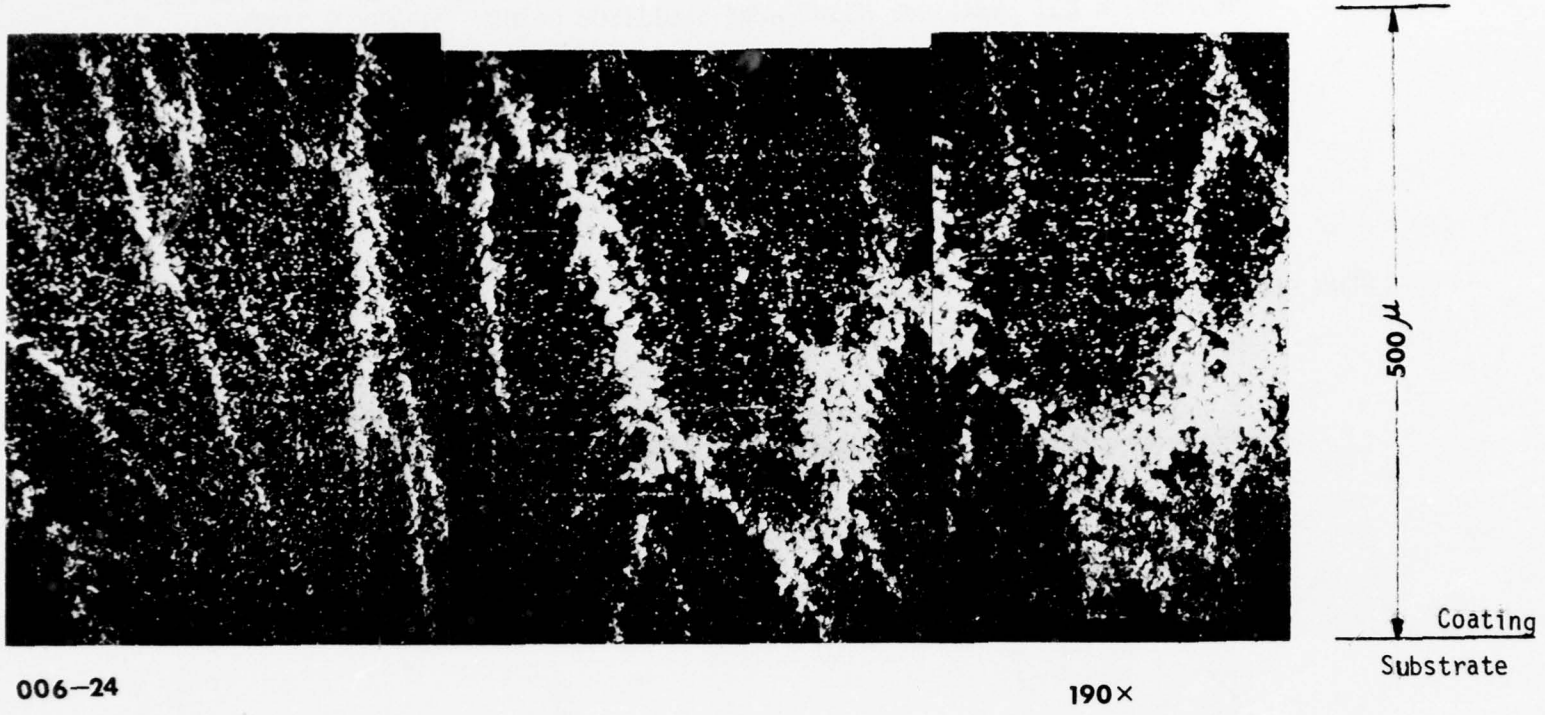

FIG. 5C X-RAY SCANNING PHOTOGRAPH. SILICON IS REPRESENTED AS WHITE AREA. HIGH SILICON CONCENTRATION OCCURS AT BOUNDARIES.

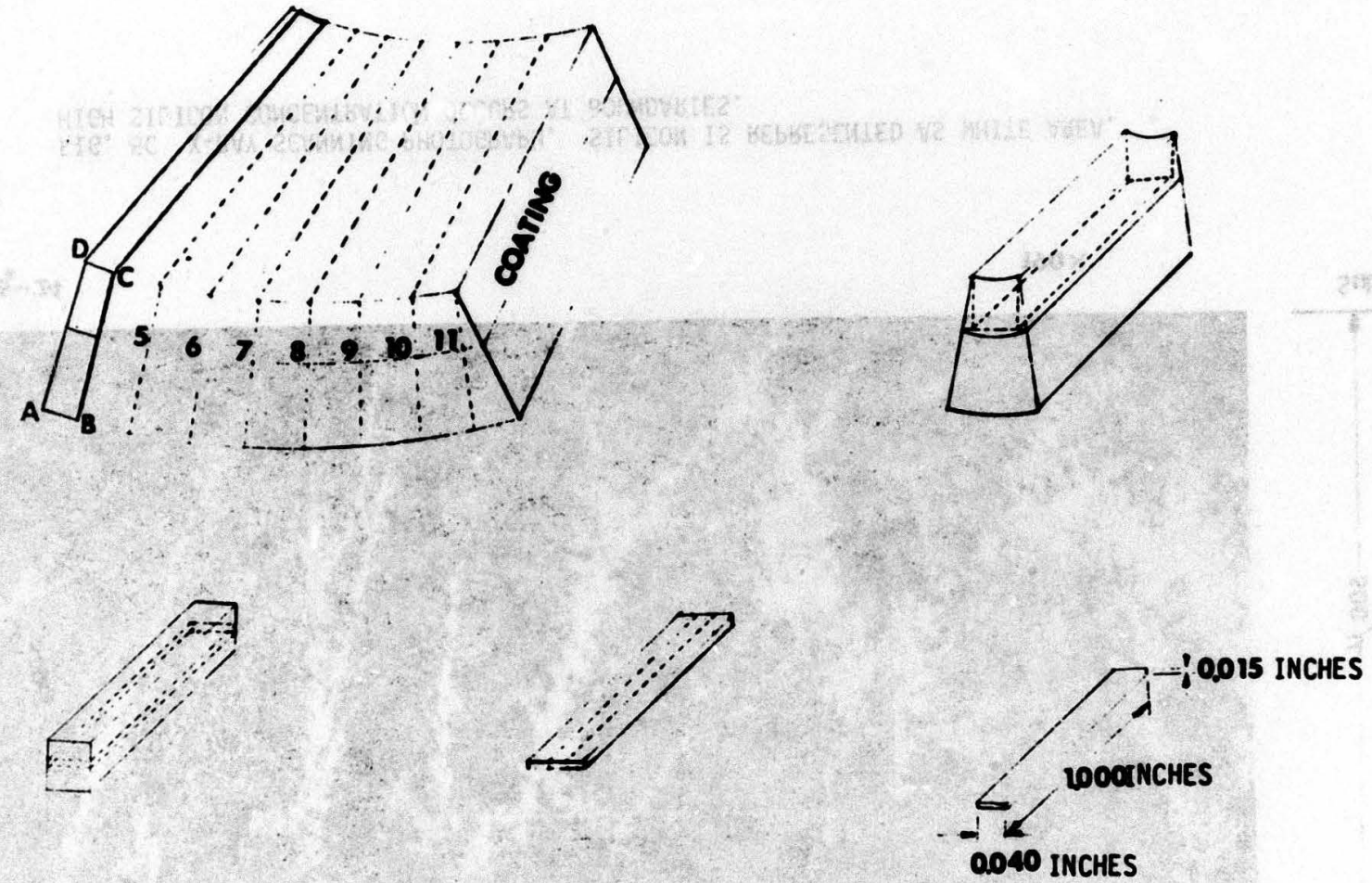

FIG. 6 SCHEMATIC DIAGRAMS SHOWING POSITIONS FROM WHICH SPECIMENS FOR MECHANICAL TESTINGS WERE CUT. FINAL DIMENSIONS OF A SPECIMEN WERE ABOUT 0.040 X 0.015 X 1.000 INCHES

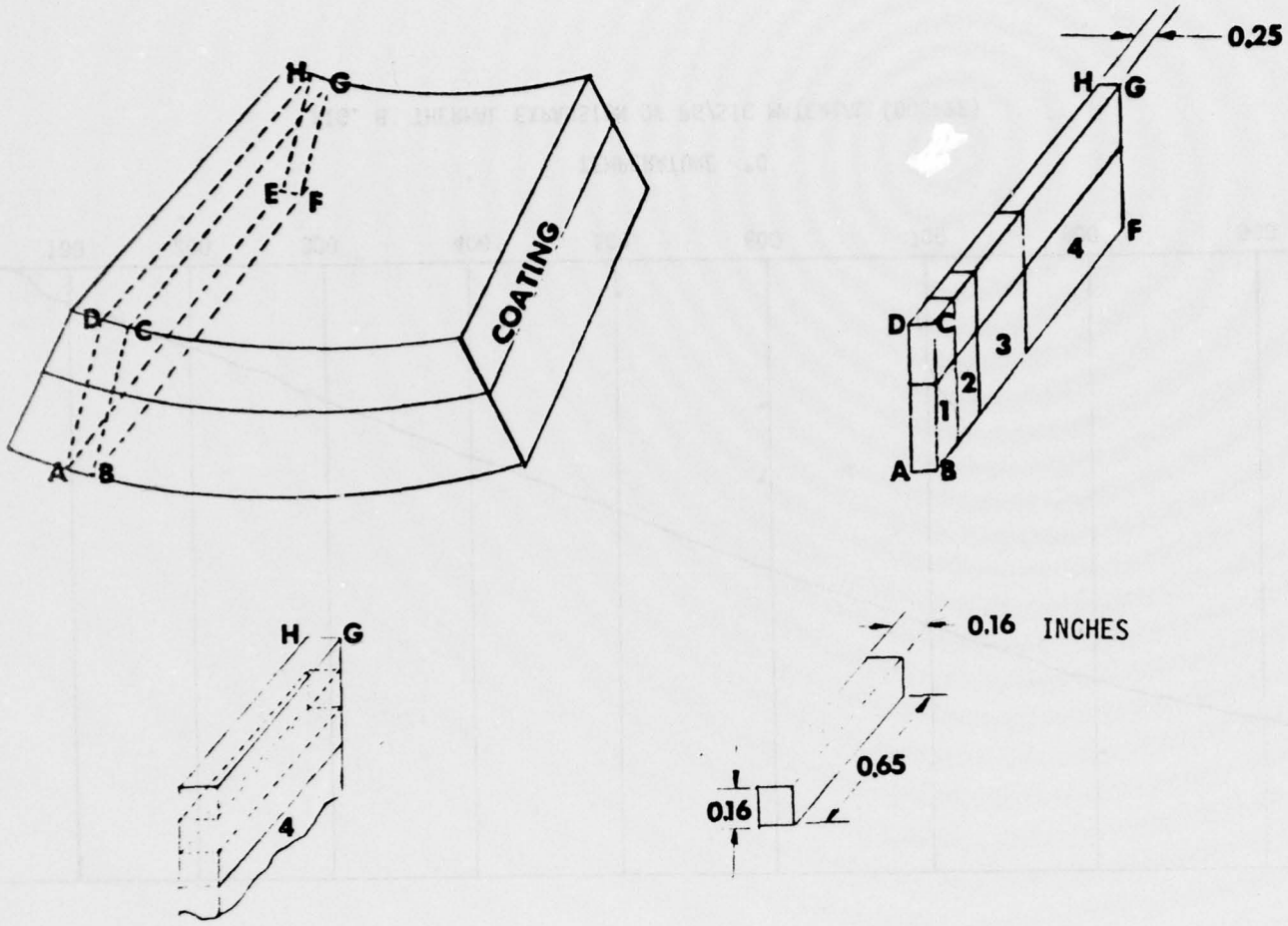

FIG. 7 SCHEMATIC DIAGRAMS SHOWING POSITIONS FROM WHICH SPECIMEN FOR THERMAL EXPANSION COEFFICIENT MEASUREMENT WERE CUT. FINAL DIMENSIONS WERE ABOUT 0.16 X 0.16 X 0.65 INCHES. MEASUREMENT WAS MADE IN A DIRECTION PARALLEL TO THE AXIS OF THE NOZZLE.

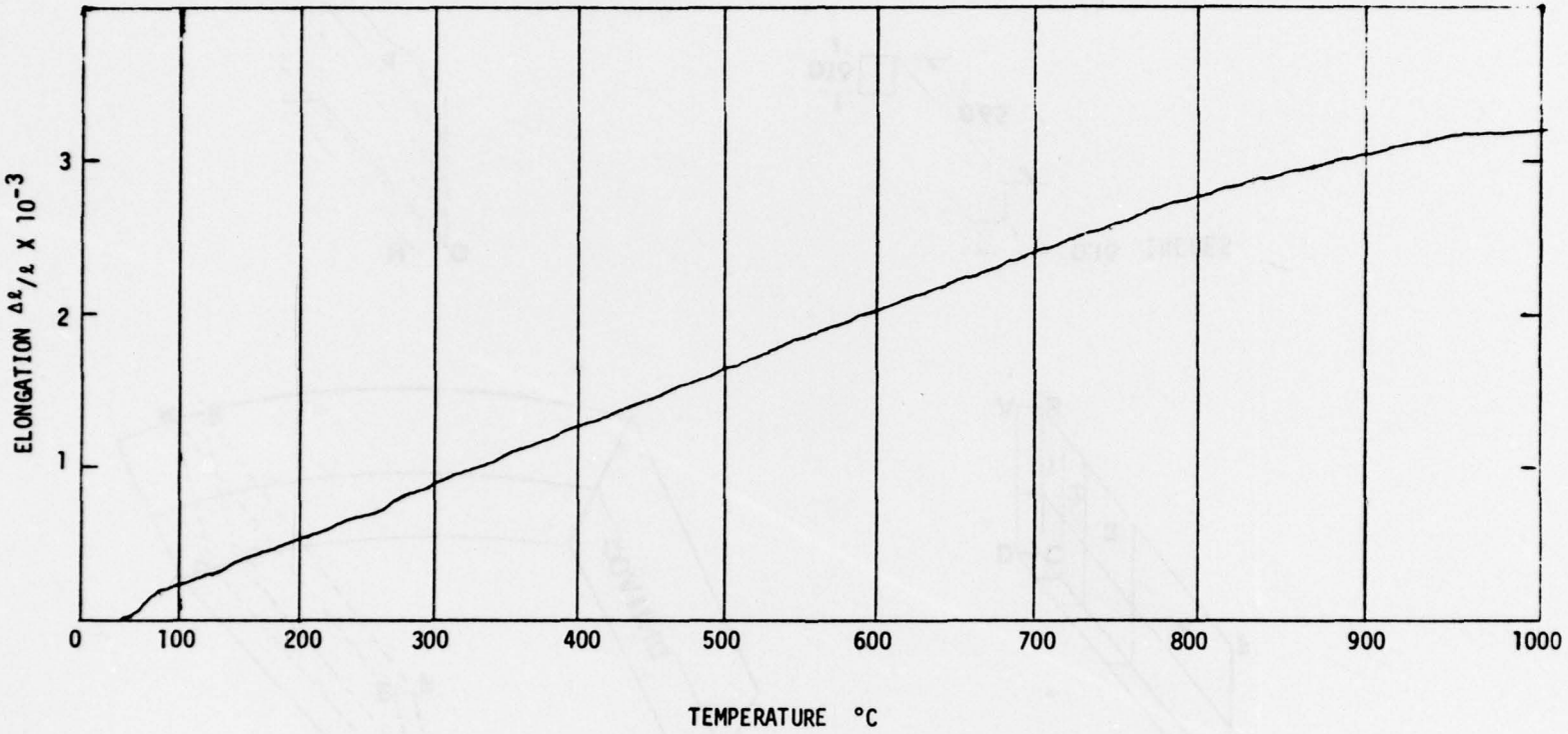

FIG. 8 THERMAL EXPANSION OF PG/SIC MATERIAL (006-22)